Study on jet angular correlations

Junya Nakamura

Particle and Nuclear Physics, School of High Energy Accelerator Science
The Graduate University for Advanced Studies, Japan

Doctoral thesis

For the degree of doctor of philosophy in physics

Abstract

This thesis discusses the azimuthal angle correlation between the two jets produced in association with a top quark pair at the LHC. A detailed calculation of the vector boson fusion contribution to the Higgs plus 2 partons process and the $Q\bar{Q}$ plus 2 partons process is presented by using the helicity amplitude technique, and the azimuthal angle correlations between the 2 partons are analytically derived. The DGLAP evolution equation is derived from an appropriate treatment of the collinear singularity which universally exists in the QCD parton radiation from incoming partons. Then it is discussed how to generate radiation according to the probabilities predicted by the DGLAP equation, by using a Monte Carlo approach. After discussing the weak and strong points in jet simulation based on matrix elements and on the DGLAP equation, the merging algorithm which combines the two approaches is explained. The CKKW-L merging algorithm is chosen in this study and our practical implementation of the algorithm with the PYTHIA8 parton shower program is presented. After testing the implementation carefully, the algorithm is applied to the event generation of the top quark pair production the LHC. The generated event samples exhibit the strong azimuthal angle correlation between the two highest p_T jets with large rapidity separation, when the $t\bar{t}$ plus up to 2 or 3 partons matrix elements are merged under the appropriate conditions. Our results are compared to the result of a naive approach in which parton shower evolution is applied to the matrix elements of only the $t\bar{t}$ plus 2 partons process. We find a non-negligible difference in the distribution of the azimuthal angle correlation, which is induced by the strong Sudakov suppression of events with relatively low p_T jets. The impacts of merging the $t\bar{t}$ plus 3 partons matrix elements are studied in detail, and they are found to improve significantly the prediction of the azimuthal angle correlation.

Contents

1 Introduction

The objective of particle physics is to understand the most fundamental constituents of the world, namely elementary particles. One of promising approaches toward it is to accelerate two particles, collide them and study produced particles. Experimental equipments are often called accelerator or collider. In the past and currently, this approach has achieved great success in development of our current best understanding, the standard model of particle physics.

The Large Hadron Collider (LHC) at CERN is one of the colliders which we possess. There are four detectors along the LHC ring built and used by the ALICE, ATLAS, CMS and LHCb collaborations. The ATLAS and CMS experiments use general purpose detectors, where they collide two protons and are capable of probing the highest energy scale ever in history. In 2012, a huge success has been achieved by the ATLAS and CMS, the discovery of the Higgs boson. The Higgs boson had been the last missing particle in the particle content of the standard model, therefore its discovery has finally established the standard model.

Despite the large success of the standard model in accurate predictions for experimental measurements, the standard model possesses theoretical problems which makes it inappropriate as the most fundamental theory. The problems which I currently recognize include, it does not say anything about the gravity which is one of the four fundamental forces, and it does not provide a reasonable reason for the lightness of the Higgs boson mass, which is often called the hierarchy problem. These considerations have motivated further work on theories of physics beyond the standard model, such as supersymmetry and extra dimensions. New theories predict new particles and/or new interactions, which should be probed by comparing experimental measurements with the standard model prediction. Contradiction can be regarded as a signal of new theories. Probing new theories at the tera electron volt (TeV) scale is one of the primary aims of the LHC.

The LHC had operated with a total energy of 7 TeV and 8 TeV between 2010 and early 2013, before its temporary shutdown for maintenance and improvement. The operation was very successful, i.e. a large amount of collisions is delivered to the detectors. However, any signals of new theories have not been reported so far, despite expectations of them by many physicists.

It is announced that the next operation will start in 2015 with a total energy of 13 TeV, in which further searches for a signal of new theories will be performed with a higher energy and more collisions. They include precise measurements of the properties of the Higgs boson. The Higgs sector of the standard model respects the charge-conjugation and parity (CP) symmetry and the Higgs boson should be CP even. Therefore if an admixture of the CP odd component is observed, it will be a direct evidence of CP violation in the Higgs sector and thus a signal of new theories.

From the analyses on the tree level matrix elements, it has been shown that the azimuthal angle difference between two partons (gluon, quarks or antiquarks) produced in association

with the Higgs boson produced by gluon fusion is very sensitive to the CP property of the Higgs boson [1, 2, 3, 4]. Several analyses including effects of higher order corrections show that the correlation found at the tree level matrix elements can be observed as the azimuthal angle difference between the two hardest *jets* despite smearing, see e.g. refs. [5, 6, 7, 8, 9]. When trying to probe CP violation in the Higgs sector by measuring the azimuthal angle correlation, one of the difficulties is the smallness of CP violation which can be expected from the Higgs measurements at the LHC that have so far been supporting the standard model predictions [10, 11, 12, 13]. This requires very accurate calculations of the azimuthal angle correlation.

Recently it has been pointed out in ref. [14] that two partons produced in association with a top quark pair has a large azimuthal angle correlation near the threshold $m_{t\bar{t}} \sim 2m_t$ and it is similar to that of two partons produced together with the CP odd Higgs boson via gluon fusion. The claim of ref. [14] is that the technique to measure such an angular correlation between jets can be established first by using these standard model processes which have large cross sections. More precisely, we measure the azimuthal angle difference between two jets produced in association with a top quark pair and tune the Monte Carlo event generator to reproduce the data quantitatively. If an event generator tuned in this way is used, the theoretical uncertainty of the prediction of the azimuthal angle correlation between two jets produced in association with the Higgs boson can be reduced significantly, i.e. accurate calculations are achieved.

In this thesis the azimuthal angle correlation between the two jets in the top quark pair production at the LHC is studied. In Section 2, a detailed calculation of the vector boson fusion contribution to the process $pp \to X + 2$-parton, where X denotes a heavy object, is performed by using the helicity amplitude technique [15, 16, 17, 18]. By identifying X with the Higgs boson and the heavy quark pair, the azimuthal angle correlations are studied both analytically and numerically.

Section 3 reviews the Monte Carlo approach for jet simulation. At first, the collinear singularity which universally appears in the QCD parton radiation from incoming partons is derived, again by using the helicity amplitude technique. The evolution equation for the parton distribution functions, namely the DGLAP equation[19, 20, 21], is introduced by the appropriate treatment of the universal collinear singularity. Then, it is discussed how to carry out the generation of parton radiation numerically according to the probabilities given by the DGLAP equation. The weak and the strong points of this approach and those of the matrix element approach for jet simulation are made clear at the end.

In Section 4, an algorithm which combines the above two approaches for jet simulation is introduced. This is called the merging algorithm [22, 23, 24, 25, 26, 27, 28, 29, 30, 31, 32, 33, 34, 35]. At first, the basic idea of the merging algorithm, on which all the proposed merging algorithms are built, is explained by employing an approach in which the DGLAP equation derived in Section 3 is improved with the help of tree level matrix elements. Next, the CKKW-L merging algorithm [24, 27, 35], which is used in this study, is reviewed. It turns out that the construction of the PYTHIA8 parton shower history is necessary for the

implementation of the CKKW-L merging algorithm with PYTHIA8 [36, 37]. This procedure is presented in detail. The implementation of the algorithm is carefully tested, and the comparison of the predictions with experimental data is also presented.

In Section 5, the merging algorithm is applied to the event generation of the top quark pair production at the LHC and the azimuthal angle correlation between the two jets is studied. At first, the dependence of the simulation result on the parameters which exist in the merging algorithm is studied, namely the merging scale and the parton shower starting scale. An appropriate relation between the merging scale and the jet definition is investigated. The special emphasis is put on the impacts of merging the $t\bar{t}$ + 3-parton matrix elements.

Section 6 gives conclusions and outlook.

The work presented in this thesis is based on the following publication,

- K. Hagiwara and J. Nakamura, "Study on the azimuthal angle correlation between two jets in the top quark pair plus multi-jet process," arXiv:1501.00794 [hep-ph].

2 Azimuthal angle correlations

Azimuthal angle correlations between two partons produced in association with heavy objects are analytically derived in this section [1]. For our calculation, the helicity amplitude technique is introduced at first in Section 2.1. Then, the so-called vector boson fusion contribution to a process $pp \to X + 2$-parton is calculated without specifying the heavy object X in Section 2.2. Finally in Section 2.3 the heavy object X is specified with a Higgs boson or a heavy quark pair, and the azimuthal angle correlations are studied both analytically and numerically

2.1 Helicity amplitude formalism

The helicity amplitude formalism, which is used in the following sections, is described in this section. The explicit forms of free fermion wave functions and those of vector boson wave functions in the helicity basis are derived by solving the equation of motion for these fields. My phase conventions completely follow the conventions [15, 16] adopted by the HELAS subroutines [17, 18].

We start from the Dirac equation

$$(i\gamma^\mu\partial_\mu - m)\psi(x) = 0, \tag{2.1}$$

which is the equation of motion for a free and spin one half fermion field $\psi(x)$. When the matrices γ^μ satisfies the anticommutation relations

$$\{\gamma^\mu, \gamma^\nu\} = 2g^{\mu\nu}, \tag{2.2}$$

it is confirmed that the Dirac equation implies the Klein-Gordon equation

$$\begin{aligned} 0 &= \big(-i\gamma^\mu\partial_\mu - m\big)\big(i\gamma^\mu\partial_\mu - m\big)\psi(x) \\ &= \big(\gamma^\mu\gamma^\nu\partial^\mu\partial^\nu + m^2\big)\psi(x) \\ &= \Big(\frac{\gamma^\mu\gamma^\nu + \gamma^\nu\gamma^\mu}{2}\partial^\mu\partial^\nu + m^2\Big)\psi(x) \\ &= \big(\partial^2 + m^2\big)\psi(x). \end{aligned} \tag{2.3}$$

This is not surprising, since the Dirac field $\psi(x)$ merely consists of four complex scalar fields. As a representation of the matrices γ^μ, we choose the chiral representation

$$\gamma^\mu = \begin{pmatrix} 0 & \sigma_+^\mu \\ \sigma_-^\mu & 0 \end{pmatrix}, \quad \sigma_\pm^\mu = \big(1, \pm\sigma^i\big). \tag{2.4}$$

It can be easily confirmed that this representation satisfies the relations in eq. (2.2) as follows.

$$\gamma^\mu\gamma^\nu + \gamma^\nu\gamma^\mu = \begin{pmatrix} \sigma_+^\mu\sigma_-^\nu + \sigma_+^\nu\sigma_-^\mu & 0 \\ 0 & \sigma_-^\mu\sigma_+^\nu + \sigma_-^\nu\sigma_+^\mu. \end{pmatrix} \tag{2.5}$$

[1] We distinguish jets from partons. Jets are obtained only after a jet clustering algorithm is applied.

For $\mu = \nu = 0$,

$$\gamma^0\gamma^0 + \gamma^0\gamma^0 = 2\begin{pmatrix} 1 & 0 \\ 0 & 1 \end{pmatrix}, \tag{2.6a}$$

for $\mu = 0$ and $\nu = i$

$$\gamma^0\gamma^i + \gamma^i\gamma^0 = \begin{pmatrix} -\sigma^i + \sigma^i & 0 \\ 0 & \sigma^i - \sigma^i \end{pmatrix} = \begin{pmatrix} 0 & 0 \\ 0 & 0 \end{pmatrix}, \tag{2.6b}$$

and for $\mu = i$ and $\nu = j$

$$\gamma^i\gamma^j + \gamma^j\gamma^i = \begin{pmatrix} -\sigma^i\sigma^j - \sigma^j\sigma^i & 0 \\ 0 & -\sigma^i\sigma^j - \sigma^j\sigma^i \end{pmatrix} = \begin{pmatrix} -2\delta^{ij} & 0 \\ 0 & -2\delta^{ij} \end{pmatrix} = -2\delta^{ij}\begin{pmatrix} 1 & 0 \\ 0 & 1 \end{pmatrix}. \tag{2.6c}$$

We divide the four-component field $\psi(x)$ into two objects by introducing an additional matrix

$$\gamma^5 \equiv i\gamma^0\gamma^1\gamma^2\gamma^3, \tag{2.7}$$

which has the following properties

$$\begin{aligned} \left(\gamma^5\right)^\dagger &= \gamma^5, \\ \left(\gamma^5\right)^2 &= 1, \\ \left\{\gamma^5, \gamma^\mu\right\} &= 0. \end{aligned} \tag{2.8}$$

This matrix has the relation

$$\left[\gamma^5, S^{\mu\nu}\right] = 0 \tag{2.9}$$

with the Lorentz transformation generator for $\psi(x)$

$$S^{\mu\nu} = \frac{i}{4}\left[\gamma^\mu, \gamma^\nu\right]. \tag{2.10}$$

The relation in eq. (2.9) indicates that the eigenvectors of the operator γ^5 with different eigenvalues will never be mixed with the other eigenvectors under Lorentz transformation. In our chiral representation

$$\gamma^5 = \begin{pmatrix} -1 & 0 \\ 0 & 1 \end{pmatrix}, \tag{2.11}$$

therefore applying the operator γ^5 on the four-component field $\psi(x)$, we find

$$\gamma^5\psi = \gamma^5\begin{pmatrix} \psi_- \\ \psi_+ \end{pmatrix} = \begin{pmatrix} -1 & 0 \\ 0 & 1 \end{pmatrix}\begin{pmatrix} \psi_- \\ \psi_+ \end{pmatrix} = \begin{pmatrix} -\psi_- \\ \psi_+ \end{pmatrix}. \tag{2.12}$$

The upper two-component labeled by ψ_- is the eigenvector of γ^5 with eigenvalue -1 and the lower two-component labeled by ψ_+ is the eigenvector of γ^5 with eigenvalue $+1$. Since these two fields $\psi_\pm$ will not mix with the other under Lorentz transformation as I mentioned below eq. (2.10), it is always meaningful to write

$$\psi = \begin{pmatrix} \psi_- \\ \psi_+ \end{pmatrix}. \tag{2.13}$$

This is the largest advantage in the chiral representation. This property can, of course, be shown explicitly by confirming that the generator $S^{\mu\nu}$ is written in a diagonal form in our representation,

$$\begin{aligned} S^{\mu\nu} &= \frac{i}{4}\left[\gamma^\mu, \gamma^\nu\right] \\ &= \frac{i}{4}\begin{pmatrix} \sigma_+^\mu\sigma_-^\nu - \sigma_+^\nu\sigma_-^\mu & 0 \\ 0 & \sigma_-^\mu\sigma_+^\nu - \sigma_-^\nu\sigma_+^\mu \end{pmatrix}. \end{aligned} \tag{2.14}$$

For $\mu = i$ and $\nu = j$,

$$S^{ij} = \frac{1}{2}\epsilon^{ijk}\begin{pmatrix} \sigma^k & 0 \\ 0 & \sigma^k \end{pmatrix} \tag{2.15}$$

which is the generator for rotation around the k-axis. For $\mu = 0$ and $\nu = i$,

$$S^{0i} = \frac{i}{2}\begin{pmatrix} -\sigma^i & 0 \\ 0 & \sigma^i \end{pmatrix} \tag{2.16}$$

which is the generator for boost along the i-axis. The eigenvalues of γ^5 are often called chirality, ψ_- has chirality -1 and ψ_+ has chirality $+1$.

Let us introduce the helicity operator,

$$\frac{\vec{p}\cdot\vec{\sigma}}{|\vec{p}|}\chi_\lambda(p) = \lambda\chi_\lambda(p). \tag{2.17}$$

The eigenvectors χ_λ whose eigenvalue is λ are used as the two base vectors to measure a spin state of a fermion with momentum p. The eigenvalues λ take two values ± 1 and are called helicity. If we parametrize momentum $\vec{p}$ as $\vec{p} = |\vec{p}|(\sin\theta\cos\phi, \sin\theta\sin\phi, \cos\theta)$, the operator is

$$\frac{\vec{p}\cdot\vec{\sigma}}{|\vec{p}|} = \begin{pmatrix} \cos\theta & \sin\theta e^{-i\phi} \\ \sin\theta e^{i\phi} & -\cos\theta \end{pmatrix}. \tag{2.18}$$

The eigenvectors χ_λ can be obtained easily by using eqs. (2.17) and (2.18). However they are not uniquely determined, since overall phase is not physical. In the HELAS convention, the eigenvector $\chi_+(p)$ with helicity $+1$ is chosen as

$$\chi_+(p) = \begin{pmatrix} \cos\frac{\theta}{2} \\ \sin\frac{\theta}{2}e^{i\phi} \end{pmatrix}. \tag{2.19}$$

It is normalized as $\chi_+^\dagger \chi_+ = 1$. Another eigenvector $\chi_-(p)$ with helicity -1 can be obtained from $\chi_+(p)$ with replacements $\theta \to \pi - \theta$ and $\phi \to \phi + \pi$, since the following is true,

$$\frac{-\vec{p}\cdot\vec{\sigma}}{|\vec{p}|}\chi_-(p) = \chi_-(p). \tag{2.20}$$

$$\begin{aligned}\chi_-(p) &= \begin{pmatrix} \sin\frac{\theta}{2} \\ -\cos\frac{\theta}{2}e^{i\phi} \end{pmatrix} \\ &= -e^{i\phi}\begin{pmatrix} -\sin\frac{\theta}{2}e^{-i\phi} \\ \cos\frac{\theta}{2} \end{pmatrix}.\end{aligned} \tag{2.21}$$

In the HELAS convention, it is adopted that

$$\chi_-(p) = \begin{pmatrix} -\sin\frac{\theta}{2}e^{-i\phi} \\ \cos\frac{\theta}{2} \end{pmatrix}. \tag{2.22}$$

With the HELAS choices in eqs. (2.19) and (2.22), the following relation holds,

$$\chi_{-\lambda} = -\lambda i\sigma^2\chi_\lambda^*. \tag{2.23}$$

This can be useful when helicity flipping is considered.

Now that we have the two-component chiral notation in eq. (2.13) and the two helicity eigenvectors in eqs. (2.19) and (2.22), we find a solution of the Dirac equation, namely the fermion four-component spinor u and the antifermion four-component spinor v in terms of chirality and helicity. The Dirac equation for the fermion spinor u in momentum space is given by

$$\big(\gamma\cdot p - m\big)u(p,\lambda) = 0. \tag{2.24}$$

This is written in our chiral representation as

$$\begin{pmatrix} -m & p\cdot\sigma_+ \\ p\cdot\sigma_- & -m \end{pmatrix}\begin{pmatrix} u(p,\lambda)_- \\ u(p,\lambda)_+ \end{pmatrix} = 0. \tag{2.25}$$

Once we put

$$u(p,\lambda)_\alpha = w(\alpha,\lambda,p)\chi_\lambda(p), \tag{2.26}$$

eq. (2.25) gives

$$\begin{pmatrix} -m & E-\vec{p}\cdot\vec{\sigma} \\ E+\vec{p}\cdot\vec{\sigma} & -m \end{pmatrix}\begin{pmatrix} w(-,\lambda,p)\chi_\lambda(p) \\ w(+,\lambda,p)\chi_\lambda(p) \end{pmatrix} = 0. \tag{2.27}$$

By using the definition of χ_λ in eq. (2.17), we find

$$\begin{pmatrix} -m & E-|\vec{p}|\lambda \\ E+|\vec{p}|\lambda & -m \end{pmatrix} \begin{pmatrix} w(-,\lambda,p)\chi_\lambda(p) \\ w(+,\lambda,p)\chi_\lambda(p) \end{pmatrix} = 0. \tag{2.28}$$

One possible solution to this equation is

$$w(\alpha,\lambda,p) = \sqrt{E+\alpha\lambda|\vec{p}|}. \tag{2.29}$$

The two-component u spinor is, therefore,

$$u(p,\lambda)_\alpha = \sqrt{E+\alpha\lambda|\vec{p}|}\ \chi_\lambda(p). \tag{2.30}$$

In the high energy limit where light fermion masses can be neglected, it reduces to

$$u(p,\lambda)_\alpha = \sqrt{2E}\ \chi_\lambda(p)\delta_{\lambda\alpha}. \tag{2.31}$$

The antifermion spinor v is calculated by using a relation

$$v(p,\lambda) = -ia\gamma^2 u(p,\lambda)^*. \tag{2.32}$$

This can be obtained from the charge-conjugation of the quantized fermion field ψ, namely $\psi^c = C\bar{\psi}^T$ which annihilate an antifermion and create a fermion. C is the charge-conjugation unitary operator and is defined by

$$C(\gamma^\mu)^T C^\dagger = -\gamma^\mu, \tag{2.33}$$

therefore it is found that

$$C = ia\gamma^0\gamma^2, \quad |a|^2 = 1. \tag{2.34}$$

Here we choose $a=-1$. Then we obtain

$$\begin{aligned} v(p,\lambda)_\alpha &= \alpha\sqrt{E-\alpha\lambda|\vec{p}|}\ \left(-i\sigma_2\chi_\lambda(p)^*\right) \\ &= \alpha\lambda\sqrt{E-\alpha\lambda|\vec{p}|}\ \chi_{-\lambda}(p), \end{aligned} \tag{2.35}$$

where at the last equality, eq. (2.23) is used.

Next, we find vector boson wave functions. We start from the equation of motion for a massive vector boson field $A^\mu(x)$, namely

$$\left(\partial^2+m^2\right)A^\mu(x) = 0, \quad \partial^\mu A_\mu(x) = 0. \tag{2.36}$$

These equations constrain the wave function vectors $\epsilon^\mu(p,s)$ as

$$p\cdot\epsilon(p,s) = 0. \tag{2.37}$$

Let us first assume a massive vector boson in its rest frame $p^\mu = (m, 0, 0, 0)$. The following three vectors can be chosen for $\epsilon^\mu(p, s)$,

$$\epsilon^\mu(p, 1) = (0, 1, 0, 0), \tag{2.38a}$$
$$\epsilon^\mu(p, 2) = (0, 0, 1, 0), \tag{2.38b}$$
$$\epsilon^\mu(p, 3) = (0, 0, 0, 1), \tag{2.38c}$$

which trivially satisfies eq. (2.37). By boosting the particle along the z-axis, $\epsilon^\mu(p, 3)$ becomes

$$\epsilon^\mu(p, 3) = \frac{1}{m}\big(|\vec{p}|, 0, 0, E\big) \tag{2.39}$$

for $p^\mu = (E, 0, 0, |\vec{p}|)$, while $\epsilon^\mu(p, 1)$ and $\epsilon^\mu(p, 2)$ remain the same. The helicity operator for vector bosons is given by

$$\frac{\vec{p}\cdot\vec{J}}{|\vec{p}|}\epsilon^\mu(p, \lambda) = \lambda\epsilon^\mu(p, \lambda), \tag{2.40}$$

where $\vec{J}$ are generators for rotation. For the momentum $p^\mu = (E, 0, 0, |\vec{p}|)$, the operator is written as

$$\frac{\vec{p}\cdot\vec{J}}{|\vec{p}|} = J^3 = i\begin{pmatrix} 0 & 0 & 0 & 0 \\ 0 & 0 & -1 & 0 \\ 0 & 1 & 0 & 0 \\ 0 & 0 & 0 & 0 \end{pmatrix}. \tag{2.41}$$

Since $\epsilon^\mu(p, 3)$ in eq. (2.39) is a solution with $\lambda = 0$ of eq. 2.40, this vector can be chosen as the eigenvector with helicity $\lambda = 0$,

$$\begin{aligned}\epsilon^\mu(p, \lambda = 0) &= \epsilon^\mu(p, 3) \\ &= \frac{1}{m}\big(|\vec{p}|, 0, 0, E\big).\end{aligned} \tag{2.42}$$

The eigenvectors with helicity $\lambda = +1, -1$ for the momentum $p^\mu = (E, 0, 0, |\vec{p}|)$ are easily obtained and they are

$$\epsilon^\mu(p, \lambda = +1) = \frac{a}{\sqrt{2}}\big(0, 1, +i, 0\big), \quad |a|^2 = 1, \tag{2.43a}$$
$$\epsilon^\mu(p, \lambda = -1) = \frac{b}{\sqrt{2}}\big(0, 1, -i, 0\big), \quad |b|^2 = 1. \tag{2.43b}$$

According to the HELAS convention, we choose $a = -1$ and $b = +1$,

$$\epsilon^\mu(p, \lambda) = \frac{1}{\sqrt{2}}\big(0, -\lambda, -i, 0\big). \tag{2.44}$$

The vectors can be expressed in terms of $\epsilon^\mu(p, 1)$ and $\epsilon^\mu(p, 2)$,

$$\epsilon^\mu(p, \lambda) = -\lambda\epsilon^\mu(p, 1) - i\epsilon^\mu(p, 2). \tag{2.45}$$

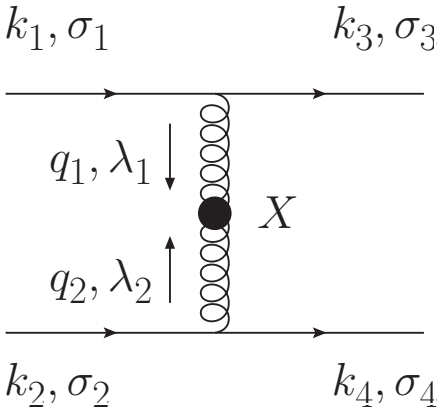

Figure 1: The Feynman diagram representing one of the vector boson fusion contributions to $pp \to X + 2$-parton process.

For a general momentum parametrized as $p^\mu = \big(E, |\vec{p}| \sin\theta\cos\phi, |\vec{p}| \sin\theta \sin\phi, |\vec{p}| \cos\theta\big)$, the wave function vectors in the rectangular basis given in eq. (2.38) are

$$\epsilon^\mu(p,1) = \big(0, \cos\theta\cos\phi, \cos\theta\sin\phi, -\sin\theta\big), \tag{2.46a}$$
$$\epsilon^\mu(p,2) = \big(0, -\sin\phi, \cos\phi, 0\big), \tag{2.46b}$$
$$\epsilon^\mu(p,3) = \frac{E}{m|\vec{p}|}\big(|\vec{p}|^2/E, \vec{p}\big). \tag{2.46c}$$

The helicity eigenvectors for this momentum are easily obtained from the above vectors in eq. (2.46) by using the relations in eqs. (2.42) and (2.45).

Up to now we have evaluated the wave function vectors for massive vector bosons. For massless vector bosons such as gluons, we use the same vectors, although only $\epsilon^\mu(p,1)$ and $\epsilon^\mu(p,2)$ or $\epsilon^\mu(p,\lambda=+1)$ and $\epsilon^\mu(p,\lambda=-1)$ are physical.

2.2 VBF amplitudes

The vector boson fusion contribution to a process $pp \to X + 2$-parton, where X denotes some heavy object, is calculated in this section. The statement of the vector boson fusion contribution means that we do not calculate the full amplitudes for this process but calculate the contribution only from a Feynman diagram shown in Figure 1. The object X is produced from a collision of the two gluons emitted from the two incoming light quarks. Note that the quarks cane be replaced with antiquarks or gluons. This process is often called the vector boson fusion (VBF) process [2]. The VBF contribution can be enhanced when the outgoing

[2]When the colliding partons are weak bosons, it is often called the weak boson fusion process.

quarks are collinear to their mother quark, due to the propagator factor of the gluons, since

$$\begin{aligned}(q_1)^2 &= (k_1 - k_3)^2 \\ &= -2k_1 \cdot k_3 \\ &= -2E_1E_3(1-\cos\theta_{13}) \\ &= -E_1E_3\theta_{13}^2 + O(\theta_{13}^4).\end{aligned} \tag{2.47}$$

It has been numerically confirmed in refs. [4, 14] that the VBF contribution dominates all the other contributions when kinematic cuts are appropriately applied on the two outgoing partons, namely a large rapidity separation between the outgoing partons [3]. The calculation in this section follows refs. [4, 14]. We do not specify the heavy object X yet, therefore our results are given with the amplitudes $\mathcal{M}(gg \to X)_{\lambda_1\lambda_2}$ where λ_1 and λ_2 are helicities of the colliding gluons.

The VBF subprocesses contributing to the inclusive $pp \to X$ + 2-parton process are summarized as follows

$$qq \to qqg^*g^* \to qqX, \tag{2.48a}$$
$$qg \to qgg^*g^* \to qgX, \tag{2.48b}$$
$$gg \to ggg^*g^* \to ggX, \tag{2.48c}$$

where g^* is a t-channel intermediate off-shell gluon and q stands for a quark or an antiquark of any light flavor. We calculate only the subprocess in eq. (2.48a) which is shown in Figure 1, since it turns out that this is enough to understand the physical origin of angular correlations between the two outgoing partons. To begin with, we define the kinematic variables for the VBF subprocess as

$$\begin{aligned}q_1(k_1,\sigma_1) + q_2(k_2,\sigma_2) &\to q_3(k_3,\sigma_3) + q_4(k_4,\sigma_4) + g_1^*(q_1,\lambda_1) + g_2^*(q_2,\lambda_2) \\ &\to q_3(k_3,\sigma_3) + q_4(k_4,\sigma_4) + X(p,\lambda)\end{aligned} \tag{2.49}$$

where $q_{1,2,3,4}$ stand for light quarks, $g_{1,2}^*$ are t-channel intermediate off-shell gluons and their momentum and helicity are shown in their parenthesis. These are specified in Figure 1 too. The helicity amplitude is written as

$$M^{\lambda}_{\sigma_1\sigma_3,\sigma_2\sigma_4} = J^{\mu_1}(k_1,k_3;\sigma_1,\sigma_3)J^{\mu_2}(k_2,k_4;\sigma_2,\sigma_4)D_{\mu_1\mu_1'}(q_1)D_{\mu_2\mu_2'}(q_2)\Gamma^{\mu_1'\mu_2'}(q_1,q_2;\lambda). \tag{2.50}$$

The external quark currents are denoted by $J^{\mu_i}(k_i,k_{i+2};\sigma_i,\sigma_{i+2})$, and $D_{\mu_i\mu_i'}(q_i)$ denotes a gluon propagator. The X production via gluon fusion is represented by $\Gamma^{\mu_1'\mu_2'}(q_1,q_2;\lambda)$. The gluon propagator has the following feature when the gluon is on-shell $q^2 \to 0$,

$$D_{\mu\mu'}(q) = \frac{1}{q^2}\big(-g_{\mu\mu'} + \cdots\big) \tag{2.51a}$$
$$\to \frac{1}{q^2}\sum_{\lambda=+1,-1}\epsilon_\mu^*(q,\lambda)\epsilon_{\mu'}(q,\lambda), \tag{2.51b}$$

[3] Parton denotes a gluon, a light quark or a light antiquark.

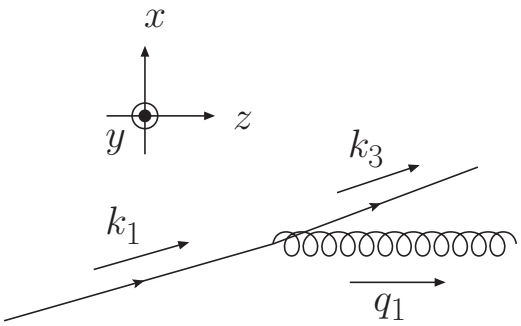

Figure 2: A frame for calculating the helicity amplitudes $(\mathcal{J}^{g_1}_{q_1q_3})^{\lambda_1}_{\sigma_1\sigma_3}$.

which is required from the optical theorem. The dotted part in eq. (2.51a) depends on a gauge fixing term which is needed for quantization of the gluon field. This is not an issue here, since we use the form in eq. (2.51b) as the on-shell gluon approximation. By using the on-shell gluon approximation, the amplitude in eq. (2.50) is approximated by

$$\begin{aligned}\mathcal{M}^{\lambda}_{\sigma_1\sigma_3,\sigma_2\sigma_4} &\simeq \frac{1}{q_1^2q_2^2}\sum_{\lambda_1=\pm1}\sum_{\lambda_2=\pm1}(\mathcal{J}^{g_1}_{q_1q_3})^{\lambda_1}_{\sigma_1\sigma_3}(\mathcal{J}^{g_2}_{q_2q_4})^{\lambda_2}_{\sigma_2\sigma_4}\epsilon_{\mu_1'}(q_1,\lambda_1)\epsilon_{\mu_2'}(q_2,\lambda_2)\Gamma^{\mu_1'\mu_2'}(q_1,q_2;\lambda)\\ &= \frac{1}{q_1^2q_2^2}\sum_{\lambda_1=\pm1}\sum_{\lambda_2=\pm1}(\mathcal{J}^{g_1}_{q_1q_3})^{\lambda_1}_{\sigma_1\sigma_3}(\mathcal{J}^{g_2}_{q_2q_4})^{\lambda_2}_{\sigma_2\sigma_4}(\hat{\mathcal{M}}^{X}_{g_1g_2})^{\lambda}_{\lambda_1\lambda_2},\end{aligned} \tag{2.52a}$$

where at the first equality, the incoming current amplitudes are written as

$$(\mathcal{J}^{g_i}_{q_iq_{i+2}})^{\lambda_i}_{\sigma_i\sigma_{i+2}} = J^{\mu_i}(k_i,k_{i+2};\sigma_i,\sigma_{i+2})\epsilon^*_{\mu_i}(q_i,\lambda_i), \tag{2.53}$$

and at the second equality, the X production amplitude via gluon fusion is written as

$$(\hat{\mathcal{M}}^{X}_{g_1g_2})^{\lambda}_{\lambda_1\lambda_2} = \epsilon_{\mu_1'}(q_1,\lambda_1)\epsilon_{\mu_2'}(q_2,\lambda_2)\Gamma^{\mu_1'\mu_2'}(q_1,q_2;\lambda). \tag{2.54}$$

The helicity amplitudes $(\mathcal{J}^{g_1}_{q_1q_3})^{\lambda_1}_{\sigma_1\sigma_3}$ and $(\mathcal{J}^{g_2}_{q_2q_4})^{\lambda_2}_{\sigma_2\sigma_4}$ in eq. (2.53) are calculated in the following. We take a simple frame described in Figure 2 for calculating $(\mathcal{J}^{g_1}_{q_1q_3})^{\lambda_1}_{\sigma_1\sigma_3}$. The momenta are parametrized as

$$k_1^\mu = E_1\big(1,\ \sin\theta_1\cos\phi_1,\ \sin\theta_1\sin\phi_1,\ \cos\theta_1\big), \tag{2.55a}$$
$$k_3^\mu = E_3\big(1,\ \sin\theta_3\cos\phi_1,\ \sin\theta_3\sin\phi_1,\ \cos\theta_3\big), \tag{2.55b}$$
$$q_1^\mu = \Big(q_1^0,\ 0,\ 0,\ \sqrt{(q_1^0)^2+Q_1^2}\Big), \tag{2.55c}$$

where $0<\theta_1,\theta_3<\pi/2$, $0<\phi_1<2\pi$ and $Q_1^2=-(q_1)^2>0$ is the virtuality of the gluon. Note that in ref. [4], a more sophisticated frame called the Breit frame is employed. In the collinear limit $\theta_1\to0$ and $\theta_3\to0$, the momenta are approximated by

$$k_1^\mu \sim E_1\big(1,\ \theta_1\cos\phi_1,\ \theta_1\sin\phi_1,\ 1\big), \tag{2.56a}$$
$$k_3^\mu \sim E_3\big(1,\ \theta_3\cos\phi_1,\ \theta_3\sin\phi_1,\ 1\big), \tag{2.56b}$$

and the gluon virtuality Q_1^2 goes to zero as given in eq. (2.47). The explicit form of the quark current amplitude $(\mathcal{J}^{g_1}_{q_1q_3})^{\lambda_1}_{\sigma_1\sigma_3}$ is given by

$$(\mathcal{J}^{g_1}_{q_1q_3})^{\lambda_1}_{\sigma_1\sigma_3} = -ig(t^{a_1})_{i_3i_1}\bar{u}(k_3,\sigma_3,i_3)\gamma^\mu u(k_1,\sigma_1,i_1)\epsilon^*_\mu(q_1,\lambda_1,a_1), \tag{2.57}$$

where i_1, i_3 and a_1 denote the color indices, g is the gauge coupling constant and t^a are the generators of the SU(3) gauge group. A treatment of the coupling and color factors is trivial. If we make the amplitude squared and sum over color indices, we find an overall factor

$$\begin{aligned}\sum_{i_1,i_3,a_1}\left|(\mathcal{J}^{g_1}_{q_1q_3})^{\lambda_1}_{\sigma_1\sigma_3}\right|^2 &= \sum_{i_1,i_3,a_1} g^2(t^{a_1})_{i_1i_3}(t^{a_1})_{i_3i_1} \\ &= \sum_{a_1} g^2\mathrm{tr}\left[t^{a_1}t^{a_1}\right] \\ &= 3g^2C_F.\end{aligned} \tag{2.58}$$

We completely forget the coupling and color factors in the following. Now the quark current amplitude is

$$(\mathcal{J}^{g_1}_{q_1q_3})^{\lambda_1}_{\sigma_1\sigma_3} = \bar{u}(k_3,\sigma_3)\gamma^\mu u(k_1,\sigma_1)\epsilon^*_\mu(q_1,\lambda_1). \tag{2.59}$$

It is easily confirmed that the antiquark current amplitude is identical to the quark current amplitude as follows.

$$\begin{aligned}\bar{v}(k_1,\sigma_1)\gamma^\mu v(k_3,\sigma_3) &= \left(i\gamma^2u(k_1,\sigma_1)^*\right)^\dagger\gamma^0\gamma^\mu\left(i\gamma^2u(k_3,\sigma_3)^*\right) \\ &= u(k_1,\sigma_1)^T\gamma^0\gamma^2\gamma^\mu\gamma^2u(k_3,\sigma_3)^* \\ &= u(k_1,\sigma_1)^T\gamma^0(\gamma^\mu)^*u(k_3,\sigma_3)^* \\ &= u(k_3,\sigma_3)^\dagger(\gamma^\mu)^\dagger\gamma^0u(k_1,\sigma_1) \\ &= \bar{u}(k_3,\sigma_3)\gamma^\mu u(k_1,\sigma_1),\end{aligned} \tag{2.60}$$

where at the first equality eq. (2.32) is used, at the third equality a property $\gamma^2\gamma^\mu\gamma^2 = (\gamma^\mu)^*$ is used, at the fourth equality a transpose is performed and at the last equality a property $\gamma^0(\gamma^\mu)^\dagger\gamma^0 = \gamma^\mu$ is used. In the chiral representation eq. (2.4), the quark current amplitude is expanded as

$$(\mathcal{J}^{g_1}_{q_1q_3})^{\lambda_1}_{\sigma_1\sigma_3} = \bar{u}(k_3,\sigma_3)_+\sigma^\mu_+u(k_1,\sigma_1)_+\epsilon^*_\mu(q_1,\lambda_1) + \bar{u}(k_3,\sigma_3)_-\sigma^\mu_-u(k_1,\sigma_1)_-\epsilon^*_\mu(q_1,\lambda_1). \tag{2.61}$$

Here one of the features in the quark current amplitude can be emphasized. The helicity of the incoming quark and that of the outgoing quark must be the same i.e. $\sigma_1 = \sigma_3$, since helicity is identical to chirality in the high energy limit where light quark masses can be neglected, see eq. (2.31). Therefore, by defining $\sigma = \sigma_1 = \sigma_3$, eq. (2.61) reduces to

$$(\mathcal{J}^{g_1}_{q_1q_3})^{\lambda_1}_{\sigma\sigma} = \sqrt{2E_1}\sqrt{2E_3}\ \chi^\dagger_\sigma(k_3)\sigma^\mu_\sigma\chi_\sigma(k_1)\epsilon^*_\mu(q_1,\lambda_1). \tag{2.62}$$

Below I calculate only the amplitude with $\sigma = +1$ explicitly, and later the amplitude with $\sigma = -1$ is easily derived by using a trick. The helicity eigenvectors necessary for this purpose are given in eqs. (2.19), (2.45) and (2.46). For the approximated momenta in eq. (2.56),

$$\chi_+(k_1) = \begin{pmatrix} 1 \\ \theta_1/2\ e^{i\phi_1} \end{pmatrix}, \quad \chi_+(k_3) = \begin{pmatrix} 1 \\ \theta_3/2\ e^{i\phi_1} \end{pmatrix} \tag{2.63a}$$

$$\epsilon^\mu(q_1,+) = \frac{1}{\sqrt{2}}\big(0,-1,-i,0\big), \quad \epsilon^\mu(q_1,-) = \frac{1}{\sqrt{2}}\big(0,1,-i,0\big). \tag{2.63b}$$

Plugging eq. 2.63a into eq. 2.62 at first, we find

$$(\mathcal{J}^{g_1}_{q_1q_3})^{\lambda_1}_{++} = \sqrt{2E_1}\sqrt{2E_3}\bigg[1,\ \frac{\theta_1}{2}e^{i\phi_1} + \frac{\theta_3}{2}e^{-i\phi_1},\ -i\frac{\theta_1}{2}e^{i\phi_1} + i\frac{\theta_3}{2}e^{-i\phi_1},\ 1\bigg]^\mu \epsilon^*_\mu(q_1,\lambda_1). \tag{2.64}$$

Then, plugging eq. 2.63b into the above equation, we find

$$(\mathcal{J}^{g_1}_{q_1q_3})^{+}_{++} = +\sqrt{2E_1}\sqrt{2E_3}\frac{\theta_3}{\sqrt{2}}e^{-i\phi_1}, \tag{2.65a}$$

$$(\mathcal{J}^{g_1}_{q_1q_3})^{-}_{++} = -\sqrt{2E_1}\sqrt{2E_3}\frac{\theta_1}{\sqrt{2}}e^{+i\phi_1}. \tag{2.65b}$$

Let us introduce an energy fraction variable z_1 and an polar angle difference θ,

$$z_1 = \frac{q_1^0}{E_1}, \tag{2.66a}$$

$$\theta = \theta_3 - \theta_1. \tag{2.66b}$$

From a transverse momentum conservation $E_1\theta_1 = E_3\theta_3$, it is easy to write $\theta_{1,3}$ in terms of z_1 and θ,

$$\theta_1 = \frac{1-z_1}{z_1}\theta, \quad \theta_3 = \frac{1}{z_1}\theta. \tag{2.67}$$

Furthermore, eq. (2.47) is now written as

$$Q_1 = \sqrt{1-z_1}E_1\theta. \tag{2.68}$$

By using eqs. (2.67) and (2.68), eq. (2.65) becomes

$$(\mathcal{J}^{g_1}_{q_1q_3})^{+}_{++} = +\sqrt{2}Q_1\frac{1}{z_1}e^{-i\phi_1}, \tag{2.69a}$$

$$(\mathcal{J}^{g_1}_{q_1q_3})^{-}_{++} = -\sqrt{2}Q_1\frac{1-z_1}{z_1}e^{+i\phi_1}. \tag{2.69b}$$

The amplitudes in eq. 2.62 with $\sigma = -1$, namely $(\mathcal{J}^{g_1}_{q_1q_3})^{-}_{--}$ and $(\mathcal{J}^{g_1}_{q_1q_3})^{+}_{--}$ are calculated in the following. From eq. (2.45), we find a relation

$$\epsilon^{\mu}(p,-\lambda) = -\epsilon^{\mu *}(p,\lambda). \tag{2.70}$$

When all the helicities in eq. (2.62) are flipped, the amplitudes are

$$\begin{aligned}
(\mathcal{J}^{g_1}_{q_1q_3})^{-\lambda_1}_{-\sigma-\sigma} &= \sqrt{2E_1}\sqrt{2E_3}\ \chi^{\dagger}_{-\sigma}(k_3)\sigma^{\mu}_{-\sigma}\chi_{-\sigma}(k_1)\epsilon^{*}_{\mu}(q_1,-\lambda_1). \\
&= -\sqrt{2E_1}\sqrt{2E_3}\ \big(-\sigma i\sigma_2\chi^{*}_{\sigma}(k_3)\big)^{\dagger}\sigma^{\mu}_{-\sigma}\big(-\sigma i\sigma_2\chi^{*}_{\sigma}(k_1)\big)\epsilon_{\mu}(q_1,\lambda_1) \\
&= -\sqrt{2E_1}\sqrt{2E_3}\ \chi^{T}_{\sigma}(k_3)\sigma_2\sigma^{\mu}_{-\sigma}\sigma_2\chi^{*}_{\sigma}(k_1)\epsilon_{\mu}(q_1,\lambda_1) \\
&= -\sqrt{2E_1}\sqrt{2E_3}\ \chi^{T}_{\sigma}(k_3)\big(\sigma^{\mu}_{\sigma}\big)^{*}\chi^{*}_{\sigma}(k_1)\epsilon_{\mu}(q_1,\lambda_1) \\
&= -\sqrt{2E_1}\sqrt{2E_3}\ \Big(\chi^{\dagger}_{\sigma}(k_3)\sigma^{\mu}_{\sigma}\chi_{\sigma}(k_1)\epsilon^{*}_{\mu}(q_1,\lambda_1)\Big)^{*} \\
&= -\big((\mathcal{J}^{g_1}_{q_1q_3})^{\lambda_1}_{\sigma\sigma}\big)^{*},
\end{aligned} \tag{2.71}$$

where at the second equality eqs. (2.23) and (2.70) are used, and at the fourth equality a property $\sigma_2\sigma^{\mu}_{-\sigma}\sigma_2 = \big(\sigma^{\mu}_{\sigma}\big)^{*}$ is used. Applying this relation to eq. (2.69), we obtain

$$(\mathcal{J}^{g_1}_{q_1q_3})^{-}_{--} = -\sqrt{2}Q_1\frac{1}{z_1}e^{+i\phi_1}, \tag{2.72a}$$

$$(\mathcal{J}^{g_1}_{q_1q_3})^{+}_{--} = +\sqrt{2}Q_1\frac{1-z_1}{z_1}e^{-i\phi_1}. \tag{2.72b}$$

Note that the useful relation in eq. (2.71) is correct only in our phase convention i.e. the HELAS convention. This is obvious, since eqs. (2.23) and (2.70) used in its derivation are guaranteed only in our phase convention. The quark current amplitudes $(\mathcal{J}^{g_1}_{q_1q_3})^{\lambda_1}_{\sigma_1\sigma_3}$ are now completed.

The amplitudes for the quark current on the other side $(\mathcal{J}^{g_2}_{q_2q_4})^{\lambda_2}_{\sigma_2\sigma_4}$ can be calculated in the similar manner, thus we give only the results below. The frame for evaluation is obtained with replacements $\theta \to \pi - \theta$ and $\phi \to \phi + \pi$ in the kinematics in eq. 2.55,

$$k_2^{\mu} = E_2\big(1,\ -\sin\theta_2\cos\phi_2,\ -\sin\theta_2\sin\phi_2,\ -\cos\theta_2\big), \tag{2.73a}$$

$$k_4^{\mu} = E_4\big(1,\ -\sin\theta_4\cos\phi_2,\ -\sin\theta_4\sin\phi_2,\ -\cos\theta_4\big), \tag{2.73b}$$

$$q_2^{\mu} = \Big(q_2^0,\ 0,\ 0,\ -\sqrt{(q_2^0)^2+Q_2^2}\Big), \tag{2.73c}$$

where $0 < \theta_2, \theta_4 < \pi/2$, $0 < \phi_2 < 2\pi$ and $Q_2^2 = -(q_2)^2 > 0$ is the virtuality of the gluon. The amplitudes are

$$(\mathcal{J}^{g_2}_{q_2q_4})^{+}_{++} = -\sqrt{2}Q_2\frac{1}{z_2}e^{i\phi_2}, \tag{2.74a}$$

$$(\mathcal{J}^{g_2}_{q_2q_4})^{-}_{++} = +\sqrt{2}Q_2\frac{1-z_2}{z_2}e^{-i\phi_2}, \tag{2.74b}$$

$$(\mathcal{J}^{g_2}_{q_2q_4})^{-}_{--} = +\sqrt{2}Q_2\frac{1}{z_2}e^{-i\phi_2}, \tag{2.74c}$$

$$(\mathcal{J}^{g_2}_{q_2q_4})^{+}_{--} = -\sqrt{2}Q_2\frac{1-z_2}{z_2}e^{+i\phi_2}. \tag{2.74d}$$

We are now ready to calculate the approximated amplitudes given in eq. (2.52a). For brevity, we simplify its notation as

$$\mathcal{M}_{\sigma_1\sigma_3\sigma_2\sigma_4} = \frac{1}{Q_1^2 Q_2^2} \sum_{\lambda_1=\pm1} \sum_{\lambda_2=\pm1} (\mathcal{J}_1)^{\lambda_1}_{\sigma_1\sigma_3} (\mathcal{J}_2)^{\lambda_2}_{\sigma_2\sigma_4} \hat{\mathcal{M}}_{\lambda_1\lambda_2}. \tag{2.75}$$

There are four combinations for $\sigma_{1,2,3,4}$,

$$(\sigma_1,\sigma_3,\sigma_2,\sigma_4) = (+,+,+,+),\ (+,+,-,-),\ (-,-,+,+),\ (-,-,-,-). \tag{2.76}$$

For the first combination, the calculation goes as follows.

$$\begin{aligned}
&\mathcal{M}_{++++} \\
&= \frac{1}{Q_1^2 Q_2^2} \sum_{\lambda_1=\pm1} \sum_{\lambda_2=\pm1} (\mathcal{J}_1)^{\lambda_1}_{++} (\mathcal{J}_2)^{\lambda_2}_{++} \hat{\mathcal{M}}_{\lambda_1\lambda_2} \\
&= \frac{1}{Q_1^2 Q_2^2} \Big[(\mathcal{J}_1)^{+}_{++} (\mathcal{J}_2)^{+}_{++} \hat{\mathcal{M}}_{++} + (\mathcal{J}_1)^{+}_{++} (\mathcal{J}_2)^{-}_{++} \hat{\mathcal{M}}_{+-} + (\mathcal{J}_1)^{-}_{++} (\mathcal{J}_2)^{+}_{++} \hat{\mathcal{M}}_{-+} + (\mathcal{J}_1)^{-}_{++} (\mathcal{J}_2)^{-}_{++} \hat{\mathcal{M}}_{--} \Big] \\
&= \frac{2}{Q_1 Q_2 z_1 z_2} \Big[-e^{-i(\phi_1-\phi_2)} \hat{\mathcal{M}}_{++} + \bar{z}_2 e^{-i(\phi_1+\phi_2)} \hat{\mathcal{M}}_{+-} + \bar{z}_1 e^{i(\phi_1+\phi_2)} \hat{\mathcal{M}}_{-+} - \bar{z}_1\bar{z}_2 e^{i(\phi_1-\phi_2)} \hat{\mathcal{M}}_{--} \Big],
\end{aligned} \tag{2.77}$$

where $\bar{z}_i = 1 - z_i$ are introduced following ref. [14]. The overall factor $2/Q_1 Q_2 z_1 z_2$ always appears, therefore we omit it during our calculation and add it at the very end. The amplitude squared gives

$$\begin{aligned}
&\left|\mathcal{M}_{++++}\right|^2 \\
&= \left|\hat{\mathcal{M}}_{++}\right|^2 + \bar{z}_2^2 \left|\hat{\mathcal{M}}_{+-}\right|^2 + \bar{z}_1^2 \left|\hat{\mathcal{M}}_{-+}\right|^2 + \bar{z}_1^2 \bar{z}_2^2 \left|\hat{\mathcal{M}}_{--}\right|^2 - 2\bar{z}_1 Re(\hat{\mathcal{M}}_{++} \hat{\mathcal{M}}^*_{-+}) \cos 2\phi_1 \\
&- 2\bar{z}_2 Re(\hat{\mathcal{M}}^*_{++} \hat{\mathcal{M}}_{+-}) \cos 2\phi_2 - 2\bar{z}_1 \bar{z}_2^2 Re(\hat{\mathcal{M}}_{+-} \hat{\mathcal{M}}^*_{--}) \cos 2\phi_1 - 2\bar{z}_1^2 \bar{z}_2 Re(\hat{\mathcal{M}}_{--} \hat{\mathcal{M}}^*_{-+}) \cos 2\phi_2 \\
&+ 2\bar{z}_1 \bar{z}_2 Re(\hat{\mathcal{M}}_{++} \hat{\mathcal{M}}^*_{--}) \cos 2(\phi_1 - \phi_2) + 2\bar{z}_1 \bar{z}_2 Re(\hat{\mathcal{M}}_{+-} \hat{\mathcal{M}}^*_{-+}) \cos 2(\phi_1 + \phi_2) \\
&+ \{Re \to Im,\ \ \cos \to \sin\}.
\end{aligned} \tag{2.78a}$$

For the other helicity combinations, the amplitude squared is given below.

$$\begin{aligned}
&\left|\mathcal{M}_{++--}\right|^2 \\
&= \bar{z}_2^2 \left|\hat{\mathcal{M}}_{++}\right|^2 + \left|\hat{\mathcal{M}}_{+-}\right|^2 + \bar{z}_1^2 \bar{z}_2^2 \left|\hat{\mathcal{M}}_{-+}\right|^2 + \bar{z}_1^2 \left|\hat{\mathcal{M}}_{--}\right|^2 - 2\bar{z}_1 \bar{z}_2^2 Re(\hat{\mathcal{M}}_{++} \hat{\mathcal{M}}^*_{-+}) \cos 2\phi_1 \\
&- 2\bar{z}_2 Re(\hat{\mathcal{M}}^*_{++} \hat{\mathcal{M}}_{+-}) \cos 2\phi_2 - 2\bar{z}_1 Re(\hat{\mathcal{M}}_{+-} \hat{\mathcal{M}}^*_{--}) \cos 2\phi_1 - 2\bar{z}_1^2 \bar{z}_2 Re(\hat{\mathcal{M}}_{--} \hat{\mathcal{M}}^*_{-+}) \cos 2\phi_2 \\
&+ 2\bar{z}_1 \bar{z}_2 Re(\hat{\mathcal{M}}_{++} \hat{\mathcal{M}}^*_{--}) \cos 2(\phi_1 - \phi_2) + 2\bar{z}_1 \bar{z}_2 Re(\hat{\mathcal{M}}_{+-} \hat{\mathcal{M}}^*_{-+}) \cos 2(\phi_1 + \phi_2) \\
&+ \{Re \to Im,\ \ \cos \to \sin\}.
\end{aligned} \tag{2.78b}$$

$$
\begin{aligned}
&\left|\mathcal{M}_{--++}\right|^2 \\
&= \bar{z}_1^2\left|\hat{\mathcal{M}}_{++}\right|^2 + \bar{z}_1^2\bar{z}_2^2\left|\hat{\mathcal{M}}_{+-}\right|^2 + \left|\hat{\mathcal{M}}_{-+}\right|^2 + \bar{z}_2^2\left|\hat{\mathcal{M}}_{--}\right|^2 - 2\bar{z}_1 Re(\hat{\mathcal{M}}_{++}\hat{\mathcal{M}}^*_{-+})\cos 2\phi_1 \\
&- 2\bar{z}_1^2\bar{z}_2 Re(\hat{\mathcal{M}}^*_{++}\hat{\mathcal{M}}_{+-})\cos 2\phi_2 - 2\bar{z}_1\bar{z}_2^2 Re(\hat{\mathcal{M}}_{+-}\hat{\mathcal{M}}^*_{--})\cos 2\phi_1 - 2\bar{z}_2 Re(\hat{\mathcal{M}}_{--}\hat{\mathcal{M}}^*_{-+})\cos 2\phi_2 \\
&+ 2\bar{z}_1\bar{z}_2 Re(\hat{\mathcal{M}}_{++}\hat{\mathcal{M}}^*_{--})\cos 2(\phi_1-\phi_2) + 2\bar{z}_1\bar{z}_2 Re(\hat{\mathcal{M}}_{+-}\hat{\mathcal{M}}^*_{-+})\cos 2(\phi_1+\phi_2) \\
&+ \{Re \to Im, \quad \cos \to \sin\}.
\end{aligned}
\tag{2.78c}
$$

$$
\begin{aligned}
&\left|\mathcal{M}_{----}\right|^2 \\
&= \bar{z}_1^2\bar{z}_2^2\left|\hat{\mathcal{M}}_{++}\right|^2 + \bar{z}_1^2\left|\hat{\mathcal{M}}_{+-}\right|^2 + \bar{z}_2^2\left|\hat{\mathcal{M}}_{-+}\right|^2 + \left|\hat{\mathcal{M}}_{--}\right|^2 - 2\bar{z}_1\bar{z}_2^2 Re(\hat{\mathcal{M}}_{++}\hat{\mathcal{M}}^*_{-+})\cos 2\phi_1 \\
&- 2\bar{z}_1^2\bar{z}_2 Re(\hat{\mathcal{M}}^*_{++}\hat{\mathcal{M}}_{+-})\cos 2\phi_2 - 2\bar{z}_1 Re(\hat{\mathcal{M}}_{+-}\hat{\mathcal{M}}^*_{--})\cos 2\phi_1 - 2\bar{z}_2 Re(\hat{\mathcal{M}}_{--}\hat{\mathcal{M}}^*_{-+})\cos 2\phi_2 \\
&+ 2\bar{z}_1\bar{z}_2 Re(\hat{\mathcal{M}}_{++}\hat{\mathcal{M}}^*_{--})\cos 2(\phi_1-\phi_2) + 2\bar{z}_1\bar{z}_2 Re(\hat{\mathcal{M}}_{+-}\hat{\mathcal{M}}^*_{-+})\cos 2(\phi_1+\phi_2) \\
&+ \{Re \to Im, \quad \cos \to \sin\}.
\end{aligned}
\tag{2.78d}
$$

After integrations over ϕ_1 and ϕ_2, the sum of the amplitude squared gives a term which contributes to the total cross section,

$$
\int d\phi_1 \int d\phi_2 \sum_{\sigma_1\sigma_3\sigma_2\sigma_4} \left|\mathcal{M}_{\sigma_1\sigma_3\sigma_2\sigma_4}\right|^2 = \frac{4}{Q_1^2Q_2^2}\frac{1+\bar{z}_1^2}{z_1^2}\frac{1+\bar{z}_2^2}{z_2^2}\left(\left|\hat{\mathcal{M}}_{++}\right|^2 + \left|\hat{\mathcal{M}}_{+-}\right|^2 + \left|\hat{\mathcal{M}}_{-+}\right|^2 + \left|\hat{\mathcal{M}}_{--}\right|^2\right),
\tag{2.79}
$$

where the omitted overall factor $2/Q_1Q_2z_1z_2$ is added. The azimuthal angle correlation terms, in which we are most interested, are

$$
\begin{aligned}
\sum_{\sigma_1\sigma_3\sigma_2\sigma_4} \left|\mathcal{M}_{\sigma_1\sigma_3\sigma_2\sigma_4}\right|^2\Big|_{\text{corr.}} =& \frac{32}{Q_1^2Q_2^2}\frac{\bar{z}_1}{z_1^2}\frac{\bar{z}_2}{z_2^2}\Big(Re(\hat{\mathcal{M}}_{++}\hat{\mathcal{M}}^*_{--})\cos 2(\phi_1-\phi_2) + Re(\hat{\mathcal{M}}_{+-}\hat{\mathcal{M}}^*_{-+})\cos 2(\phi_1+\phi_2)\Big) \\
&+ \{Re \to Im, \quad \cos \to \sin\}.
\end{aligned}
\tag{2.80}
$$

These two eqs. (2.79) and (2.80) are the most important findings in this section. The amount of the correlations are estimated by looking at the ratio between these two,

$$
\begin{aligned}
&\frac{\sum_{\sigma_1\sigma_3\sigma_2\sigma_4}\left|\mathcal{M}_{\sigma_1\sigma_3\sigma_2\sigma_4}\right|^2\Big|_{\text{corr.}}}{\int d\phi_1 \int d\phi_2 \sum_{\sigma_1\sigma_3\sigma_2\sigma_4}\left|\mathcal{M}_{\sigma_1\sigma_3\sigma_2\sigma_4}\right|^2} = 8\frac{\bar{z}_1\bar{z}_2}{(1+\bar{z}_1^2)(1+\bar{z}_1^2)} \\
&\times\frac{Re(\hat{\mathcal{M}}_{++}\hat{\mathcal{M}}^*_{--})\cos 2(\phi_1-\phi_2) + Re(\hat{\mathcal{M}}_{+-}\hat{\mathcal{M}}^*_{-+})\cos 2(\phi_1+\phi_2) + \{Re \to Im, \quad \cos \to \sin\}}{\left|\hat{\mathcal{M}}_{++}\right|^2 + \left|\hat{\mathcal{M}}_{+-}\right|^2 + \left|\hat{\mathcal{M}}_{-+}\right|^2 + \left|\hat{\mathcal{M}}_{--}\right|^2}.
\end{aligned}
\tag{2.81}
$$

The first factor on the right hand side of eq. (2.81) given in terms of $\bar{z}_1$ and $\bar{z}_2$ determines the amount of the correlations according to kinematics. This is maximized when $\bar{z}_1 \to 1$ and $\bar{z}_2 \to 1$ i.e. the colliding gluon is soft with respect to its mother parton. The rest on the

right hand side is dependent on the hard process producing X.

Although we have calculated only the quark current process in eq. (2.48a), it terms out that the above result captures all the important properties. The difference appears only in the kinematic factor given in terms of z_1 and z_2. To make it clear, we rewrite eqs. (2.79) and (2.80) in the following forms,

$$\int d\phi_1 \int d\phi_2 \sum_{\sigma_1\sigma_3\sigma_2\sigma_4} \left|\mathcal{M}_{\sigma_1\sigma_3\sigma_2\sigma_4}\right|^2 = \frac{4}{Q_1^2 Q_2^2} F_0[a_1 a_2]\left(\left|\hat{\mathcal{M}}_{++}\right|^2 + \left|\hat{\mathcal{M}}_{+-}\right|^2 + \left|\hat{\mathcal{M}}_{-+}\right|^2 + \left|\hat{\mathcal{M}}_{--}\right|^2\right), \tag{2.82}$$

and

$$\begin{aligned}\sum_{\sigma_1\sigma_3\sigma_2\sigma_4} \left|\mathcal{M}_{\sigma_1\sigma_3\sigma_2\sigma_4}\right|^2\Big|_{\text{corr.}} =& \frac{32}{Q_1^2 Q_2^2} F_3[a_1 a_2]\Big(Re(\hat{\mathcal{M}}_{++}\hat{\mathcal{M}}^*_{--})\cos 2(\phi_1-\phi_2) + \\ & Re(\hat{\mathcal{M}}_{+-}\hat{\mathcal{M}}^*_{-+})\cos 2(\phi_1+\phi_2)\Big) + \{Re \to Im, \quad \cos \to \sin\},\end{aligned} \tag{2.83}$$

where $a_1 a_2$ is one of the three possible incoming states, qq, qg or gg. The kinematic factors F_0 and F_3 for all the incoming states are summarized as [14]

$$F_0[qq] = \frac{1+\bar{z}_1^2}{z_1^2}\frac{1+\bar{z}_2^2}{z_2^2}, \tag{2.84a}$$

$$F_0[qg] = \frac{1+\bar{z}_1^2}{z_1^2}\frac{1+z_2^4+\bar{z}_2^4}{z_2^2\bar{z}_2}, \tag{2.84b}$$

$$F_0[gg] = \frac{1+z_1^4+\bar{z}_1^4}{z_1^2\bar{z}_1}\frac{1+z_2^4+\bar{z}_2^4}{z_2^2\bar{z}_2}, \tag{2.84c}$$

and

$$F_3[qq] = F_3[qg] = F_3[gg] = \frac{\bar{z}_1}{z_1^2}\frac{\bar{z}_2}{z_2^2}. \tag{2.85}$$

It is remarkable that the kinematic factor of the correlation term F_3 is the same for all the three incoming states. Kinematic enhancement of the correlation is evaluated from F_3/F_0,

$$F_3/F_0[qq] = \frac{\bar{z}_1\bar{z}_2}{(1+\bar{z}_1^2)(1+\bar{z}_1^2)}, \tag{2.86a}$$

$$F_3/F_0[qg] = \frac{\bar{z}_1\bar{z}_2^2}{(1+\bar{z}_1^2)(1+z_2^4+\bar{z}_2^4)}, \tag{2.86b}$$

$$F_3/F_0[gg] = \frac{\bar{z}_1^2\bar{z}_2^2}{(1+z_1^4+\bar{z}_1^4)(1+z_2^4+\bar{z}_2^4)}. \tag{2.86c}$$

From the above equations, we can read that maximal enhancement of the correlation is achieved when $\bar{z}_1 \to 1$ and $\bar{z}_2 \to 1$, not only for the qq initial state but also for the qg and

gg initial states.

Before closing this section, one important issue should be remarked. Since we have assumed gluon fusion as the hard process producing X, only the vector boson wave functions with helicity $+1$ and -1 are used. However, if a massive gauge boson fusion is assumed, the wave function with helicity 0 is also relevant. In such a case, the azimuthal angle dependence given in eq. (2.78) will be more complicated. This is studied in detail in ref. [4], to which I refer the reader.

2.3 Azimuthal angle correlations in the Higgs and $Q\bar{Q}$ productions

In this section, the process dependent factor in eq. (2.81) is calculated for the Higgs boson production and $Q\bar{Q}$ production.

We start from the Higgs boson production. For a scalar boson production, the amplitudes $\hat{\mathcal{M}}_{+-}$ and $\hat{\mathcal{M}}_{-+}$ vanish, therefore eq. (2.81) reduces to

$$R_{\rm corr.} = \frac{8F_3}{F_0}\frac{Re(\hat{\mathcal{M}}_{++}\hat{\mathcal{M}}^*_{--})\cos 2(\phi_1-\phi_2) + \{Re\to Im,\ \ \cos\to\sin\}}{\left|\hat{\mathcal{M}}_{++}\right|^2 + \left|\hat{\mathcal{M}}_{--}\right|^2}, \tag{2.87}$$

where eq. (2.81) is rewritten in a simpler form and defined by $R_{\rm corr.}$.

The Higgs boson field in the standard model does not have a tree level coupling with the gluon field, thus the Higgs boson production via gluon fusion is induced at the leading order by a quark 1-loop exchange. The couplings between the Higgs boson field and quark fields are relevant, therefore. In the standard model, they are described by

$$\mathcal{L}_{\rm SM} = -y_f\bar{\psi}_f\psi_f h. \tag{2.88}$$

Here we assume a non-standard coupling, namely [3]

$$\mathcal{L}_{\rm non-SM} = -y_f\cos\alpha\ \bar{\psi}_f\psi_f h - y_f\sin\alpha\bar{\psi}_f i\gamma^5\psi_f h, \tag{2.89}$$

where $-\pi/2<\alpha<\pi/2$ and the second term leads to violation of the parity symmetry unless $\alpha=0$ or $|\alpha|=\pi/2$. The helicity amplitudes after the 1-loop calculation are given by

$$\begin{aligned}(\hat{\mathcal{M}}^h_{g_1g_2})_{\lambda_1\lambda_2} = \frac{\alpha_s}{4\pi}T_R\delta_{a_1a_2}\frac{\sqrt{2}m_h^2}{v}\Bigg[&(1+\lambda_1\lambda_2)\cos\alpha\int_0^1 dx\int_0^{1-x}dy\frac{1-4xy}{1-(m_h^2/m_f^2)xy}\\ &+i(\lambda_1+\lambda_2)\sin\alpha\int_0^1 dx\int_0^{1-x}dy\frac{1}{1-(m_h^2/m_f^2)xy}\Bigg],\end{aligned} \tag{2.90}$$

where a_i denote the color indices for the gluons, m_h is the Higgs boson mass and m_f is the loop running quark mass. The amplitudes vanish unless $\lambda_1=\lambda_2$ as mentioned above. By

introducing $\lambda = \lambda_1 = \lambda_2$, it can be written as

$$(\hat{\mathcal{M}}^h_{g_1 g_2})_{\lambda\lambda} = \frac{\alpha_s}{4\pi} T_R \delta_{a_1 a_2} \frac{2\sqrt{2} m_h^2}{v} \Bigg[\cos\alpha \int_0^1 dx \int_0^{1-x} dy \frac{1-4xy}{1-(m_h^2/m_f^2)xy} + i\lambda \sin\alpha \int_0^1 dx \int_0^{1-x} dy \frac{1}{1-(m_h^2/m_f^2)xy} \Bigg]. \quad (2.91)$$

When the loop running quark mass is so large that m_h^2/m_f^2 terms can be neglected, the above integration is easily performed and we find

$$(\hat{\mathcal{M}}^h_{g_1 g_2})_{\lambda\lambda} = \frac{\alpha_s}{4\pi} T_R \delta_{a_1 a_2} \frac{2\sqrt{2} m_h^2}{3v} \Bigg[\cos\alpha + i\lambda \frac{3}{2} \sin\alpha \Bigg]. \quad (2.92)$$

It is straightforward to derive $R_{\text{corr.}}$ for the non-standard Higgs boson production via gluon fusion by plugging the helicity amplitudes in eq. 2.92 into eq. 2.87,

$$R_{\text{corr.}} = \frac{4F_3}{F_0} \frac{\left(\cos^2\alpha - \frac{9}{4}\sin^2\alpha\right)\cos 2(\phi_1 - \phi_2) + 3\sin\alpha\cos\alpha \ \sin 2(\phi_1 - \phi_2)}{\cos^2\alpha + \frac{9}{4}\sin^2\alpha}. \quad (2.93)$$

It should be worth looking at the two extreme cases, namely $\alpha = 0$ and $|\alpha| = \pi/2$,

$$R_{\text{corr.}}\big(\alpha = 0\big) = +\frac{4F_3}{F_0} \cos 2(\phi_1 - \phi_2), \quad (2.94a)$$

$$R_{\text{corr.}}\big(|\alpha| = \pi/2\big) = -\frac{4F_3}{F_0} \cos 2(\phi_1 - \phi_2). \quad (2.94b)$$

The overall different sign indicates a clear discrimination in the $\phi_1 - \phi_2$ distribution for the standard model Higgs boson ($\alpha = 0$) and the parity odd non-standard Higgs boson ($|\alpha| = \pi/2$). This is confirmed in the left graph of Figure 3, where the blue solid curve represents $\alpha = 0$ and the red dashed curve $|\alpha| = \pi/2$. The event samples are generated according to the exact tree level matrix elements for a Higgs plus 2-parton process by using MadGraph5_aMC@NLO [38] version 5.2.2.1. An implemented model file named heft 1.5.0 is used. Kinematic cuts $y_1 \times y_2 > 0$ and $|y_1 - y_2| > 4$, which are called the VBF cuts, are applied on the two partons, in order to enhance the VBF contribution. A cut on transverse momentum $p_T > 20$ GeV is also applied. The scale in the parton distribution functions is set to 20 GeV. A parton with positive rapidity is always chosen for ϕ_1 and another parton with negative rapidity is chosen for ϕ_2. The initial condition is proton-proton and the center-of-mass energy is 14 TeV.

When the mixing angle $|\alpha|$ is neither 0 nor $\pi/2$ i.e. the parity symmetry is broken, the $\sin 2(\phi_1 - \phi_2)$ dependence appears. From eq. (2.93), the dependence is maximized when $\cos^2\alpha = (9/4)\sin^2\alpha$, that is, $\sin\alpha \simeq \pm 0.55$,

$$R_{\text{corr.}}\big(\cos^2\alpha = (9/4)\sin^2\alpha\big) = \frac{4F_3}{F_0} \frac{\sin\alpha}{|\sin\alpha|} \sin 2(\phi_1 - \phi_2). \quad (2.95)$$

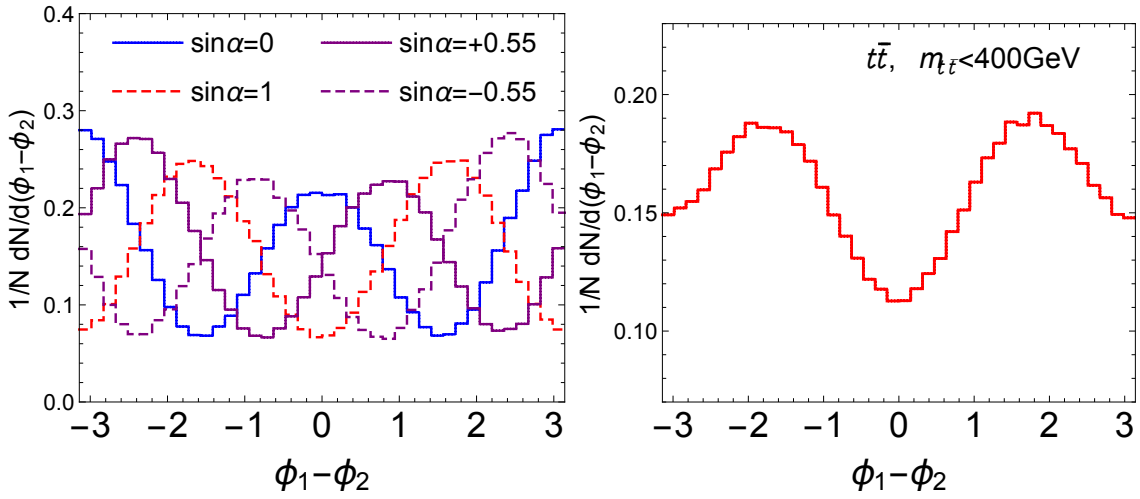

Figure 3: *left*: The $\phi_1 - \phi_2$ distribution for the Higgs boson production, according to the exact tree level matrix elements. The blue solid curve represents the standard model Higgs boson ($\alpha = 0$), the red dashed curve the parity odd Higgs boson ($|\alpha| = \pi/2$), the purple solid curve a mixed Higgs boson with $\sin\alpha = +0.55$ and the purple dashed curve a mixed Higgs boson with $\sin\alpha = -0.55$. The vector boson fusion cuts $y_1 \times y_2 < 0$ and $|y_1 - y_2| > 4$ are applied. *right*: The same with the left figure but the production of the top quark pair plus two partons. A phase space cut $m_{t\bar{t}} < 400$ GeV is additionally imposed.

In the left graph of Figure 3, the $\phi_1 - \phi_2$ distribution for $\sin\alpha = +0.55$ is shown by the purple solid line and that for $\sin\alpha = -0.55$ is shown by the purple dashed line. The event samples are generated with the same strategy above. A small modification is needed in the model file [4]. It should be emphasized that, if a parton with higher p_T had been always chosen for ϕ_1 and another parton with lower p_T had been chosen for ϕ_2, the $\sin 2(\phi_1 - \phi_2)$ correlation would have completely disappeared, simply because of its property $\sin(-x) = -\sin x$. Both a complex phase and a helicity λ dependence are necessary to obtain the $\sin 2(\phi_1 - \phi_2)$ correlation, which is exactly the case in the amplitudes in eq. 2.92.

Although we have evaluated the three extreme cases in eqs. (2.94) and (2.95), it is important to learn that a small shift of the peak point from 0 in the $\phi_1 - \phi_2$ distribution indicates a parity violation in the Higgs sector.

Let us study the second case, a heavy quark pair production. Here a heavy quark means a bottom quark or a top quark. Unlike the above study, only the standard model QCD interactions are assumed. The helicity amplitudes for the $gg \to Q\bar{Q}$ process at the leading

[4] I modified the parameters 'scalarf' and 'axialf' in the subroutine setpara in couplings.f.

order are given in a compact form in ref. [14],

$$(\hat{\mathcal{M}}^{Q\bar{Q}}_{g_1g_2})^{\sigma\bar{\sigma}i\hat{i}}_{\lambda_1\lambda_2a_1a_2} = g_s^2\left[\frac{1}{2}\{t^{a_1},t^{a_2}\}_{i\bar{i}}\hat{\mathcal{M}}^{\sigma\bar{\sigma}}_{\lambda_1\lambda_2} + \frac{1}{2}[t^{a_1},t^{a_2}]_{i\bar{i}}\hat{\mathcal{N}}^{\sigma\bar{\sigma}}_{\lambda_1\lambda_2}\right], \tag{2.96a}$$

$$\hat{\mathcal{N}}^{\sigma\bar{\sigma}}_{\lambda_1\lambda_2} = \hat{\mathcal{M}}^{\sigma\bar{\sigma}}_{\lambda_1\lambda_2}\times\beta\cos\theta, \tag{2.96b}$$

where a_1, a_2 denote the color indices for the gluons and i, $\bar{i}$ denote the color indices for the heavy quark and the heavy antiquark, respectively. The amplitudes $\hat{\mathcal{M}}^{\sigma\bar{\sigma}}_{\lambda_1\lambda_2}$ are [14]

$$\hat{\mathcal{M}}^{\sigma-\sigma}_{\lambda-\lambda} = 2\beta\sin\theta(\sigma\lambda+\cos\theta)/(1-\beta^2\cos^2\theta), \tag{2.97a}$$

$$\hat{\mathcal{M}}^{\sigma\sigma}_{\lambda\lambda} = -2\sqrt{1-\beta^2}(\lambda+\sigma\beta)/(1-\beta^2\cos^2\theta), \tag{2.97b}$$

$$\hat{\mathcal{M}}^{\sigma\sigma}_{\lambda-\lambda} = 2\beta\sqrt{1-\beta^2}\,\sigma\sin^2\theta/(1-\beta^2\cos^2\theta), \tag{2.97c}$$

$$\hat{\mathcal{M}}^{\sigma-\sigma}_{\lambda\lambda} = 0, \tag{2.97d}$$

where β is the velocity of the heavy quark $\beta=\sqrt{1-4m_Q^2/m_{Q\bar{Q}}^2}$ and θ is the polar angle for the heavy quark, $0<\theta<\pi$. At first, we evaluate the color factors. Because the first term in the right hand side of eq. (2.96a) is symmetric under exchanging a_1 and a_2 while the second term is antisymmetric, these two terms do not interfere. The amplitude squared gives

$$\begin{aligned}\sum_{\text{color}}\left|(\hat{\mathcal{M}}^{Q\bar{Q}}_{g_1g_2})^{\sigma\bar{\sigma}i\hat{i}}_{\lambda_1\lambda_2a_1a_2}\right|^2 &= \frac{g_s^4}{4}\sum_{\text{color}}\left[\{t^{a_1},t^{a_2}\}_{i\bar{i}}\{t^{a_2},t^{a_1}\}_{\bar{i}i}\left|\hat{\mathcal{M}}^{\sigma\bar{\sigma}}_{\lambda_1\lambda_2}\right|^2 + [t^{a_1},t^{a_2}]_{i\bar{i}}[t^{a_2},t^{a_1}]_{\bar{i}i}\left|\hat{\mathcal{N}}^{\sigma\bar{\sigma}}_{\lambda_1\lambda_2}\right|^2\right]\\ &= \frac{g_s^4}{4}\sum_{\text{color}}\left[\text{tr}\left[\{t^{a_1},t^{a_2}\}\{t^{a_2},t^{a_1}\}\right]\left|\hat{\mathcal{M}}^{\sigma\bar{\sigma}}_{\lambda_1\lambda_2}\right|^2 + \text{tr}\left[[t^{a_1},t^{a_2}][t^{a_2},t^{a_1}]\right]\left|\hat{\mathcal{N}}^{\sigma\bar{\sigma}}_{\lambda_1\lambda_2}\right|^2\right]\end{aligned} \tag{2.98}$$

The first term is evaluated as follows,

$$\begin{aligned}&\sum_{\text{color}}\text{tr}\left[\{t^{a_1},t^{a_2}\}\{t^{a_2},t^{a_1}\}\right]\\ &= 2\sum_{\text{color}}\text{tr}\left[t^{a_1}t^{a_1}t^{a_2}t^{a_2} + t^{a_1}t^{a_2}t^{a_1}t^{a_2}\right]\\ &= 2\sum_{\text{color}}(t^{a_1}t^{a_1})_{ij}(t^{a_2}t^{a_2})_{ji} + (t^{a_1})_{ij}(t^{a_2})_{jk}(t^{a_1})_{kl}(t^{a_2})_{li}\\ &= 2\sum_{\text{color}}T_R^2\frac{(N^2-1)^2}{N^2}\delta_{ij}\delta_{ji} + T_R^2(\delta_{il}\delta_{jk}-1/N\delta_{ij}\delta_{kl})(\delta_{ji}\delta_{kl}-1/N\delta_{jk}\delta_{li})\\ &= 2\left\{T_R^2\frac{(N^2-1)^2}{N} + T_R^2\left(-N+\frac{1}{N}\right)\right\}\\ &= 2T_R^2(N^2-1)\frac{N^2-2}{N},\end{aligned} \tag{2.99}$$

where at the third equality, the Fierz identity $\sum_a(t^a)_{ij}(t^a)_{kl} = T_R(\delta_{il}\delta_{jk}-1/N\delta_{ij}\delta_{kl})$ and some identity derived from the Fierz identity $\sum_a(t^at^a)_{ij} = T_R\delta_{ij}(N^2-1)/N$ are used. The

second term goes similarly,

$$\begin{aligned}
&\sum_{\text{color}} \text{tr}\Big[\big[t^{a_1}, t^{a_2}\big]\big[t^{a_2}, t^{a_1}\big]\Big] \\
&= 2\sum_{\text{color}} \text{tr}\Big[t^{a_1}t^{a_1}t^{a_2}t^{a_2} - t^{a_1}t^{a_2}t^{a_1}t^{a_2}\Big] \\
&= 2\bigg\{T_R^2\frac{(N^2-1)^2}{N} - T_R^2\Big(-N+\frac{1}{N}\Big)\bigg\} \\
&= 2T_R^2\big(N^2-1\big)N.
\end{aligned} \tag{2.100}$$

Thus, eq. (2.98) has a factorized form

$$\begin{aligned}
\sum_{\text{color}}\big|(\hat{\mathcal{M}}^{Q\bar{Q}}_{g_1g_2})^{\sigma\bar{\sigma}i\bar{i}}_{\lambda_1\lambda_2 a_1 a_2}\big|^2 &= g_s^2\frac{T_R^2}{2}\big(N^2-1\big)\bigg\{\frac{N^2-2}{N}\big|\hat{\mathcal{M}}^{\sigma\bar{\sigma}}_{\lambda_1\lambda_2}\big|^2 + N\big|\hat{\mathcal{N}}^{\sigma\bar{\sigma}}_{\lambda_1\lambda_2}\big|^2\bigg\} \\
&= g_s^2\frac{T_R^2}{2}\big(N^2-1\big)\bigg\{\frac{N^2-2}{N} + N\beta^2\cos^2\theta\bigg\}\big|\hat{\mathcal{M}}^{\sigma\bar{\sigma}}_{\lambda_1\lambda_2}\big|^2,
\end{aligned} \tag{2.101}$$

where at the last equality eq. (2.96b) is used. This expression allows us to evaluate the correlation terms by using only the helicity amplitudes $\hat{\mathcal{M}}^{\sigma\bar{\sigma}}_{\lambda_1\lambda_2}$. Eq. (2.81) is written as

$$\begin{aligned}
&R_{\text{corr.}} \\
&= \frac{8F_3}{F_0}\frac{\sum_{\sigma\bar{\sigma}} Re(\hat{\mathcal{M}}^{\sigma\bar{\sigma}}_{++}\hat{\mathcal{M}}^{\sigma\bar{\sigma}*}_{--})\cos 2(\phi_1-\phi_2) + Re(\hat{\mathcal{M}}^{\sigma\bar{\sigma}}_{+-}\hat{\mathcal{M}}^{\sigma\bar{\sigma}*}_{-+})\cos 2(\phi_1+\phi_2) + \{Re\to Im, \cos\to\sin\}}{\sum_{\sigma\bar{\sigma}}\big|\hat{\mathcal{M}}^{\sigma\bar{\sigma}}_{++}\big|^2 + \big|\hat{\mathcal{M}}^{\sigma\bar{\sigma}}_{+-}\big|^2 + \big|\hat{\mathcal{M}}^{\sigma\bar{\sigma}}_{-+}\big|^2 + \big|\hat{\mathcal{M}}^{\sigma\bar{\sigma}}_{--}\big|^2}.
\end{aligned} \tag{2.102}$$

By plugging the amplitudes in eq. (2.97) into the above equation, we can find

$$R_{\text{corr.}} = \frac{4F_3}{F_0}\frac{-(1-\beta^2)^2\cos 2(\phi_1-\phi_2) - \beta^4\sin^4\theta\cos 2(\phi_1+\phi_2)}{1+2\beta^2\sin^2\theta - \beta^4(1+\sin^4\theta)}. \tag{2.103}$$

The $\sin 2(\phi_1 \pm \phi_2)$ correlation term is not present, since the amplitudes in eq. (2.97) are purely real. Again we look at the two kinematically extreme cases, namely $\beta = 0$ and $\beta = 1$,

$$R_{\text{corr.}}\big(\beta=0\big) = -\frac{4F_3}{F_0}\cos 2(\phi_1-\phi_2), \tag{2.104a}$$

$$R_{\text{corr.}}\big(\beta=1\big) = -\frac{4F_3}{F_0}\frac{\sin^2\theta}{1+\cos^2\theta}\cos 2(\phi_1+\phi_2). \tag{2.104b}$$

The correlation term with $\beta = 0$ is identical to the one of the parity odd Higgs boson in eq. (2.94b), while that with $\beta = 1$ is found for the first time. Let us investigate why a heavy quark pair with $\beta = 0$ shows the same azimuthal angle correlation with the parity odd Higgs boson. When $\beta = 0$, both the quark and the antiquark have little momentum and they construct a orbital angular momentum $L = 0$ quark-antiquark bound state, which has odd parity. Thus, if the colliding two gluons have the same helicity $\lambda_1 = \lambda_2$, the bound state

should behave as odd parity scalar.

At the LHC, a heavy quark pair with $\beta = 0$ can be achieved by a top quark pair with applying an upper cut on the $t\bar{t}$ invariant mass $m_{t\bar{t}}$ [14]. A heavy quark pair with $\beta = 1$ can be easily achieved by a bottom quark pair with applying a lower cut on $m_{b\bar{b}}$. In the following we concentrate only on the top quark pair production at the 14 TeV LHC. In the right graph of Figure 3, the $\phi_1 - \phi_2$ distribution for the $t\bar{t}$ production is shown. The event samples are generated with the same philosophy for the samples in the right graph. A kinematic cut $m_{t\bar{t}} < 400$ GeV is applied in addition to the VBF cuts. The distribution is very similar to the one of the parity odd Higgs boson, as expected from the above discussion.

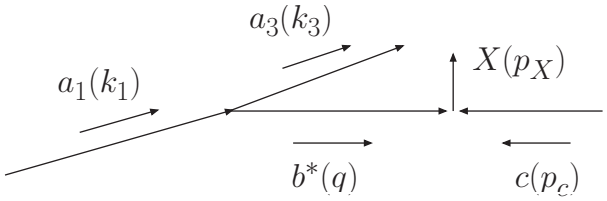

Figure 4: A hard collision process $b^* + c \to X$ and one QCD parton radiation $a_1 \to a_3 b^*$.

3 Parton shower Monte Carlo based on the DGLAP equation

The predictions for the $\phi_1 - \phi_2$ distribution in Section 2.3 are produced from event generation according to the tree level matrix elements for $pp \to H + 2$-parton process and $pp \to t\bar{t} + 2$-parton process. Since this is the order α_s^2 real emission correction to the leading order process, it is required that $\sigma(H+0\text{-parton}) \gg \sigma(H+2\text{-parton})$ or $\sigma(t\bar{t}+0\text{-parton}) \gg \sigma(t\bar{t}+2\text{-parton})$, for the fixed order perturbation theory to be applicable. However it turns out that it is easily achieved that $\sigma(H+0\text{-parton}) \sim \sigma(H+2\text{-parton})$ or $\sigma(t\bar{t}+0\text{-parton}) \sim \sigma(t\bar{t}+2\text{-parton})$, when the 2 partons are soft and/or collinear. This section is devoted to describing methods to solve this problem. In Section 3.1, the collinear singularity which universally exits in the QCD radiation is derived. The treatment of this universal singularity brings the scale dependence of the parton distribution function (PDF) and furthermore the evolution equation for the PDFs, which is the topic in Section 3.2. In Section 3.3, it is discussed how to carry out event generation according to the evolution equation for the PDFs. In Section 3.4, the result of the event generation is compared with the result obtained in Section 2.3. [5]

3.1 Universal singularity

Let us examine the process described in Figure 4. There is a hard collision process $b^* + c \to X$ and one parton radiation $a_1 \to a_3 b^*$. The whole process is

$$\begin{aligned} a_1(k_1, \sigma_1) + c(p_c) &\to a_3(k_3, \sigma_3) + b^*(q, \lambda) + c(p_c) \\ &\to a_3(k_3, \sigma_3) + X(p_X), \end{aligned} \tag{3.1}$$

where momentum and helicity are shown in parentheses. Note that, if we assume that quarks for $a_{1,3}$ and a gluon for b^*, the process is identical to the half part of the process in eq. (2.49). We are actually going to repeat some parts of the calculation which we have done in Section 2.2. By using the on-shell approximation for the parton $b^*(q, \lambda)$, the helicity amplitudes for the process are written as

$$\mathcal{M}_{\sigma_1 \sigma_3} \simeq \frac{1}{q^2} \sum_{\lambda = \pm 1} (\mathcal{J}^b_{a_1 a_3})^{\lambda}_{\sigma_1 \sigma_3} (\hat{\mathcal{M}}^X_{b\ c})_{\lambda}, \tag{3.2}$$

[5] I have learned these topics from refs. [30, 39, 40, 41, 42, 43].

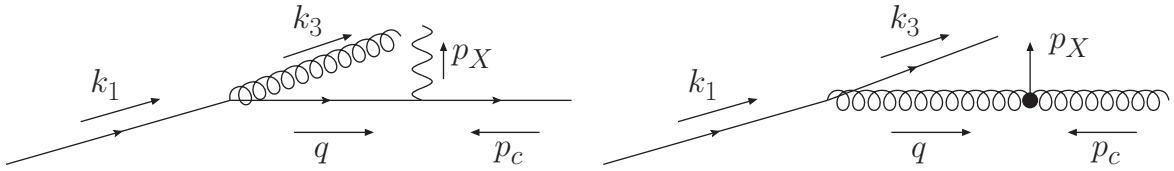

Figure 5: Two example processes described by eq. (3.2). .

where $(\mathcal{J}^b_{a_1a_3})^\lambda_{\sigma_1\sigma_3}$ are the QCD current amplitudes and $(\hat{\mathcal{M}}^X_{b\ c})_\lambda$ are the hard process amplitudes. It should be stressed that this structure of the amplitudes is quite general. If a process given in the left of Figure 5 is considered for example, the pieces in eq. (3.2) are

$$(\mathcal{J}^b_{a_1a_3})^\lambda_{\sigma_1\sigma_3} = \bar{u}(q,\lambda)\gamma^\mu u(k_1,\sigma_1)\epsilon^*_\mu(k_3,\sigma_3), \tag{3.3a}$$

$$(\hat{\mathcal{M}}^X_{b\ c})_\lambda = \epsilon^*_\nu(p_X)\bar{v}(p_c)\gamma^\nu u(q,\lambda), \tag{3.3b}$$

and, if a process given in the right of Figure 5 is considered for example, the pieces are

$$(\mathcal{J}^b_{a_1a_3})^\lambda_{\sigma_1\sigma_3} = \bar{u}(k_3,\sigma_3)\gamma^\mu u(k_1,\sigma_1)\epsilon^*_\mu(q,\lambda), \tag{3.4a}$$

$$(\hat{\mathcal{M}}^X_{b\ c})_\lambda = \epsilon_\nu(q,\lambda)\Gamma^{\nu\rho}(p_X)\epsilon_\rho(p_c), \tag{3.4b}$$

where couplings and the color factors are suppressed and the helicity for the parton c and X is implicit.

Now we evaluate the process in the left of Figure 5 in detail. Our goal is to obtain the cross section of this process, which is calculated from

$$d\sigma(q+c\to X+g) = \frac{1}{2s}\frac{1}{2}\sum_{\sigma_1,\sigma_3}|\mathcal{M}_{\sigma_1\sigma_3}|^2 d\Phi(k_3+p_X), \tag{3.5}$$

where $s=(k_1+p_c)^2$ and $d\Phi(k_3+p_X)$ is the Lorentz invariant phase space integral. The current amplitudes are

$$(\mathcal{J}^q_{qg})^\lambda_{\sigma_1\sigma_3} = \bar{u}(q,\lambda)\gamma^\mu u(k_1,\sigma_1)\epsilon^*_\mu(k_3,\sigma_3). \tag{3.6}$$

We use the same momentum parametrization in eq. (2.55), namely

$$k_1^\mu = E_1\big(1,\ \sin\theta_1\cos\phi_1,\ \sin\theta_1\sin\phi_1,\ \cos\theta_1\big), \tag{3.7a}$$

$$k_3^\mu = E_3\big(1,\ \sin\theta_3\cos\phi_1,\ \sin\theta_3\sin\phi_1,\ \cos\theta_3\big), \tag{3.7b}$$

$$q^\mu = \Big(q^0,\ 0,\ 0,\ \sqrt{(q^0)^2+Q^2}\Big). \tag{3.7c}$$

By using the helicity amplitude technique described in Section 2.1, we can easily find

$$(\mathcal{J}^q_{qg})^+_{++} = -(\mathcal{J}^q_{qg})^-_{--} = -\sqrt{2}Q\frac{1}{\sqrt{z(1-z)}}, \tag{3.8a}$$

$$(\mathcal{J}^q_{qg})^+_{+-} = -(\mathcal{J}^q_{qg})^-_{-+} = \sqrt{2}Q\frac{\sqrt{z}}{\sqrt{z(1-z)}}, \tag{3.8b}$$

where z is the energy fraction variable and defined by $z = q^0/E_1$.

The helicity summation of the amplitude squared is

$$\begin{aligned}
&\frac{1}{2}\sum_{\sigma_1,\sigma_3}|\mathcal{M}_{\sigma_1\sigma_3}|^2 \\
&= \frac{4\pi\alpha_s C_F}{2Q^4}\Big(\big|(\mathcal{J}^q_{qg})^+_{++}(\hat{\mathcal{M}}^X_{qc})_+\big|^2 + \big|(\mathcal{J}^q_{qg})^+_{+-}(\hat{\mathcal{M}}^X_{qc})_+\big|^2 + \big|(\mathcal{J}^q_{qg})^-_{--}(\hat{\mathcal{M}}^X_{qc})_-\big|^2 + \big|(\mathcal{J}^q_{qg})^-_{-+}(\hat{\mathcal{M}}^X_{qc})_-\big|^2\Big) \\
&= \frac{4\pi\alpha_s}{Q^2}\frac{1}{z}C_F\frac{1+z^2}{1-z}\Big(\big|(\hat{\mathcal{M}}^X_{qc})_+\big|^2 + \big|(\hat{\mathcal{M}}^X_{qc})_-\big|^2\Big) \\
&= \frac{8\pi\alpha_s}{Q^2}\frac{1}{z}C_F\frac{1+z^2}{1-z}\frac{1}{2}\sum_\lambda\big|(\hat{\mathcal{M}}^X_{qc})_\lambda\big|^2,
\end{aligned} \tag{3.9}$$

where the coupling constant and the color factor are included, which are calculated as follows.

$$\begin{aligned}
g_s^2\frac{1}{N_c}\sum_a \mathrm{tr}\big[t^a t^a\big] &= g^2 C_F \\
&= 4\pi\alpha_s C_F.
\end{aligned} \tag{3.10}$$

The next step is to evaluate the phase space integral.

$$\begin{aligned}
d\Phi(k_3 + p_X) &= \frac{d^3k_3}{(2\pi)^3 2E_3}d\Phi(p_X) \\
&= \frac{1}{8\pi^2}E_3 dE_3 d\cos\theta_3\frac{d\phi}{2\pi}d\Phi(p_X) \\
&= \frac{1}{8\pi^2}E_3 dE_3 d\cos(\theta_3-\theta_1)\frac{d\phi}{2\pi}d\Phi(p_X) \\
&= \frac{1}{8\pi^2}E_3 dE_3 \sin\theta d\theta\frac{d\phi}{2\pi}d\Phi(p_X) \\
&\simeq \frac{1}{8\pi^2}E_3 dE_3 \theta d\theta\frac{d\phi}{2\pi}d\Phi(p_X) \\
&= \frac{1}{16\pi^2}E_3 dE_3 d\theta^2\frac{d\phi}{2\pi}d\Phi(p_X) \\
&= \frac{1}{16\pi^2}dz dQ^2\frac{d\phi}{2\pi}d\Phi(p_X).
\end{aligned} \tag{3.11}$$

After plugging eqs. (3.9) and (3.11) into eq. (3.5) and defining $\hat{s} = (q+p_c)^2 \simeq zs$, we finally arrive at

$$\begin{aligned}
d\sigma\big(q + c \to X + g; s\big) &= \frac{\alpha_s}{2\pi}\frac{dQ^2}{Q^2}dz\frac{d\phi}{2\pi}C_F\frac{1+z^2}{1-z}\frac{1}{2\hat{s}}\frac{1}{2}\sum_\lambda\big|(\hat{\mathcal{M}}^X_{qc})_\lambda\big|^2 d\Phi(p_X) \\
&= \frac{\alpha_s}{2\pi}\frac{dQ^2}{Q^2}dz\frac{d\phi}{2\pi}C_F\frac{1+z^2}{1-z}\sigma\big(q + c \to X; \hat{s} = zs\big),
\end{aligned} \tag{3.12}$$

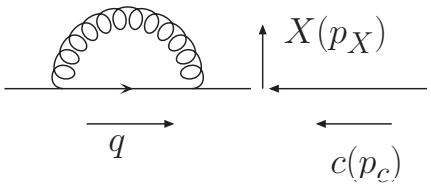

Figure 6: The order α_s virtual correction to the hard process $q + c \to X$.

therefore

$$\sigma\big(q + c \to X + g; s\big) = \frac{\alpha_s}{2\pi} \int_0^{Q_h^2} \frac{dQ^2}{Q^2} \int_0^1 dz \hat{P}_{qq}(z) \sigma\big(q + c \to X; \hat{s} = zs\big), \tag{3.13}$$

where

$$\hat{P}_{qq}(z) = C_F \frac{1 + z^2}{1 - z}. \tag{3.14}$$

The upper limit Q_h^2 in the Q^2 integration is the scale determined from the hard collision process $q + c \to X$. Note that Q_h^2 is not necessary equal to $\hat{s}$.

The above result is considered as the order α_s real emission correction to the process $q + c \to X$. The order α_s virtual correction to the process $q + c \to X$ is also needed. It is shown in Figure 6. Here we use a trick rather than doing the exact calculation. The integration over z in eq. (3.13) is divergent at $z = 1$ i.e. the emitted gluon has very little energy compared to the mother parton that emits it. This soft divergence should be canceled with another divergence coming from the virtual correction, thus at the end we should have a finite result. This statement means that the virtual correction should be identical to the real emission correction with the opposite sign in the soft limit,

$$\begin{aligned} &- \frac{\alpha_s}{2\pi} \int_0^{Q_h^2} \frac{dQ^2}{Q^2} \int_0^1 dz \hat{P}_{qq}(z) \sigma(q + c \to X; \hat{s} = zs) \Big|_{z=1} \\ = &- \frac{\alpha_s}{2\pi} \int_0^{Q_h^2} \frac{dQ^2}{Q^2} \int_0^1 dz \hat{P}_{qq}(z) \sigma(q + c \to X; \hat{s} = s). \end{aligned} \tag{3.15}$$

By including this term in eq. (3.13), we find the complete order α_s result

$$\sigma(q + c \to X + g; s) = \frac{\alpha_s}{2\pi} \int_0^{Q_h^2} \frac{dQ^2}{Q^2} \int_0^1 dz \hat{P}_{qq}(z) \Big\{ \sigma(q + c \to X; \hat{s} = zs) - \sigma(q + c \to X; \hat{s} = s) \Big\}. \tag{3.16}$$

The term in the parenthesis tends to zero in the soft limit, which kills the divergence in $\hat{P}_{qq}(z)$. To simplify writing, we introduce the plus prescription defined by

$$\int_0^1 dz \ \big[g(z)\big]_+ f(z) = \int_0^1 dz \ g(z) \big(f(z) - f(1)\big). \tag{3.17}$$

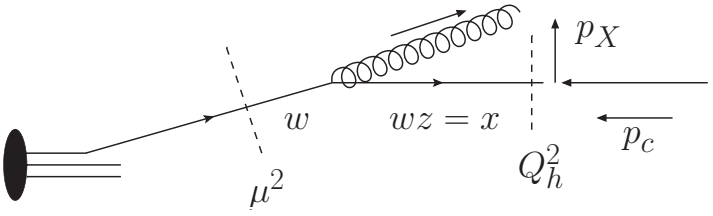

Figure 7: A picture showing that the gluon radiation is evaluated only above the scale μ^2.

Note that the plus prescription is defined only in integrals. By using this, Eq. (3.16) reduces to

$$\sigma(q + c \to X + g; s) = \frac{\alpha_s}{2\pi} \int_0^{Q_h^2} \frac{dQ^2}{Q^2} \int_0^1 dz P_{qq}(z) \sigma(q + c \to X; \hat{s} = zs), \tag{3.18}$$

where

$$P_{qq}(z) = C_F \left(\frac{1 + z^2}{1 - z} \right)_+ . \tag{3.19}$$

This is the most important result in this section. This form of the cross section in eq. (3.18) is universal i.e. it does not depends on the nature of the hard process under consideration, as it is clear from the fact that we have assumed only that a quark is participating in the hard process, when we have derived this. Only the splitting function $P_{qq}(z)$ will be replaced with different one for the other radiation processes. Thus by using the notation in eq. (3.1), the general expression will be

$$\sigma(a_1 + c \to X + a_3; s) = \frac{\alpha_s}{2\pi} \int_0^{Q_h^2} \frac{dQ^2}{Q^2} \int_0^1 dz P_{a_1 \to b a_3}(z) \sigma(b + c \to X; \hat{s} = zs). \tag{3.20}$$

We will derive the other processes too in Section 3.5. What we should notice in eqs. (3.18) or (3.20) is that the integration over Q^2 is divergent at $Q^2 = 0$, despite that this result includes both the real emission correction and the virtual correction. This divergence is often called collinear singularity or collinear divergence, since $Q^2 \simeq E_1 E_3 (\theta_1 - \theta_3)^2$. The treatment of this divergence will be discussed in Section 3.2.

3.2 The DGLAP evolution equation

In order to remove the collinear divergence in eq. (3.18) consistently, we need to introduce two artificial ingredients, namely a cutoff scale μ^2 and parton distribution functions (PDFs) $q(x, \mu^2)$ which is the number density of the quark q carrying a fraction x of the momentum of a proton. The idea is that the integration is carried out only between $\mu^2 < Q^2 < Q_h^2$ and that we assume that the extra contribution from the integration between $0 < Q^2 < \mu^2$ is included in the PDF $q(x, \mu^2)$. The process configuration is described in Figure 7. The fraction which is initially w is changed to $wz = x$ after one gluon emission. Note that x is always the fraction relevant to the hard process $q + c \to X$, and $x = w$ is true only at

the leading order i.e. the order α_s^0. The momentum of the proton is p and we redefine s as $s = (p + p_c)^2$, such that $(k_1 + p_c)^2 = ws$. The order α_s contribution is given by

$$\int_0^1 dw\ q(w,\mu^2)\frac{\alpha_s}{2\pi}\int_{\mu^2}^{Q_h^2}\frac{dQ^2}{Q^2}\int_0^1 dz P_{qq}(z)\sigma(q+c\to X;\hat{s}=zws). \tag{3.21}$$

The leading order term to which the above contribution can be a correction should be written as

$$\int_0^1 dw\ q(w,\mu^2)\sigma(q+c\to X;\hat{s}=ws). \tag{3.22}$$

Considering the idea that a contribution from the integration between $0 < Q^2 < \mu^2$ is included in the PDF $q(x,\mu^2)$, the following relation should be correct at the order α_s accuracy,

$$\begin{aligned}&\int_0^1 dx\ q(x,Q_h^2)\sigma(X;\hat{s}=xs)\\ &=\int_0^1 dw\ q(w,\mu^2)\sigma(X;\hat{s}=ws)+\int_0^1 dw\ q(w,\mu^2)\frac{\alpha_s}{2\pi}\int_{\mu^2}^{Q_h^2}\frac{dQ^2}{Q^2}\int_0^1 dz P_{qq}(z)\sigma(X;\hat{s}=zws),\end{aligned} \tag{3.23}$$

where a short notation $\sigma(X;\hat{s}) = \sigma(q + c \to X;\hat{s})$ is used. In the left hand side (LHS) of eq. (3.23), the contribution from the integration between $0 < Q^2 < Q_h^2$ is included in the PDF $q(x,Q_h^2)$. The right hand side (RHS) is the sum of eqs. (3.21) and (3.22), where the PDF takes care of the integration only between $0 < Q^2 < \mu^2$ and the rest of the integration between $\mu^2 < Q^2 < Q_h^2$ is explicitly carried out at the order α_s. The RHS is simplified as

$$\begin{aligned}\text{RHS}&=\int_0^1 dw\ q(w,\mu^2)\int_0^1 dz\left\{\delta(1-z)+\frac{\alpha_s}{2\pi}\int_{\mu^2}^{Q_h^2}\frac{dQ^2}{Q^2}P_{qq}(z)\right\}\sigma(X;\hat{s}=zws)\\ &=\int_0^1 dx\ \int_0^1\frac{dz}{z}\left\{\delta(1-z)+\frac{\alpha_s}{2\pi}\int_{\mu^2}^{Q_h^2}\frac{dQ^2}{Q^2}P_{qq}(z)\right\}q\Big(\frac{x}{z},\mu^2\Big)\sigma(X;\hat{s}=xs),\end{aligned} \tag{3.24}$$

from which we find

$$q(x,Q_h^2)=\int_0^1\frac{dz}{z}\left\{\delta(1-z)+\frac{\alpha_s}{2\pi}\int_{\mu^2}^{Q_h^2}\frac{dQ^2}{Q^2}P_{qq}(z)\right\}q\Big(\frac{x}{z},\mu^2\Big), \tag{3.25}$$

or

$$q(x,Q_h^2)=q(x,\mu^2)+\frac{\alpha_s}{2\pi}\int_{\mu^2}^{Q_h^2}\frac{dQ^2}{Q^2}\int_0^1\frac{dz}{z}P_{qq}(z)q\Big(\frac{x}{z},\mu^2\Big). \tag{3.26}$$

Since $q(x,Q_h^2)$ does not depend on μ^2, it follows that

$$\frac{d}{d\mu^2}q(x,Q_h^2)=0. \tag{3.27}$$

This leads to the following equation at the order α_s accuracy,

$$\mu^2 \frac{d}{d\mu^2} q(x,\mu^2) = \frac{\alpha_s}{2\pi} \int_0^1 \frac{dz}{z} q\Big(\frac{x}{z},\mu^2\Big) P_{qq}(z). \tag{3.28}$$

This is called the DGLAP (evolution) equation [19, 20, 21] [6]. This equation is incomplete, since the proton contains gluons and antiquarks too. Because this equation is necessary and enough in order to discuss the role and physical meaning of the DGLAP equation, let us continue our discussion with this result and postpone the derivation of the complete result until Section 3.5.

Let us introduce a scale variable $t = \mu^2$ and $dp(z) = dz/z(\alpha_s/2\pi)P_{qq}(z)$, just in order to simplify writing. Now the DGLAP equation is written as

$$t \frac{d}{dt} q(x,t) = \int_0^1 dp(z) q\Big(\frac{x}{z},t\Big). \tag{3.29}$$

First of all, we introduce two scales t_X and t_Λ, where t_X is the scale associated with a hard process producing an object X and t_Λ is an arbitrary lower cutoff scale. We assume that the hard process is induced by a quark carrying a fraction x of the momentum of the proton. We carry out the t integration in the DGLAP equation between $t_\Lambda < t < t_X$, which leads to

$$q(x,t_X) = q(x,t_\Lambda) + \int_{t_\Lambda}^{t_X} \frac{dt_1}{t_1} \int_0^1 dp(z_1) q\Big(\frac{x}{z_1},t_1\Big). \tag{3.30}$$

What we should be careful at this point is that this integrated form of the DGLAP equation is not identical to eq. (3.26). The quark PDF $q(x/z_1,t_1)$ includes every contribution below t_1. Thus, the contribution of each term on the RHS can be read as follows.

$$q(x,t_\Lambda) : \text{ 0 rad. above } \mathrm{t}_\Lambda$$

$$\int_{t_\Lambda}^{t_X} \frac{dt_1}{t_1} \int_0^1 dp(z_1) q\Big(\frac{x}{z_1},t_1\Big) : \text{ 1 rad. above } \mathrm{t}_1 \text{ and at least 1 rad. above } \mathrm{t}_\Lambda$$

The first term should be clear. The second term includes not only the one radiation contribution at the scale t_1 but also all possible radiation between $t_\Lambda < t < t_1$. In other words, there is only one radiation exclusively above t_1. This statement can be explicitly confirmed by using eq. (3.30) iteratively. After one iteration,

$$\begin{aligned}
&q(x,t_X) \\
&= q(x,t_\Lambda) + \int_{t_\Lambda}^{t_X} \frac{dt_1}{t_1} \int_0^1 dp(z_1) q\Big(\frac{x}{z_1},t_1\Big) \\
&= q(x,t_\Lambda) + \int_{t_\Lambda}^{t_X} \frac{dt_1}{t_1} \int_0^1 dp(z_1) \left\{ q\Big(\frac{x}{z_1},t_\Lambda\Big) + \int_{t_\Lambda}^{t_1} \frac{dt_2}{t_2} \int_0^1 dp(z_2) q\Big(\frac{x}{z_1 z_2},t_2\Big) \right\} \\
&= q(x,t_\Lambda) + \int_{t_\Lambda}^{t_X} \frac{dt_1}{t_1} \int_0^1 dp(z_1) q\Big(\frac{x}{z_1},t_\Lambda\Big) + \int_{t_\Lambda}^{t_X} \frac{dt_1}{t_1} \int_0^1 dp(z_1) \int_{t_\Lambda}^{t_1} \frac{dt_2}{t_2} \int_0^1 dp(z_2) q\Big(\frac{x}{z_1 z_2},t_2\Big).
\end{aligned} \tag{3.31}$$

[6] DGLAP: Dokshitzer, Gribov, Lipatov, Altarelli, Parisi

The contribution of each term can be understood as follows.

$$
\begin{aligned}
q(x,t_\Lambda) &: \text{ 0 rad. above } t_\Lambda \\
\int_{t_\Lambda}^{t_X}\frac{dt_1}{t_1}\int_0^1 dp(z_1) q\left(\frac{x}{z_1},t_\Lambda\right) &: \text{ 1 rad. above } t_\Lambda \\
\int_{t_\Lambda}^{t_X}\frac{dt_1}{t_1}\int_0^1 dp(z_1)\int_{t_\Lambda}^{t_1}\frac{dt_2}{t_2}\int_0^1 dp(z_2) q\left(\frac{x}{z_1 z_2},t_2\right) &: \text{ 2 rad. above } t_2 \text{ and at least 2 rad. above } t_\Lambda
\end{aligned}
$$

where one more radiation is made explicit. After infinite iterations, we find

$$
\begin{aligned}
& q(x,t_X) \\
&= q(x,t_\Lambda) + \int_{t_\Lambda}^{t_X}\frac{dt_1}{t_1}\int_0^1 dp(z_1) q\left(\frac{x}{z_1},t_\Lambda\right) + \int_{t_\Lambda}^{t_X}\frac{dt_1}{t_1}\int_0^1 dp(z_1)\int_{t_\Lambda}^{t_1}\frac{dt_2}{t_2}\int_0^1 dp(z_2) q\left(\frac{x}{z_1 z_2},t_\Lambda\right) + \cdots \\
&\quad + \int_{t_\Lambda}^{t_X}\frac{dt_1}{t_1}\int_0^1 dp(z_1)\int_{t_\Lambda}^{t_1}\frac{dt_2}{t_2}\int_0^1 dp(z_2)\cdots\int_{t_\Lambda}^{t_{n-1}}\frac{dt_n}{t_n}\int_0^1 dp(z_n) q\left(\frac{x}{z_1 z_2\cdots z_n},t_\Lambda\right) + \cdots \\
&= q(x,t_\Lambda) + \ln\frac{t_X}{t_\Lambda}\int_0^1 dp(z_1) q\left(\frac{x}{z_1},t_\Lambda\right) + \frac{1}{2}\ln^2\frac{t_X}{t_\Lambda}\int_0^1 dp(z_1)\int_0^1 dp(z_2) q\left(\frac{x}{z_1 z_2},t_\Lambda\right) + \cdots \\
&\quad + \frac{1}{n!}\ln^n\frac{t_X}{t_\Lambda}\int_0^1 dp(z_1)\int_0^1 dp(z_2)\cdots\int_0^1 dp(z_n) q\left(\frac{x}{z_1 z_2\cdots z_n},t_\Lambda\right) + \cdots ,
\end{aligned}
\tag{3.32}
$$

from which it should be clear that the logarithmic term

$$
\frac{\alpha_s}{2\pi}\ln\frac{t_X}{t_\Lambda}, \tag{3.33}
$$

which can be large if $t_\Lambda \ll t_X$, is summed up to infinite orders. In other words, the effects of the infinite number of radiation which can occur during the scale evolution from t_Λ to t_X can be included in $q(x,t_X)$ by using the DGLAP equation and $q(x,t_\Lambda)$ as an initial condition.

Let us discuss the event generation for the Higgs plus 2-parton production which we have already encountered in Section 2.3, by using the knowledge which we have gained so far [7]. By using the universal expression in eq. (3.20), the parton level cross section of the Higgs plus 2-parton initiated by the qq state is

$$
\begin{aligned}
& \sigma(q+q\to H+q+q;s) \\
&= \left(\frac{\alpha_s}{2\pi}\right)^2\int_0^{m_H^2}\frac{dQ_1^2}{Q_1^2}\int_0^1 dz_1 P_{gq}(z_1)\int_0^{m_H^2}\frac{dQ_2^2}{Q_2^2}\int_0^1 dz_2 P_{gq}(z_2)\ \sigma(g+g\to H;\hat{s}=z_1 z_2 s) \\
&\simeq \left(\frac{\alpha_s}{2\pi}\right)^2\int_0^{m_H^2}\frac{dp_{T3}^2}{p_{T3}^2}\int_0^1 dz_1 P_{gq}(z_1)\int_0^{m_H^2}\frac{dp_{T4}^2}{p_{T4}^2}\int_0^1 dz_2 P_{gq}(z_2)\ \sigma(g+g\to H;\hat{s}=z_1 z_2 s),
\end{aligned}
\tag{3.34}
$$

[7] The discussion on the $t\bar{t}$ plus 2-parton production should be equivalent.

where the virtuality of the colliding gluons is replaced with the transverse momentum of the emitted quark, which is a good approximation. We introduce the quark PDFs with a cut off scale $p_{T\mathrm{cut}}$ as we did in eq. (3.23), then the above equation becomes

$$\begin{aligned}
&\int_0^1 dw_1\ q(w_1, p^2_{T\mathrm{cut}}) \int_0^1 dw_2\ q(w_2, p^2_{T\mathrm{cut}}) \\
&\times \left(\frac{\alpha_s}{2\pi}\right)^2 \int_{p^2_{T\mathrm{cut}}}^{m_H^2} \frac{dp^2_{T3}}{p^2_{T3}} \int_0^1 dz_1 P_{gq}(z_1) \int_{p^2_{T\mathrm{cut}}}^{m_H^2} \frac{dp^2_{T4}}{p^2_{T4}} \int_0^1 dz_2 P_{gq}(z_2)\ \sigma(g+g\to H; \hat{s} = w_1 z_1 w_2 z_2 s) \\
&= \int_0^1 dx_1 \int_0^1 dx_2\ \sigma(g+g\to H; \hat{s} = x_1 x_2 s) \frac{\alpha_s}{2\pi} \ln\left(\frac{m_H^2}{p^2_{T\mathrm{cut}}}\right) \int_0^1 \frac{dz_1}{z_1} P_{gq}(z_1) q\left(\frac{x_1}{z_1}, p^2_{T\mathrm{cut}}\right) \\
&\times \frac{\alpha_s}{2\pi} \ln\left(\frac{m_H^2}{p^2_{T\mathrm{cut}}}\right) \int_0^1 \frac{dz_2}{z_2} P_{gq}(z_2) q\left(\frac{x_2}{z_2}, p^2_{T\mathrm{cut}}\right), \qquad (3.35)
\end{aligned}$$

where $x_i = w_i z_i$. The logarithmic term $\ln m_H^2/p^2_{T\mathrm{cut}}$ can be larger for a smalller $p^2_{T\mathrm{cut}}$ with respect to m_H^2 and has a potential to break perturbative expansion. What we should notice by looking at this equation and eq. (3.32) is that the cross section written as

$$\int_0^1 dx_1 \int_0^1 dx_2\ \sigma(g+g\to H; \hat{s} = x_1 x_2 s) g(x_1, m_H^2) g(x_2, m_H^2) \qquad (3.36)$$

includes the term in eq. (3.35) and also more radiation effects up to the infinite number [8]. An obvious problem in the expression of the cross section in eq. (3.36) is that it does not predict anything about the kinematics of emitted partons, whose angular correlations are our interest. Section 3.3 discusses how to predict the kinematics of emitted partons, while the cross section is described in the form of eq. (3.36). The strategy will be to generate radiation according to probabilities predicted by the DGLAP equation, by using a Monte Carlo approach.

3.3 The DGLAP evolution equation with the Sudakov form factor

Let us copy eq. (3.32), which has been obtained by using the integrated form of the DGLAP equation iteratively, below after dividing by $q(x, t_X)$,

$$\begin{aligned}
1 = \frac{q(x,t_\Lambda)}{q(x,t_X)} &+ \ln\frac{t_X}{t_\Lambda} \int_0^1 dp(z_1) \frac{q\left(\frac{x}{z_1}, t_\Lambda\right)}{q(x,t_X)} + \frac{1}{2}\ln^2\frac{t_X}{t_\Lambda} \int_0^1 dp(z_1) \int_0^1 dp(z_2) \frac{q\left(\frac{x}{z_1 z_2}, t_\Lambda\right)}{q(x,t_X)} + \cdots \\
&+ \frac{1}{n!}\ln^n\frac{t_X}{t_\Lambda} \int_0^1 dp(z_1) \int_0^1 dp(z_2) \cdots \int_0^1 dp(z_n) \frac{q\left(\frac{x}{z_1 z_2 \cdots z_n}, t_\Lambda\right)}{q(x,t_X)} + \cdots . \qquad (3.37)
\end{aligned}$$

[8] The expansion in eq. (3.32) includes only a quark PDF, since we have started from the DGLAP equation which includes only a quark PDF. It is not very difficult, however, to find (guess) that the gluon PDF at the scale t_X is expanded in terms of a quark PDF at the scale t_Λ by starting from the DGLAP equation of gluon in eq. (3.104b).

Noticing that a PDF $q(x,t)$ simply represents a structure of a proton expressed by q and x at the scale t, the probability of finding a structure $q(x)$ at t_Λ in a proton whose structure used to be $q(x)$ too at t_X should be given by $q(x,t_\Lambda)/q(x,t_X)$. Therefore, the first term of the RHS in eq. (3.37) can be read as the probability of having the same structure during a scale evolution from t_X to t_Λ, in other words no radiation probability [9]. Then, the second term of the RHS represents the probability of having exclusively one radiation during an evolution from t_X to t_Λ, and so on. The LHS in eq. (3.37) ensures the probability conservation. Our goal is to generate actual radiation according to these probabilities. When we do this by using a Monte Carlo approach, it turns out that we basically obtain t and z for each radiation in order to describe the kinematics of the radiation. However, the plus prescription in the splitting functions is not suitable for this purpose. We use the splitting functions without the virtual correction instead and include the virtual correction with a different form, the Sudakov form factor which is defined by

$$\Delta(t) = \exp\left(-\int_{\mu^2}^{t}\frac{dt'}{t'}\int_0^1 dz\frac{\alpha_s}{2\pi}\hat{P}_{qq}(z)\right). \tag{3.38}$$

With the Sudakov form factor, the DGLAP equation in eq. (3.28) has the following form [39],

$$\begin{aligned} t\frac{d}{dt}q(x,t) &= \frac{\alpha_s}{2\pi}\int_0^1\frac{dz}{z}P_{qq}(z)q\Big(\frac{x}{z},t\Big) \\ &= \frac{\alpha_s}{2\pi}\int_0^1\frac{dz}{z}\hat{P}_{qq}(z)q\Big(\frac{x}{z},t\Big) - \frac{\alpha_s}{2\pi}\int_0^1 dz\hat{P}_{qq}(z)q(x,t) \\ &= \frac{\alpha_s}{2\pi}\int_0^1\frac{dz}{z}\hat{P}_{qq}(z)q\Big(\frac{x}{z},t\Big) + \frac{q(x,t)}{\Delta(t)}t\frac{d\Delta(t)}{dt}, \end{aligned} \tag{3.39}$$

thus

$$t\frac{d}{dt}\frac{q(x,t)}{\Delta(t)} = \frac{\alpha_s}{2\pi}\int_0^1\frac{dz}{z}\hat{P}_{qq}(z)\frac{q\big(\frac{x}{z},t\big)}{\Delta(t)}. \tag{3.40}$$

An integration over $t_\Lambda < t < t_X$ leads to the integrated form

$$\frac{q(x,t_X)}{\Delta(t_X)} = \frac{q(x,t_\Lambda)}{\Delta(t_\Lambda)} + \int_{t_\Lambda}^{t_X}\frac{dt}{t}\int_0^1 d\hat{p}(z)q\Big(\frac{x}{z},t\Big)\frac{1}{\Delta(t)}, \tag{3.41}$$

where a short hand notation is used,

$$d\hat{p}(z) = \frac{\alpha_s}{2\pi}\frac{dz}{z}\hat{P}_{qq}(z). \tag{3.42}$$

After the infinite iterations of eq. (3.41) , it is found that

$$\begin{aligned} \frac{q(x,t_X)}{\Delta(t_X)} =& \frac{q(x,t_\Lambda)}{\Delta(t_\Lambda)} + \int_{t_\Lambda}^{t_X}\frac{dt_1}{t_1}\int_0^1 d\hat{p}(z_1)q\Big(\frac{x}{z_1},t_\Lambda\Big)\frac{1}{\Delta(t_\Lambda)} \\ &+ \int_{t_\Lambda}^{t_X}\frac{dt_1}{t_1}\int_0^1 d\hat{p}(z_1)\int_{t_\Lambda}^{t_1}\frac{dt_2}{t_2}\int_0^1 d\hat{p}(z_2)q\Big(\frac{x}{z_1z_2},t_\Lambda\Big)\frac{1}{\Delta(t_\Lambda)} + \cdots . \end{aligned} \tag{3.43}$$

[9] I think that this is also clear from our discussion at around eq. (3.31)

By dividing this equation by $q(x,t_X)/\Delta(t_X)$, we find

$$1 = \frac{q(x,t_\Lambda)}{q(x,t_X)}\frac{\Delta(t_X)}{\Delta(t_\Lambda)} + \int_{t_\Lambda}^{t_X}\frac{dt_1}{t_1}\int_0^1 d\hat{p}(z_1)\frac{q\left(\frac{x}{z_1},t_\Lambda\right)}{q(x,t_X)}\frac{\Delta(t_X)}{\Delta(t_\Lambda)} + \int_{t_\Lambda}^{t_X}\frac{dt_1}{t_1}\int_0^1 d\hat{p}(z_1)\int_{t_\Lambda}^{t_1}\frac{dt_2}{t_2}\int_0^1 d\hat{p}(z_2)\frac{q\left(\frac{x}{z_1z_2},t_\Lambda\right)}{q(x,t_X)}\frac{\Delta(t_X)}{\Delta(t_\Lambda)} + \cdots \tag{3.44}$$

This equation, derived from the new DGLAP equation, should be compared with eq. (3.37) which has been derived from the original DGLAP equation. The same discussion below eq. (3.37) can be applied to this equation too. The first term of the RHS in eq. (3.44) can be read as the probability of no radiation during a scale evolution from t_X to t_Λ. We define this in the following form,

$$\Pi(t_1,t_2,x) = \frac{q(x,t_2)}{q(x,t_1)}\frac{\Delta(t_1)}{\Delta(t_2)}. \tag{3.45}$$

We might call this a Sudakov form factor too sometimes in this thesis. By using this form, we can express the second term in eq. (3.44), which is the probability of having one radiation exclusively during a scale evolution from t_X to t_Λ, as

$$\begin{aligned}&\int_{t_\Lambda}^{t_X}\frac{dt_1}{t_1}\int_0^1 d\hat{p}(z_1)\frac{q(x,t_1)}{q(x,t_X)}\frac{\Delta(t_X)}{\Delta(t_1)}\frac{q(x/z_1,t_1)}{q(x,t_1)}\frac{q(x/z_1,t_\Lambda)}{q(x/z_1,t_1)}\frac{\Delta(t_1)}{\Delta(t_\Lambda)}\\ &= \int_{t_\Lambda}^{t_X}\frac{dt_1}{t_1}\int_0^1 d\hat{p}(z_1)\ \Pi(t_X,t_1,x)\ \frac{q(x/z_1,t_1)}{q(x,t_1)}\ \Pi(t_1,t_\Lambda,x/z_1).\end{aligned} \tag{3.46}$$

The third term in eq. (3.44) is also expressed in the same manner. Therefore eq. (3.44) has the following expression,

$$\begin{aligned}1 = \Pi(t_X,t_\Lambda,x) &+ \int_{t_\Lambda}^{t_X}\frac{dt_1}{t_1}\int_0^1 d\hat{p}(z_1)\ \Pi(t_X,t_1,x)\ \frac{q(x/z_1,t_1)}{q(x,t_1)}\ \Pi(t_1,t_\Lambda,x/z_1)\\ &+ \int_{t_\Lambda}^{t_X}\frac{dt_1}{t_1}\int_0^1 d\hat{p}(z_1)\int_{t_\Lambda}^{t_1}\frac{dt_2}{t_2}\int_0^1 d\hat{p}(z_2)\Pi(t_X,t_1,x)\frac{q(x/z_1,t_1)}{q(x,t_1)}\Pi(t_1,t_2,x/z_1)\frac{q(x/z_1z_2,t_2)}{q(x/z_1,t_2)}\Pi(t_2,t_\Lambda,x/z_1z_2)\\ &+\cdots.\end{aligned} \tag{3.47}$$

From this equation, it is easy to guess the explicit form of $\Pi(t_1,t_2,x)$. In order to satisfy this equation at the order α_s^1 accuracy, the first term of the RHS must be[10]

$$\Pi(t_X,t_\Lambda,x) = 1 - \int_{t_\Lambda}^{t_X}\frac{dt}{t}\int_0^1 d\hat{p}(z)\frac{q(x/z,t)}{q(x,t)}. \tag{3.48}$$

[10]Remember that $d\hat{p}(z)$ includes one α_s, see eq. (3.42).

Furthermore, in order to satisfy eq. (3.47) at the order α_s^2 accuracy, it is easy to show that the first term of the RHS must be

$$\begin{aligned}\Pi(t_X, t_\Lambda, x) &= 1 - \int_{t_\Lambda}^{t_X} \frac{dt}{t} \int_0^1 d\hat{p}(z) \frac{q(x/z,t)}{q(x,t)} \\ &\quad + \int_{t_\Lambda}^{t_X} \frac{dt_1}{t_1} \int_0^1 d\hat{p}(z_1) \frac{q(x/z_1,t_1)}{q(x,t_1)} \int_{t_\Lambda}^{t_1} \frac{dt_2}{t_2} \int_0^1 d\hat{p}(z_2) \frac{q(x/z_2,t_2)}{q(x,t_2)} \\ &= 1 - \int_{t_\Lambda}^{t_X} \frac{dt}{t} \int_0^1 d\hat{p}(z) \frac{q(x/z,t)}{q(x,t)} + \frac{1}{2} \left(\int_{t_\Lambda}^{t_X} \frac{dt}{t} \int_0^1 d\hat{p}(z) \frac{q(x/z,t)}{q(x,t)} \right)^2 . \end{aligned} \tag{3.49}$$

By repeating this procedure, we should find a form [44]

$$\Pi(t_1, t_2, x) = \exp\left(- \int_{t_2}^{t_1} \frac{dt}{t} \int_0^1 d\hat{p}(z) \frac{q(x/z,t)}{q(x,t)} \right). \tag{3.50}$$

Let us think how we can generate radiations based on the set up we have developed so far. Suppose that we want to generate the first radiation described by t and z during an evolution from a higher scale t_X of the hard process producing a particle X to a lower scale t_Λ. The integrated form of the DGLAP equation in eq. (3.47) gives

$$1 - \Pi(t_X, t_\Lambda, x) = \int_{t_\Lambda}^{t_X} \frac{dt}{t} \int_0^1 d\hat{p}(z)\ \Pi(t_X, t, x)\ \frac{q(x/z,t)}{q(x,t)}, \tag{3.51}$$

where the RHS should mean the integrated probability of generating at least one radiation. Thus the probability distribution of generating the first radiation at the scale t should be given by

$$\frac{1}{t} \int_0^1 d\hat{p}(z)\ \Pi(t_X, t, x)\ \frac{q(x/z,t)}{q(x,t)}. \tag{3.52}$$

We want to generate a value of t randomly according to this probability distribution. What we should notice is that the derivative of $\Pi(t_X, t, x)$ gives the distribution, namely

$$\frac{d\Pi(t_X, t, x)}{dt} = \frac{1}{t} \int_0^1 d\hat{p}(z)\ \Pi(t_X, t, x)\ \frac{q(x/z,t)}{q(x,t)}. \tag{3.53}$$

By introducing a probability distribution $f(r)$ for random number which is distributed in the range $0 < r < 1$, thus $f(r) = 1$ by definition, the following equation can be confirmed from the probability conservation,

$$\int_0^1 dr f(r) = \int_0^{t_X} dt \frac{d\Pi(t_X, t, x)}{dt} = 1. \tag{3.54}$$

At some value of r and t, the following should be satisfied,

$$\int_r^1 dr' f(r') = \int_t^{t_X} dt' \frac{d\Pi(t_X, t', x)}{dt'}. \tag{3.55}$$

By solving this, it is found that

$$r = \Pi(t_X, t, x). \tag{3.56}$$

Therefore, we can find t randomly from the inverse function of $\Pi(t_X, x; r)$ with a random number r,

$$t = \Pi^{-1}(t_X, x; r). \tag{3.57}$$

Once the scale t is found, z is also obtained randomly by using the same method. The probability distribution of z can be read again from eq. (3.51),

$$\frac{1}{z}\hat{P}_{qq}(z)q(x/z, t), \tag{3.58}$$

where only the z dependent factors are kept. Since the integration of this probability distribution is not necessarily unity, by introducing a normalization

$$N = \int_0^1 \frac{dz}{z}\hat{P}_{qq}(z)q(x/z, t), \tag{3.59}$$

z is found from

$$r = \frac{1}{N}\int_0^z \frac{dz'}{z'}\hat{P}_{qq}(z')q(x/z', t). \tag{3.60}$$

Although the integration is infinite at $z = 1$, the integration region is kinematically constrained so that $z = 1$ is effectively avoided. We will discuss this issue below. Now that we have completed one parton generation described by t_1 and z_1, the next generation is performed in the same manner but this time the evolution starts not from t_X but from t_1, then ordering of the scale is achieved. The algorithm is repeated until the scale chosen is below the scale t_Λ. After one scale evolution from t_X to t_Λ, the event structure, which used to have only the particle X, has now X plus multi-parton in the final state. The number of partons are determined in the probabilistic manner, thus it can be 0 or even 1000. This probabilistic algorithm for generating parton radiation according to the DGLAP equation with the Sudakov form factor is called the parton shower Monte Carlo program.

So far we have discussed only the radiation from incoming partons from a proton i.e. initial state radiation. The DGLAP equation can also be used to predict the radiation from produced outgoing partons .i.e. final state radiation. For this purpose, what we should notice is only that the PDFs $q(x, t)$, which represents a structure of a proton expressed by q and x at the scale t, have a role in constraining the evolution in the DGLAP equation. Therefore, the PDFs in the DGLAP equation can be just replaced with a function which represents a configuration of produced outgoing partons and thus constraints radiation from the outgoing partons. In the following we derive the DGLAP equation which can be generally used both for initial state radiation and final state radiation, without distinguishing them.

By introducing a constraint function $f(z,t;\{p\}_n)$ where $\{p\}_n$ denotes the event configuration consisting of n-parton, eq. (3.47) is generalized to

$$
\begin{aligned}
1 &= \Pi(t_X, t_\Lambda, \{p\}_X) + \int_{t_\Lambda}^{t_X} \frac{dt_1}{t_1} \int_0^1 d\hat{p}(z_1)\ \Pi(t_X, t_1, \{p\}_X)\ f(z_1, t_1; \{p\}_X)\ \Pi(t_1, t_\Lambda, \{p\}_{X+1}) \\
&+ \int_{t_\Lambda}^{t_X} \frac{dt_1}{t_1} \int_0^1 d\hat{p}(z_1) \Pi(t_X, t_1, \{p\}_X)\ f(z_1, t_1; \{p\}_X) \\
&\quad \times \int_{t_\Lambda}^{t_1} \frac{dt_2}{t_2} \int_0^1 d\hat{p}(z_2) \Pi(t_1, t_2, \{p\}_{X+1}) f(z_2, t_2; \{p\}_{X+1})\ \Pi(t_2, t_\Lambda, \{p\}_{X+2}) \\
&+ \cdots,
\end{aligned}
\tag{3.61}
$$

and accordingly

$$
\Pi(t_1, t_2, \{p\}_n) = \exp\left(- \int_{t_2}^{t_1} \frac{dt}{t} \int_0^1 d\hat{p}(z) f(z, t; \{p\}_n) \right), \tag{3.62}
$$

which is defined as no radiation probability for the n-parton event configuration $\{p\}_n$ as a whole. In other words, this is the probability that the n-parton event configuration remains the same. Note that

$$
\begin{aligned}
d\hat{p}(z) &= \frac{dz}{z} \frac{\alpha_s}{2\pi} \hat{P}_{qq}(z) \quad \text{for initial state radiation,} \\
d\hat{p}(z) &= dz \frac{\alpha_s}{2\pi} \hat{P}_{qq}(z) \quad \text{for final state radiation.}
\end{aligned}
\tag{3.63}
$$

For initial state radiation, the constraint function $f(z,t;\{p\}_n)$ includes PDFs as well as kinematic constraint based on $\{p\}_n$ such as the energy and momentum conservation before and after a radiation, while for final state radiation it includes only kinematic constraint.

Since our discussion here is a bit too general, we introduce the constraint function $f(z,t;\{p\}_n)$ implemented in the PYTHIA8 parton shower program [42, 45]. Suppose one radiation from an outgoing parton a, $a \to bc$. One another parton r, which is called recoiler, is assigned to this radiation process. This procedure uses color information, thus it is said that a and r construct a color dipole. The process is sketched in Figure 14. Once the evolution variable $p_\perp$ is randomly obtained by the above method, the integration region of z is constrained from $m_a < m_{ar}$ by

$$
z_\pm = \frac{1}{2}\left(1 \pm \sqrt{1 - \frac{4p_\perp^2}{m_{ar}^2}}\right). \tag{3.64}
$$

This effectively avoids the soft singularity at $z = 1$. Once z is randomly found in the above range, m_a is calculated from

$$
m_a = \frac{p_\perp}{\sqrt{z(1-z)}}. \tag{3.65}
$$

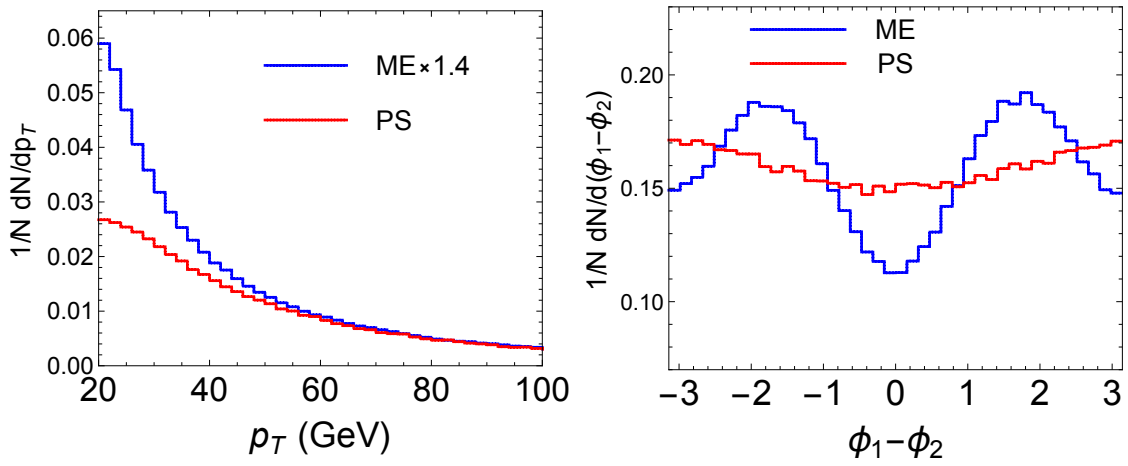

Figure 8: p_T and $\phi_1 - \phi_2$ distributions in the $t\bar{t}$ plus two-parton events.

From a constraint $p^2_{T,\ b} > 0$ or $p^2_{T,\ c} > 0$, there is a further constraint on z,

$$z_\pm = \frac{1}{2}\left(1 \pm \frac{m^2_{ar} - m^2_a}{m^2_{ar} + m^2_a}\right). \tag{3.66}$$

Next, suppose one radiation from an incoming parton a, $a \to bc$, and c becomes an outgoing parton. The recoiler r is always the parton coming from the proton on the other side. The process is sketched in Figure 13. Once the evolution variable $p_\perp$ is randomly obtained by the above method, the integration region of z is constrained by

$$x_b < z < 1 - \frac{p_\perp}{m_{br}}\left(\sqrt{1 + \frac{p^2_\perp}{4m^2_{br}}} - \frac{p_\perp}{2m_{br}}\right), \tag{3.67}$$

where the lower limit comes from $x_a = x_b/z < 1$, the upper limit comes from $p^2_{T,\ c} > 0$. Once z is randomly found in the above range, $-m_b^2$ is calculated from

$$-m_b^2 = \frac{p^2_\perp}{1-z}. \tag{3.68}$$

3.4 Jet simulation with the DGLAP equation

In this section, we present a result of the jet simulation which has been obtained by the method explained in Section 3.3. The result will be compared with the matrix elements prediction.

As a process, we take the top quark pair plus two partons production at the 14 TeV LHC. In order to produce a simulation based on the DGLAP equation, at first the event samples of the process $pp \to t\bar{t}$ are generated according to the matrix elements. Then, extra radiation is randomly generated with a parton shower program. The shower program is

stopped once two partons are generated. The scale in the PDFs i.e. factorization scale is set to the transverse energy of the top quark $\sqrt{p_T^2 + m_t^2}$. The parton shower program also starts from this scale. For another simulation based on matrix elements, the event samples are generated according to the tree level matrix elements of the $t\bar{t}$+2-parton process, which is the same procedure given in Section 2.3. The factorization scale is set to 20 GeV, which is identical to the parton p_T cut. All the matrix element event samples are generated with MadGraph5_aMC@NLO[38] version 5.2.2.1. PYTHIA8 [36, 37] is used as a parton shower program.

The p_T and the azimuthal angle difference $\phi_1 - \phi_2$ distributions after the following kinematic cuts are shown in Figure 8.

$$y_1 \times y_2 < 0, \quad |y_1 - y_2| > 4, \quad m_{t\bar{t}} < 400 \text{ GeV} \tag{3.69}$$

Let us study the left graph at first. An enhancement at the small p_T region is apparent for the matrix elements prediction. This is the logarithmic enhancement which we have discussed at the end of Section 3.2. On the other hand, the prediction with the parton shower program shows a converged distribution at the small p_T region. This convergence is often called a Sudakov suppression, since it is achieved by the Sudakov form factors as we can learn from eq. (3.61). Note that these two predictions are set equal to each other at 100 GeV which is high enough as the matrix elements prediction should be reliable. Next, let us study the right graph. Although the simulation based on the DGLAP equation gives a satisfactory prediction on the p_T distribution, the graph shows that it does not predict the angular correlation. This is what we can expect, since the DGLAP equation includes only the universal logarithmic term while azimuthal angle correlations are not universal i.e. hard process dependent.

One solution to this issue is that we use the exact matrix elements and put a higher cut on p_T such as 60 GeV at which the logarithmic enhancement is not robust anymore. One obvious problem in this method is that we lose many events. We employ the other approach, which is the topic discussed in Section 4.

3.5 The DGLAP evolution equation - complete results

In this section, we derive the complete result of the DGLAP equation, which we have postponed in Section 3.2.

Let us recall that we have derived the following DGLAP equation for the quark PDF at eq. (3.28),

$$\mu^2 \frac{d}{d\mu^2} q(x, \mu^2) = \frac{\alpha_s}{2\pi} \int_0^1 \frac{dz}{z} q\Big(\frac{x}{z}, \mu^2\Big) P_{qq}(z). \tag{3.70}$$

For the complete DGLAP equation for the quark PDF, it is needed to examine the process described in Figure 9 additionally. The calculation proceeds in the similar way as in

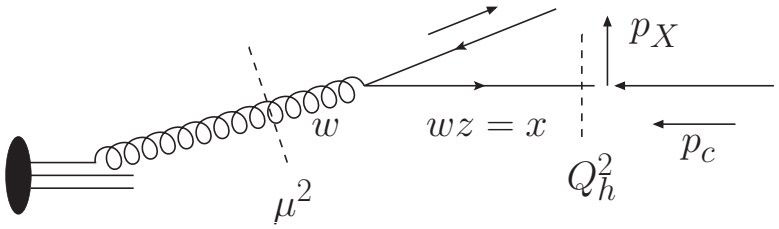

Figure 9: The $g \to q\bar{q}$ splitting which contributes to the quark PDF.

Section 3.1. The current amplitudes for this process are

$$(\mathcal{J}^q_{g\bar{q}})^{\lambda}_{\sigma_1\sigma_3} = \bar{u}(q,\lambda)\gamma^\mu v(k_3,\sigma_3)\epsilon_\mu(k_1,\sigma_1), \tag{3.71}$$

which are easily calculated and the results are

$$(\mathcal{J}^q_{g\bar{q}})^{+}_{+-} = -(\mathcal{J}^q_{g\bar{q}})^{-}_{-+} = -\sqrt{2}Q\sqrt{z}, \tag{3.72}$$

$$(\mathcal{J}^q_{g\bar{q}})^{+}_{--} = -(\mathcal{J}^q_{g\bar{q}})^{-}_{++} = -\sqrt{2}Q\sqrt{z}\frac{1-z}{z}. \tag{3.73}$$

By assigning the color index i for the quark, $\bar{i}$ for the antiquark and a for the gluon, the color factor is calculated as

$$\frac{1}{N_c^2-1}\sum_{a,i,\bar{i}}(t^a)_{i\bar{i}}(t^a)_{\bar{i}i} = \frac{N_c}{N_c^2-1}C_F = T_R. \tag{3.74}$$

We plug-in these results into the helicity amplitudes in eq. (3.2) and we find

$$\begin{aligned}
&\frac{1}{2}\sum_{\sigma_1,\sigma_3}|\mathcal{M}_{\sigma_1\sigma_3}|^2 \\
&\quad= \frac{4\pi\alpha_s T_R}{2Q^4}\Big(\big|(\mathcal{J}^q_{g\bar{q}})^{+}_{+-}(\hat{\mathcal{M}}^X_{qc})_{+}\big|^2 + \big|(\mathcal{J}^q_{g\bar{q}})^{+}_{--}(\hat{\mathcal{M}}^X_{qc})_{+}\big|^2 + \big|(\mathcal{J}^q_{g\bar{q}})^{-}_{-+}(\hat{\mathcal{M}}^X_{qc})_{-}\big|^2 + \big|(\mathcal{J}^q_{g\bar{q}})^{-}_{++}(\hat{\mathcal{M}}^X_{qc})_{-}\big|^2\Big) \\
&\quad= \frac{4\pi\alpha_s}{Q^2}\frac{1}{z}T_R\big\{z^2+(1-z)^2\big\}\Big(\big|(\hat{\mathcal{M}}^X_{qc})_{+}\big|^2 + \big|(\hat{\mathcal{M}}^X_{qc})_{-}\big|^2\Big) \\
&\quad= \frac{8\pi\alpha_s}{Q^2}\frac{1}{z}T_R\big\{z^2+(1-z)^2\big\}\frac{1}{2}\sum_{\lambda}\big|(\hat{\mathcal{M}}^X_{qc})_{\lambda}\big|^2.
\end{aligned} \tag{3.75}$$

This leads to the final result, which should be compared to eq. (3.13),

$$\sigma(g+c\to X+\bar{q};s) = \frac{\alpha_s}{2\pi}\int_0^{Q_h^2}\frac{dQ^2}{Q^2}\int_0^1\frac{dz}{z}P_{qg}(z)\sigma(q+c\to X;\hat{s}=zs), \tag{3.76}$$

where the splitting function for $g \to q\bar{q}$ is

$$P_{qg}(z) = T_R\big\{z^2+(1-z)^2\big\}. \tag{3.77}$$

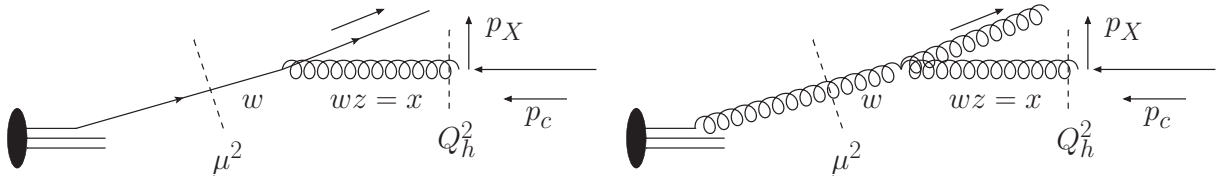

Figure 10: The $q \to gq$ splitting (left) and the $g \to gg$ splitting (right) which contribute to the gluon PDF.

Notice that there is not a soft divergence in eq. (3.76). The divergence at $Q^2 \to 0$ is treated by introducing the gluon PDF,

$$\int_0^1 dw\ g(w,\mu^2)\frac{\alpha_s}{2\pi}\int_{\mu^2}^{Q_h^2}\frac{dQ^2}{Q^2}\int_0^1\frac{dz}{z}P_{qg}(z)\sigma(q+c\to X;\hat{s}=zws). \tag{3.78}$$

This is a new contribution to RHS of eq. (3.23), thus eq. (3.25) is updated to

$$\begin{aligned} q(x,Q_h^2) &= \int_0^1\frac{dz}{z}\left\{\delta(1-z)+\frac{\alpha_s}{2\pi}\int_{\mu^2}^{Q_h^2}\frac{dQ^2}{Q^2}P_{qq}(z)\right\}q\Big(\frac{x}{z},\mu^2\Big)+\frac{\alpha_s}{2\pi}\int_{\mu^2}^{Q_h^2}\frac{dQ^2}{Q^2}\int_0^1\frac{dz}{z}P_{qg}(z)g\Big(\frac{x}{z},\mu^2\Big) \\ &= q(x,\mu^2)+\frac{\alpha_s}{2\pi}\int_{\mu^2}^{Q_h^2}\frac{dQ^2}{Q^2}\int_0^1\frac{dz}{z}\left\{P_{qq}(z)q\Big(\frac{x}{z},\mu^2\Big)+P_{qg}(z)g\Big(\frac{x}{z},\mu^2\Big)\right\}. \end{aligned} \tag{3.79}$$

This equation gives the complete DGLAP equation for the quark PDF, which will be summarized at the end of this Section.

Next, we derive the DGLAP equation for the gluon PDF, for which we need to examine the two processes in Figure 10. A gluon is participating in the hard process, $g + c \to X$ instead of a quark. The helicity amplitudes for these processes are

$$\mathcal{M}_{\sigma_1\sigma_3} \simeq \frac{1}{q^2}\sum_{\lambda=\pm1}(\mathcal{J}^g_{a_1a_3})^{\lambda}_{\sigma_1\sigma_3}(\hat{\mathcal{M}}^X_{g\ c})_\lambda. \tag{3.80}$$

For the left process, the current helicity amplitudes have been already calculated in eqs. (2.69) and (2.72). The helicity summation of the amplitude squared gives

$$\begin{aligned} &\frac{1}{2}\sum_{\sigma_1,\sigma_3}|\mathcal{M}_{\sigma_1\sigma_3}|^2 \\ &\quad= \frac{4\pi\alpha_s C_F}{2Q^4}\left(\Big|(\mathcal{J}^g_{qq})^+_{++}(\hat{\mathcal{M}}^X_{gc})_+ + (\mathcal{J}^g_{qq})^-_{++}(\hat{\mathcal{M}}^X_{gc})_-\Big|^2 + \Big|(\mathcal{J}^g_{qq})^-_{--}(\hat{\mathcal{M}}^X_{gc})_- + (\mathcal{J}^g_{qq})^+_{--}(\hat{\mathcal{M}}^X_{gc})_+\Big|^2\right) \\ &\quad= \frac{4\pi\alpha_s}{Q^2}\frac{1}{z}C_F\left\{\frac{1+(1-z)^2}{z}\Big(\big|(\hat{\mathcal{M}}^X_{gc})_+\big|^2+\big|(\hat{\mathcal{M}}^X_{gc})_-\big|^2\Big)\right. \\ &\qquad\qquad\left. -4\frac{1-z}{z}\Big(Re\big((\hat{\mathcal{M}}^X_{gc})_+(\hat{\mathcal{M}}^X_{gc})^*_-\big)\cos2\phi + Im\big((\hat{\mathcal{M}}^X_{gc})_+(\hat{\mathcal{M}}^X_{gc})^*_-\big)\sin2\phi\Big).\right\} \end{aligned} \tag{3.81}$$

Note that there are terms which depends on the azimuthal angle ϕ of the emitted quark, which induces the azimuthal angle correlations which we have encountered in Section 2.2. Since we are currently not interested in the azimuthal angle dependence, the integration over ϕ is carried out in advance. Then, we find

$$\frac{1}{2}\sum_{\sigma_1,\sigma_3}|\mathcal{M}_{\sigma_1\sigma_3}|^2 = \frac{8\pi\alpha_s}{Q^2}\frac{1}{z}C_F\frac{1+(1-z)^2}{z}\frac{1}{2}\sum_{\lambda}\left|(\hat{\mathcal{M}}^X_{gc})_\lambda\right|^2, \tag{3.82}$$

from which the cross section follows

$$\sigma(q+c\to X+q;s) = \frac{\alpha_s}{2\pi}\int_0^{Q_h^2}\frac{dQ^2}{Q^2}\int_0^1\frac{dz}{z}P_{gq}(z)\sigma(g+c\to X;\hat{s}=zs), \tag{3.83}$$

where the splitting function for $q\to gq$ is

$$P_{gq}(z) = C_F\frac{1+(1-z)^2}{z}. \tag{3.84}$$

Let us evaluate the right process in Figure 10. The current amplitudes for the triple gluon vertex are written as

$$\begin{aligned}(\mathcal{J}^g_{gg})^\lambda_{\sigma_1\sigma_3} &= \epsilon^{\nu*}(k_3,\sigma_3,i_3)\epsilon^{\rho*}(q,\lambda,a)\Gamma^{i_1i_3a}_{\mu\nu\rho}\epsilon^\mu(k_1,\sigma_1,i_1)\\ &= \big(\epsilon(k_1)\cdot\epsilon(k_3)^*\big)\big(\epsilon(q)^*\cdot(k_1+k_3)\big) + \big(\epsilon(k_3)^*\cdot\epsilon(q)^*\big)\big(\epsilon(k_1)\cdot(-k_3+q)\big)\\ &\quad + \big(\epsilon(k_1)\cdot\epsilon(q)^*\big)\big(\epsilon(k_3)^*\cdot(-q-k_1)\big),\end{aligned} \tag{3.85}$$

where at the second line the coupling and color factor $-g_sf^{i_1i_3a}$ are omitted, and the color and helicity indices in the gluon wave functions are suppressed. All of the amplitudes in our phase convention are summarized below.

$$(\mathcal{J}^g_{gg})^+_{++} = -\sqrt{2}Q\frac{1}{\sqrt{z}\sqrt{1-z}}e^{-i\phi}, \qquad (\mathcal{J}^g_{gg})^-_{--} = \sqrt{2}Q\frac{1}{\sqrt{z}\sqrt{1-z}}e^{i\phi}, \tag{3.86a}$$

$$(\mathcal{J}^g_{g\bar{g}})^-_{++} = \sqrt{2}Q\frac{(1-z)^2}{\sqrt{z}\sqrt{1-z}}e^{i\phi}, \qquad (\mathcal{J}^g_{g\bar{g}})^+_{--} = -\sqrt{2}Q\frac{(1-z)^2}{\sqrt{z}\sqrt{1-z}}e^{-i\phi}, \tag{3.86b}$$

$$(\mathcal{J}^g_{g\bar{g}})^+_{+-} = \sqrt{2}Q\frac{z}{\sqrt{z}\sqrt{1-z}}e^{-i\phi}, \qquad (\mathcal{J}^g_{g\bar{g}})^-_{-+} = -\sqrt{2}Q\frac{z}{\sqrt{z}\sqrt{1-z}}e^{i\phi}, \tag{3.86c}$$

$$(\mathcal{J}^g_{g\bar{g}})^-_{+-} = 0, \qquad (\mathcal{J}^g_{g\bar{g}})^+_{-+} = 0. \tag{3.86d}$$

The coupling and the color factor is evaluated

$$\begin{aligned}g_s^2\frac{1}{N_c^2-1}\sum_{i_1,i_3,a}f^{i_1i_3a}f^{i_1i_3a} &= g_s^2\frac{1}{N_c^2-1}C_A(N_c^2-1)\\ &= 4\pi\alpha_s^2C_A.\end{aligned} \tag{3.87}$$

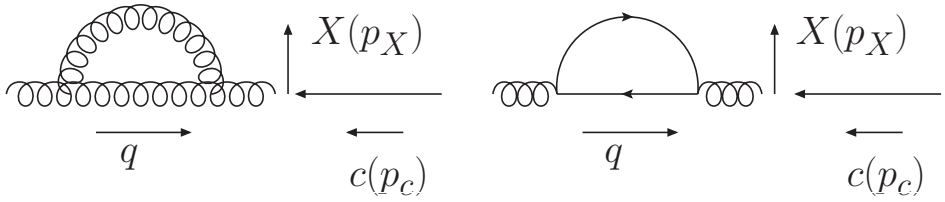

Figure 11: The order α_s virtual corrections to the process $g + c \to X$.

The helicity summation of the amplitude squared gives

$$\begin{aligned}
&\frac{1}{2}\sum_{\sigma_1,\sigma_3}|\mathcal{M}_{\sigma_1\sigma_3}|^2 \\
&\quad= \frac{4\pi\alpha_s C_A}{2Q^4}\bigg(\Big|(\mathcal{J}^g_{gg})^+_{++}(\hat{\mathcal{M}}^X_{gc})_+ + (\mathcal{J}^g_{gg})^-_{++}(\hat{\mathcal{M}}^X_{gc})_-\Big|^2 + \Big|(\mathcal{J}^g_{gg})^+_{+-}(\hat{\mathcal{M}}^X_{gc})_+\Big|^2 \\
&\qquad\qquad + \Big|(\mathcal{J}^g_{gg})^-_{-+}(\hat{\mathcal{M}}^X_{gc})_-\Big|^2 + \Big|(\mathcal{J}^g_{gg})^+_{--}(\hat{\mathcal{M}}^X_{gc})_+ + (\mathcal{J}^g_{gg})^-_{--}(\hat{\mathcal{M}}^X_{gc})_-\Big|^2\bigg) \\
&\quad= \frac{4\pi\alpha_s}{Q^2}\frac{1}{z}C_A\bigg\{\frac{1+(1-z)^4+z^4}{z(1-z)}\Big(\big|(\hat{\mathcal{M}}^X_{gc})_+\big|^2 + \big|(\hat{\mathcal{M}}^X_{gc})_-\big|^2\Big) \\
&\qquad\qquad - 4\frac{1-z}{z}\Big(Re\big((\hat{\mathcal{M}}^X_{gc})_+(\hat{\mathcal{M}}^X_{gc})^*_-\big)\cos 2\phi + Im\big((\hat{\mathcal{M}}^X_{gc})_+(\hat{\mathcal{M}}^X_{gc})^*_-\big)\sin 2\phi\Big)\bigg\}.
\end{aligned} \tag{3.88}$$

By doing the integration over ϕ in advance, we find

$$\begin{aligned}
\frac{1}{2}\sum_{\sigma_1,\sigma_3}|\mathcal{M}_{\sigma_1\sigma_3}|^2 &= \frac{8\pi\alpha_s}{Q^2}\frac{1}{z}C_A\frac{1+(1-z)^4+z^4}{z(1-z)}\frac{1}{2}\sum_\lambda\big|(\hat{\mathcal{M}}^X_{gc})_\lambda\big|^2 \\
&= \frac{8\pi\alpha_s}{Q^2}\frac{1}{z}2C_A\Big(\frac{z}{1-z}+\frac{1-z}{z}+z(1-z)\Big)\frac{1}{2}\sum_\lambda\big|(\hat{\mathcal{M}}^X_{gc})_\lambda\big|^2,
\end{aligned} \tag{3.89}$$

from which the cross section follows

$$\sigma(g+c\to X+g;s) = \frac{\alpha_s}{2\pi}\int_0^{Q^2_h}\frac{dQ^2}{Q^2}\int_0^1 dz\; 2\hat{P}_{gg}(z)\sigma(g+c\to X;\hat{s}=zs), \tag{3.90}$$

where the splitting function for $g \to gg$ is

$$\hat{P}_{gg}(z) = C_A\Big(\frac{z}{1-z}+\frac{1-z}{z}+z(1-z)\Big). \tag{3.91}$$

A factor of 2 is present in eq. (3.90), since there are two gluons after the gluon splitting $g \to gg$ and both of them can participate in the hard process $g + c \to X$. Eqs. (3.83) and (3.90) complete the order α_s real emission correction to the process $g + c \to X$.

The next task is to calculate the order α_s virtual corrections to the process $g + c \to X$ described in Figure 11. Again, by using the trick which has been used to derive eq. (3.15), they will be

$$\begin{aligned}
&-\frac{\alpha_s}{2\pi}\int_0^{Q_h^2}\frac{dQ^2}{Q^2}\int_0^1 dz\big(\hat{P}_{gg}(z)+n_f P_{qg}(z)\big)\sigma(g+c\to X;\hat{s}=zs)\Big|_{z=1}\\
=&-\frac{\alpha_s}{2\pi}\int_0^{Q_h^2}\frac{dQ^2}{Q^2}\int_0^1 dz\big(\hat{P}_{gg}(z)+n_f P_{qg}(z)\big)\sigma(g+c\to X;\hat{s}=s),
\end{aligned}\tag{3.92}$$

where n_f denotes the number of quark flavor which are considered massless. Adding this correction to eq. (3.90), the order α_s result is

$$\begin{aligned}
&\sigma(g+c\to X+g;s)\\
&=\frac{\alpha_s}{2\pi}\int_0^{Q_h^2}\frac{dQ^2}{Q^2}\int_0^1 dz\bigg\{2\hat{P}_{gg}(z)\sigma\big(g+c\to X;\hat{s}=zs\big)-\Big(\hat{P}_{gg}(z)+n_f P_{qg}(z)\Big)\sigma\big(g+c\to X;\hat{s}=s\big)\bigg\}.
\end{aligned}\tag{3.93}$$

The terms proportional to $\hat{P}_{gg}(z)$ are evaluated as follows,

$$\begin{aligned}
&\int_0^1 dz\ 2\hat{P}_{gg}(z)\sigma(zs)-\hat{P}_{gg}(z)\sigma(s)\\
&=C_A\int_0^1 dz\ 2\bigg(\frac{z}{1-z}+\frac{1-z}{z}+z(1-z)\bigg)\sigma(zs)-\bigg(\frac{z}{1-z}+\frac{1-z}{z}+z(1-z)\bigg)\sigma(s)\\
&=C_A\int_0^1 dz\ 2\bigg(\frac{z}{1-z}+\frac{1-z}{z}+z(1-z)\bigg)\sigma(zs)-\bigg(2\frac{z}{1-z}+z(1-z)\bigg)\sigma(s)\\
&=C_A\int_0^1 dz\ \bigg(2\frac{z}{1-z}+z(1-z)\bigg)\Big(\sigma(zs)-\sigma(s)\Big)+\bigg(2\frac{1-z}{z}+z(1-z)\bigg)\sigma(zs)\\
&=C_A\int_0^1 dz\ \bigg(2\frac{z}{1-z}+z(1-z)\bigg)_+\sigma(zs)+\bigg(2\frac{1-z}{z}+z(1-z)\bigg)\sigma(zs)\\
&=C_A\int_0^1 dz\ \bigg\{\bigg(2\frac{z}{1-z}+z(1-z)\bigg)_++\bigg(2\frac{1-z}{z}+z(1-z)\bigg)\bigg\}\sigma(zs).
\end{aligned}\tag{3.94}$$

Evaluation of the rest term is trivial,

$$\begin{aligned}
&-n_f\int_0^1 dz\ P_{qg}(z)\sigma(s)\\
&=-n_f T_R\int_0^1 dz\ \big\{z^2+(1-z)^2\big\}\sigma(s)\\
&=-n_f\frac{2}{3}T_R\sigma(s)\\
&=-n_f\frac{2}{3}T_R\int_0^1 dz\ \delta(1-z)\sigma(zs).
\end{aligned}\tag{3.95}$$

With these calculations, eq. (3.93) is written as

$$\sigma(g+c\to X+g;s)=\frac{\alpha_s}{2\pi}\int_0^{Q_h^2}\frac{dQ^2}{Q^2}\int_0^1 dz P_{gg}(z)\sigma(g+c\to X;\hat{s}=zs), \tag{3.96}$$

where

$$P_{gg}(z)=C_A\left(2\frac{z}{1-z}+z(1-z)\right)_+ +C_A\left(2\frac{1-z}{z}+z(1-z)\right)-n_f\frac{2}{3}T_R\delta(1-z). \tag{3.97}$$

Now that the order α_s correction to the process $g+c\to X$ is completed, we deal with the divergence at $Q^2\to 0$ by introducing a cutoff μ^2 and PDFs. Eqs. (3.83) and (3.96) give rise to, respectively,

$$\int_0^1 dw\ q(w,\mu^2)\frac{\alpha_s}{2\pi}\int_{\mu^2}^{Q_h^2}\frac{dQ^2}{Q^2}\int_0^1 dz P_{gq}(z)\sigma(\hat{s}=zws), \tag{3.98}$$

and

$$\int_0^1 dw\ g(w,\mu^2)\frac{\alpha_s}{2\pi}\int_{\mu^2}^{Q_h^2}\frac{dQ^2}{Q^2}\int_0^1 dz P_{gg}(z)\sigma(\hat{s}=zws). \tag{3.99}$$

The leading order term should be given by

$$\int_0^1 dw\ g(w,\mu^2)\sigma(\hat{s}=ws). \tag{3.100}$$

Here a short notation $\sigma(\hat{s})=\sigma(g+c\to X;\hat{s})$ has been used. The sum of these gives

$$\begin{aligned}
&\int_0^1 dw\int_0^1 dz\left[g(w,\mu^2)\left\{\delta(1-z)+\frac{\alpha_s}{2\pi}\int_{\mu^2}^{Q_h^2}\frac{dQ^2}{Q^2}P_{gg}(z)\right\}+q(w,\mu^2)\frac{\alpha_s}{2\pi}\int_{\mu^2}^{Q_h^2}\frac{dQ^2}{Q^2}P_{gq}(z)\right]\sigma(\hat{s}=zws)\\
&=\int_0^1 dx\int_0^1\frac{dz}{z}\left[g\Big(\frac{x}{z},\mu^2\Big)\left\{\delta(1-z)+\frac{\alpha_s}{2\pi}\int_{\mu^2}^{Q_h^2}\frac{dQ^2}{Q^2}P_{gg}(z)\right\}+q\Big(\frac{x}{z},\mu^2\Big)\frac{\alpha_s}{2\pi}\int_{\mu^2}^{Q_h^2}\frac{dQ^2}{Q^2}P_{gq}(z)\right]\sigma(\hat{s}=xs)\\
&=\int_0^1 dx\left[g(x,\mu^2)+\frac{\alpha_s}{2\pi}\int_{\mu^2}^{Q_h^2}\frac{dQ^2}{Q^2}\int_0^1\frac{dz}{z}\left\{P_{gg}(z)g\Big(\frac{x}{z},\mu^2\Big)+P_{gq}(z)q\Big(\frac{x}{z},\mu^2\Big)\right\}\right]\sigma(\hat{s}=xs).
\end{aligned} \tag{3.101}$$

By comparing this with

$$\int_0^1 dx g(x,Q_h^2)\sigma(\hat{s}=xs), \tag{3.102}$$

we find

$$g(x,Q_h^2)=g(x,\mu^2)+\frac{\alpha_s}{2\pi}\int_{\mu^2}^{Q_h^2}\frac{dQ^2}{Q^2}\int_0^1\frac{dz}{z}\left[P_{gg}(z)g\Big(\frac{x}{z},\mu^2\Big)+P_{gq}(z)\left\{q\Big(\frac{x}{z},\mu^2\Big)+\bar{q}\Big(\frac{x}{z},\mu^2\Big)\right\}\right], \tag{3.103}$$

where the contribution from the antiquark splitting $\bar{q} \to g\bar{q}$ is added.

Let us summarize what we have derived so far. From eqs. (3.79) and (3.103), the DGLAP equations for the quark and gluon PDFs are

$$\mu^2 \frac{d}{d\mu^2} q(x,\mu^2) = \frac{\alpha_s}{2\pi} \int_0^1 \frac{dz}{z} \left\{ P_{qq}(z) q\Big(\frac{x}{z},\mu^2\Big) + P_{qg}(z) g\Big(\frac{x}{z},\mu^2\Big) \right\}, \tag{3.104a}$$

$$\mu^2 \frac{d}{d\mu^2} g(x,\mu^2) = \frac{\alpha_s}{2\pi} \int_0^1 \frac{dz}{z} \left[P_{gg}(z) g\Big(\frac{x}{z},\mu^2\Big) + P_{gq}(z) \left\{ q\Big(\frac{x}{z},\mu^2\Big) + \bar{q}\Big(\frac{x}{z},\mu^2\Big) \right\} \right]. \tag{3.104b}$$

From eqs. (3.19), (3.77), (3.84) and (3.97), the splitting functions are

$$P_{qq}(z) = C_F \left(\frac{1+z^2}{1-z} \right)_+, \tag{3.105a}$$

$$P_{qg}(z) = T_R \big\{ z^2 + (1-z)^2 \big\}, \tag{3.105b}$$

$$P_{gq}(z) = C_F \frac{1+(1-z)^2}{z}, \tag{3.105c}$$

$$P_{gg}(z) = C_A \left(2\frac{z}{1-z} + z(1-z) \right)_+ + C_A \left(2\frac{1-z}{z} + z(1-z) \right) - n_f \frac{2}{3} T_R \delta(1-z). \tag{3.105d}$$

4 Merging matrix elements with parton showers

In Section 3.4, we have explicitly found that both the weak point and the strong point in jet simulation based on the fixed order matrix elements and on the DGLAP evolution equation. The weak point of the fixed order matrix elements calculation is that the large logarithmic terms can break the validity of the fixed order perturbation theory, while the strong point of it is that it correctly produces process dependent predictions such as angular correlation between radiated partons. The strong point of the DGLAP equation is that its prediction takes into account the infinite number of the large logarithmic term, thus convergent results can be obtained. The weak point of the DGLAP equation is that it does not provide process dependent predictions, since it includes only the universal logarithmic term. It is also the case that the DGLAP equation does not necessarily predict hard and large angle radiation correctly.

The purpose of this section is to discuss how to combine these two approaches. This algorithm is called the merging algorithm. A complete merging algorithm was first proposed in ref. [23, 25], which is called the CKKW merging algorithm. The other well-known merging algorithms include the CKKW-L [24, 27, 35] and MLM algorithms [22, 28, 32]. In Section 4.1, the basic idea of the merging algorithm, on which all the merging algorithm are built, is presented. In Section 4.2, the CKKW-L merging algorithm is introduced. Section 4.3 treats a topic which are necessary for the implementation of the CKKW-L merging algorithm with PYTHIA8, namely construction of the PYTHIA8 parton shower history. In Section 4.4, the merging procedure is explained step by step. The implementation of the merging algorithm is tested by comparing the predictions with experimental data in Section 4.5.

4.1 Improvement of the DGLAP equation with matrix elements

Let us copy eqs. (3.61) and (3.62) below, which is the generalized integrated form of the DGLAP equation with the Sudakov form factors,

$$\begin{aligned}
1 &= \Pi(t_X, t_\Lambda, \{p\}_X) + \int_{t_\Lambda}^{t_X} \frac{dt_1}{t_1} \int_0^1 d\hat{p}(z_1)\ \Pi(t_X, t_1, \{p\}_X)\ f(z_1, t_1; \{p\}_X) \\
&= \Pi(t_X, t_\Lambda, \{p\}_X) + \int_{t_\Lambda}^{t_X} \frac{dt_1}{t_1} \int_0^1 d\hat{p}(z_1)\ \Pi(t_X, t_1, \{p\}_X)\ f(z_1, t_1; \{p\}_X)\ \Pi(t_1, t_\Lambda, \{p\}_{X+1}) \\
&+ \int_{t_\Lambda}^{t_X} \frac{dt_1}{t_1} \int_0^1 d\hat{p}(z_1) \Pi(t_X, t_1, \{p\}_X)\ f(z_1, t_1; \{p\}_X) \\
&\quad \times \int_{t_\Lambda}^{t_1} \frac{dt_2}{t_2} \int_0^1 d\hat{p}(z_2) \Pi(t_1, t_2, \{p\}_{X+1}) f(z_2, t_2; \{p\}_{X+1})\ \Pi(t_2, t_\Lambda, \{p\}_{X+2}) \\
&+ \cdots,
\end{aligned} \tag{4.1}$$

$$\Pi(t_1, t_2, \{p\}_n) = \exp\left(- \int_{t_2}^{t_1} \frac{dt}{t} \int_0^1 d\hat{p}(z) f(z, t; \{p\}_n) \right). \tag{4.2}$$

The goal of this Section is to improve the above equation with the help of tree level matrix elements.

At first, let us assume a case in which there is only final state radiation. As such a case, we consider jet production at e^+e^- annihilation. The leading order cross section is given by

$$\sigma(e^+e^- \to q\bar{q}, s) = \frac{1}{2s}\int d\Phi_{q\bar{q}} \overline{\sum_{\lambda}} \left|\mathcal{M}_{q\bar{q}}\right|^2. \tag{4.3}$$

By multiplying the above cross section by eq. (4.1), the following expression is found,

$$\begin{aligned}
&\sigma(q\bar{q}, s) \\
&= \frac{1}{2s}\int d\Phi_{q\bar{q}} \overline{\sum_{\lambda}} \left|\mathcal{M}_{q\bar{q}}\right|^2 \Pi(s, t_\Lambda, \{p\}_{q\bar{q}}) \\
&\quad + \frac{1}{2s}\int d\Phi_{q\bar{q}} \overline{\sum_{\lambda}} \left|\mathcal{M}_{q\bar{q}}\right|^2 \int_{t_\Lambda}^{s} \frac{dt_1}{t_1} \int_0^1 d\hat{p}(z_1) f(z_1, t_1; \{p\}_{q\bar{q}}) \Pi(s, t_1, \{p\}_{q\bar{q}}) \\
&= \frac{1}{2s}\int d\Phi_{q\bar{q}} \overline{\sum_{\lambda}} \left|\mathcal{M}_{q\bar{q}}\right|^2 \Pi(s, t_\Lambda, \{p\}_{q\bar{q}}) \\
&\quad + \frac{1}{2s}\int d\Phi_{q\bar{q}} \overline{\sum_{\lambda}} \left|\mathcal{M}_{q\bar{q}}\right|^2 \int_{t_\Lambda}^{s} \frac{dt_1}{t_1} \int_0^1 d\hat{p}(z_1) f(z_1, t_1; \{p\}_{q\bar{q}}) \Pi(s, t_1, \{p\}_{q\bar{q}}) \Pi(t_1, t_\Lambda, \{p\}_{q\bar{q}+1}) \\
&\quad + \frac{1}{2s}\int d\Phi_{q\bar{q}} \overline{\sum_{\lambda}} \left|\mathcal{M}_{q\bar{q}}\right|^2 \int_{t_\Lambda}^{s} \frac{dt_1}{t_1} \int_0^1 d\hat{p}(z_1) f(z_1, t_1; \{p\}_{q\bar{q}}) \Pi(s, t_1, \{p\}_{q\bar{q}}) \\
&\qquad \times \int_{t_\Lambda}^{t_1} \frac{dt_2}{t_2} \int_0^1 d\hat{p}(z_2) f(z_2, t_2; \{p\}_{q\bar{q}+1}) \Pi(t_1, t_2, \{p\}_{q\bar{q}+1}) \Pi(t_2, t_\Lambda, \{p\}_{q\bar{q}+2}) \\
&\quad + \cdots .
\end{aligned} \tag{4.4}$$

The idea originally proposed in ref. [23] is to replace the terms of the leading order cross section times the factorized universal radiating probability with the cross section for the

higher parton multiplicities,

$$
\begin{aligned}
&\sigma(q\bar{q}, s) \\
&= \frac{1}{2s}\int d\Phi_{q\bar{q}} \overline{\sum_{\lambda}} \left|\mathcal{M}_{q\bar{q}}\right|^2 \Pi(s, t_\Lambda, \{p\}_{q\bar{q}}) \\
&\quad + \frac{1}{2s}\int_{\{p\}_{q\bar{q}+1}>t_\Lambda} d\Phi_{q\bar{q}+1} \bar{\sum_{\lambda}} \left|\mathcal{M}_{q\bar{q}+1}\right|^2 \Pi(s, t_1, \{p\}_{q\bar{q}}) \\
&= \frac{1}{2s}\int d\Phi_{q\bar{q}} \overline{\sum_{\lambda}} \left|\mathcal{M}_{q\bar{q}}\right|^2 \Pi(s, t_\Lambda, \{p\}_{q\bar{q}}) \\
&\quad + \frac{1}{2s}\int_{\{p\}_{q\bar{q}+1}>t_\Lambda} d\Phi_{q\bar{q}+1} \bar{\sum_{\lambda}} \left|\mathcal{M}_{q\bar{q}+1}\right|^2 \Pi(s, t_1, \{p\}_{q\bar{q}}) \Pi(t_1, t_\Lambda, \{p\}_{q\bar{q}+1}) \\
&\quad + \frac{1}{2s}\int_{\{p\}_{q\bar{q}+2}>t_\Lambda} d\Phi_{q\bar{q}+2} \bar{\sum_{\lambda}} \left|\mathcal{M}_{q\bar{q}+2}\right|^2 \Pi(s, t_1, \{p\}_{q\bar{q}}) \Pi(t_1, t_2, \{p\}_{q\bar{q}+1}) \Pi(t_2, t_\Lambda, \{p\}_{q\bar{q}+2}) \\
&\quad + \cdots .
\end{aligned}
\tag{4.5}
$$

This expression states that the kinematics of $q\bar{q}$ plus additional partons are determined according to the exact tree level matrix elements. The soft and collinear divergences in the matrix elements for multi-parton are regularized by a cutoff t_Λ. This cut off scale is called the merging scale. The largest advantage in the merging algorithm is that in principle any number of partons are made generated according to tree level exact matrix elements. The another advantage is that we can choose the merging scale freely as long as it is reasonable. This plays a serious role when we want to simulate angular correlations between jets for instance.

Next, let us assume a case in which there is only initial state radiation. As such a case, we study the Z boson production at proton proton collisions. We write the leading order cross section as

$$
\int_0^1 dx_1 \int_0^1 dx_2 q(x_1, m_z^2)\bar{q}(x_2, m_z^2)\sigma(q\bar{q} \to Z; m_z^2 = x_1 x_2 s). \tag{4.6}
$$

By multiplying the above cross section by eq. (4.1) as before, the following expression is

found.

$$
\begin{aligned}
&\int_0^1 dx_1 \int_0^1 dx_2 q(x_1, m_z^2)\bar{q}(x_2, m_z^2)\sigma(q\bar{q} \to Z; m_z^2 = x_1 x_2 s) \\
&= \int_0^1 dx_1 \int_0^1 dx_2 q(x_1, m_z^2)\bar{q}(x_2, m_z^2)\sigma(q\bar{q} \to Z; m_z^2 = x_1 x_2 s)\Pi(m_z^2, t_\Lambda, \{p\}_Z) \\
&\quad + \int_0^1 dx_1 \int_0^1 dx_2 q(x_1, m_z^2)\bar{q}(x_2, m_z^2)\sigma(q\bar{q} \to Z; m_z^2 = x_1 x_2 s) \\
&\quad \times \int_{t_\Lambda}^{m_z^2} \frac{dt_1}{t_1} \int_0^1 d\hat{p}(z_1) f'(z_1, t_1; \{p\}_Z) \frac{q(x_i/z_1, t_1)}{q(x_i, t_1)} \Pi(m_z^2, t_1, \{p\}_Z) \\
&= \int_0^1 dx_1 \int_0^1 dx_2 q(x_1, m_z^2)\bar{q}(x_2, m_z^2)\sigma(q\bar{q} \to Z; m_z^2 = x_1 x_2 s)\Pi(m_z^2, t_\Lambda, \{p\}_Z) \\
&\quad + \int_0^1 dx_1 \int_0^1 dx_2 q(x_1, m_z^2)\bar{q}(x_2, m_z^2)\sigma(q\bar{q} \to Z; m_z^2 = x_1 x_2 s) \\
&\quad \times \int_{t_\Lambda}^{m_z^2} \frac{dt_1}{t_1} \int_0^1 d\hat{p}(z_1) f'(z_1, t_1; \{p\}_Z) \frac{q(x_i/z_1, t_1)}{q(x_i, t_1)} \Pi(m_z^2, t_1, \{p\}_Z)\Pi(t_1, t_\Lambda, \{p\}_{Z+1}) \\
&\quad + \cdots ,
\end{aligned}
\tag{4.7}
$$

where the PDF factors are extracted from the constraint functions and are explicitly shown. Note that $\{p\}_{Z+n}$ includes the incoming two partons implicitly. The last term in the above equation, which contributes to the one radiation exclusive above t_Λ, will be corrected with the fixed order prediction for the $Z+1$-parton process, as follows.

$$
\begin{aligned}
&\int_0^1 dx_1 \int_0^1 dx_2 q(x_1, m_z^2)\bar{q}(x_2, m_z^2)\sigma\big(q\bar{q} \to Z; m_z^2 = x_1 x_2 s\big) \\
&\quad \times \int_{t_\Lambda}^{m_z^2} \frac{dt_1}{t_1} \int_0^1 d\hat{p}(z_1) f'(z_1, t_1; \{p\}_Z) \frac{q(x_1/z_1, t_1)}{q(x_1, t_1)} \Pi(m_z^2, t_1, \{p\}_Z)\Pi(t_1, t_\Lambda, \{p\}_{Z+1}) \\
&= \int_0^1 dx_1 \int_0^1 dx_2 q(x_1, m_z^2)\bar{q}(x_2, m_z^2)\ \sigma\big(q\bar{q} \to Z+1; \hat{s} = (x_1/z_1)x_2 s, \{p\}_{Z+1} > t_\Lambda\big) \frac{1}{z_1} \frac{q(x_1/z_1, t_1)}{q(x_1, t_1)} \\
&\quad \times \Pi(m_z^2, t_1, \{p\}_Z)\Pi(t_1, t_\Lambda, \{p\}_{Z+1}) \\
&= \int_0^1 dw_1 \int_0^1 dx_2 q(z_1 w_1, m_z^2)\bar{q}(x_2, m_z^2)\ \sigma\big(q\bar{q} \to Z+1; \hat{s} = w_1 x_2 s, \{p\}_{Z+1} > t_\Lambda\big) \frac{q(w_1, t_1)}{q(z_1 w_1, t_1)} \\
&\quad \times \Pi(m_z^2, t_1, \{p\}_Z)\Pi(t_1, t_\Lambda, \{p\}_{Z+1}) \\
&= \int_0^1 dw_1 \int_0^1 dx_2 q(w_1, t_1)\bar{q}(x_2, m_z^2)\ \sigma\big(q\bar{q} \to Z+1; \hat{s} = w_1 x_2 s, \{p\}_{Z+1} > t_\Lambda\big) \frac{q(z_1 w_1, m_z^2)}{q(z_1 w_1, t_1)} \\
&\quad \times \Pi(m_z^2, t_1, \{p\}_Z)\Pi(t_1, t_\Lambda, \{p\}_{Z+1}).
\end{aligned}
\tag{4.8}
$$

Note that $w_1 = x_1/z_1$ and that $1/z_1$ at the first equality comes from $d\hat{p}(z_1)$. The only difference from the correction of final state radiation in eq. (4.5) is that there are PDF factors.

Eqs. (4.5) and (4.8) uniquely complete the basic idea of the CKKW merging which has been designed for the improvement of the DGLAP equation with tree level matrix elements.

However a procedure to actually generate event samples based on these equations is not so unique, therefore several merging algorithms have been proposed. For detailed comparisons of these, refer to refs. [31, 26, 29]. In my study the CKKW-L merging algorithm is entirely used [24, 27, 35].

4.2 The CKKW-L merging algorithm

In this section, the CKKW-L merging algorithm [24, 27, 35] is reviewed by using the improved DGLAP equation which we have presented in Section 4.1. Let us copy eq. (4.5) below.

$$
\begin{aligned}
&\sigma(q\bar{q}, s) \\
&= \frac{1}{2s}\int d\Phi_{q\bar{q}} \overline{\sum_{\lambda}} \left|\mathcal{M}_{q\bar{q}}\right|^2 \Pi(s, t_{\rm cut}, \{p\}_{q\bar{q}}) + \frac{1}{2s}\int_{\{p\}_{q\bar{q}+1}>t_{\rm cut}} d\Phi_{q\bar{q}+1} \overline{\sum_{\lambda}} \left|\mathcal{M}_{q\bar{q}+1}\right|^2 \Pi(s, t_1, \{p\}_{q\bar{q}}) \\
&= \frac{1}{2s}\int d\Phi_{q\bar{q}} \overline{\sum_{\lambda}} \left|\mathcal{M}_{q\bar{q}}\right|^2 \Pi(s, t_{\rm cut}, \{p\}_{q\bar{q}}) \\
&\quad + \frac{1}{2s}\int_{\{p\}_{q\bar{q}+1}>t_{\rm cut}} d\Phi_{q\bar{q}+1} \overline{\sum_{\lambda}} \left|\mathcal{M}_{q\bar{q}+1}\right|^2 \Pi(s, t_1, \{p\}_{q\bar{q}}) \Pi(t_1, t_{\rm cut}, \{p\}_{q\bar{q}+1}) \\
&\quad + \frac{1}{2s}\int_{\{p\}_{q\bar{q}+2}>t_{\rm cut}} d\Phi_{q\bar{q}+2} \overline{\sum_{\lambda}} \left|\mathcal{M}_{q\bar{q}+2}\right|^2 \Pi(s, t_1, \{p\}_{q\bar{q}}) \Pi(t_1, t_2, \{p\}_{q\bar{q}+1}) \Pi(t_2, t_{\rm cut}, \{p\}_{q\bar{q}+2}) \\
&\quad + \cdots .
\end{aligned}
\tag{4.9}
$$

Here we assume that the definition of the merging scale $t_{\rm cut}$ is equivalent to that of the shower evolution scale t. Later, we consider a general case in which this is not the case.
Let us assume that we have a matrix element event generator which generate unweighted event samples according to exact tree level matrix elements and a parton shower generator. Parton shower generators have a cut off scale on their evolution variable, and once the evolution scale is reached to the cut off scale, the shower generation is turned off and all the produced partons are passed to a hadronization model. The goal of this section is to generate multi-parton final states which can be passed to a hadronization model according to the improved DGLAP equation. In other words, the parton shower program will not be stopped until its evolution scale reaches its cut off scale, $t_{\rm had}$.

We will examine each term, one by one, in the above equation. In order to generate event samples according to the probability of the first term

$$
\frac{1}{2s}\int d\Phi_{q\bar{q}} \overline{\sum_{\lambda}} \left|\mathcal{M}_{q\bar{q}}\right|^2 \Pi(s, t_{\rm cut}, \{p\}_{q\bar{q}}), \tag{4.10}
$$

at first the $q\bar{q}$ event samples are generated with the matrix elements. The next step is to calculate the Sudakov form factor. The CKKW-L algorithm uses the parton shower generator to calculate Sudakov form factors. We execute the shower program, whose shower starting scale is set to s, on the $q\bar{q}$ events. If the first evolution scale randomly chosen is higher than $t_{\rm cut}$, then we throw away this event sample and go to the next event sample. This is

equivalent to accepting event samples with the probability equal to $\Pi(s, t_{\rm cut}, \{p\}_{q\bar{q}})$, since $\Pi(s, t_{\rm cut}, \{p\}_{q\bar{q}})$ is the probability of no radiation between s and $t_{\rm cut}$. If the first evolution scale is lower than $t_{\rm cut}$, this evolution is continued until the cut off scale $t_{\rm had}$ and this event sample contributes to the inclusive event samples.

Let us look at the second term,

$$\frac{1}{2s}\int_{\{p\}_{q\bar{q}+1}>t_{\rm cut}} d\Phi_{q\bar{q}+1}\overline{\sum_{\lambda}}\left|\mathcal{M}_{q\bar{q}+1}\right|^2\Pi(s, t_1, \{p\}_{q\bar{q}})\Pi(t_1, t_{\rm cut}, \{p\}_{q\bar{q}+1}). \tag{4.11}$$

At first we generate the $q\bar{q}+1$ event samples according to the tree level matrix elements. The next step is to calculate $\Pi(s, t_1, \{p\}_{q\bar{q}})$. Here we notice that we have neither the scale t_1 nor the $q\bar{q}$ events which are needed for calculating $\Pi(s, t_1, \{p\}_{q\bar{q}})$. s is known in e^+e^- annihilation, but it will not be the case in pp collisions. Thus we need to obtain these information from the $q\bar{q}+1$ event samples. In the CKKW-L algorithm, this procedure is the exact inverse of the shower generation in the shower program which we use. Let us assume that a $q\bar{q}+1$ event is generated from a $q\bar{q}$ event with an evolution scale t_1 by the shower program. In the inverse procedure, a $q\bar{q}$ event together with an evolution scale t_1 is constructed from a $q\bar{q}+1$ event in such a way that, if the shower program generates the radiation t_1 from the $q\bar{q}$, it must lead to the $q\bar{q}+1$ event. This backward flow from the $q\bar{q}+1$ event to the $q\bar{q}$ event is often called parton shower history. The construction of parton shower history completely depends on the shower program which are used. In Section 4.3, the construction of the PYTHIA8 parton shower history is presented. For now let us assume that we construct the shower history and obtain the $q\bar{q}$ event and the scale t_1. In order to calculate $\Pi(s, t_1, \{p\}_{q\bar{q}})$, we execute the shower program on the $q\bar{q}$ event from the scale s as before. If the first evolution scale is higher than t_1, throw away this event and go to the next event sample. If not, we calculate the second Sudakov form factor $\Pi(t_1, t_{\rm cut}, \{p\}_{q\bar{q}+1})$. We execute the shower program on the $q\bar{q}+1$ event from the scale t_1. If the first evolution scale is higher than $t_{\rm cut}$, then we throw away this event sample and go to the next event sample. If the first evolution scale is lower than $t_{\rm cut}$, this evolution is continued until the cut off scale $t_{\rm had}$ and this event sample contributes to the inclusive event samples.

The event generation according to the third term and higher terms can be carried out with the same strategy. Although the CKKW type merging algorithms including the CKKW-L can treat tree level matrix elements of any number of additional partons, there is limitation in the matrix element calculation. When we decide not to include the matrix elements for the $q\bar{q}+2$-parton process for instance, what we should do is to remove the last Sudakov form factor $\Pi(t_1, t_{\rm cut}, \{p\}_{q\bar{q}+1})$ in the second term. The event generation should follow the first equality in eq. (4.9), thus the second term can include all the contribution below the scale t_1.

The discussion up to now has assumed that the definition of the merging scale $t_{\rm cut}$ is equivalent to that of the shower evolution scale t. It has been discussed in the original paper of the CKKW-L algorithm [24] that the definition of the merging scale $t_{\rm cut}$ can be arbitrary, as long as it regularizes the singularity in matrix elements. Here we define the merging scale

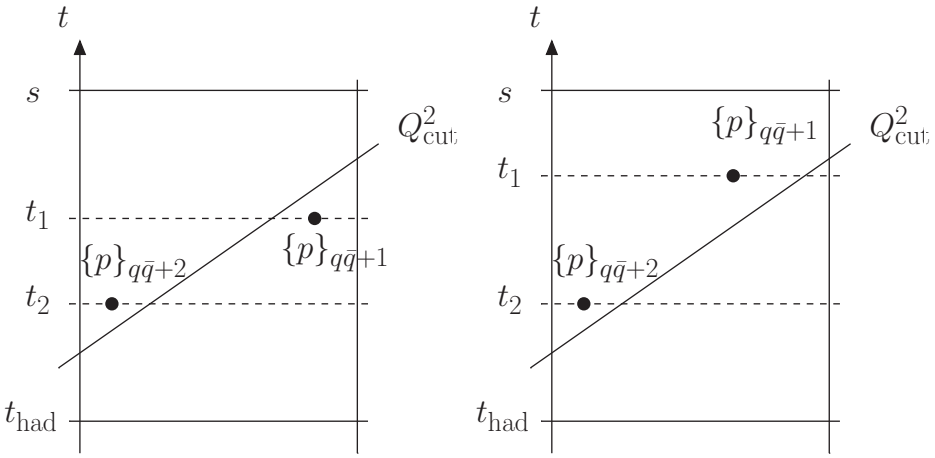

Figure 12: Panels for explaining how to avoid the double counting problem. See the text for the details.

$Q^2_{\rm cut}$, which can be the $k_\perp$ definition of the Durham jet clustering algorithm [47] for instance. Let us rewrite the above equation by replacing $t_{\rm cut}$ with $Q^2_{\rm cut}$,

$$
\begin{aligned}
&\sigma(q\bar{q}, s) \\
&= \frac{1}{2s}\int d\Phi_{q\bar{q}} \overline{\sum_\lambda} \left|\mathcal{M}_{q\bar{q}}\right|^2 \Pi(s, Q^2_{\rm cut}, \{p\}_{q\bar{q}}) + \frac{1}{2s}\int_{\{p\}_{q\bar{q}+1} > Q^2_{\rm cut}} d\Phi_{q\bar{q}+1} \bar{\sum_\lambda} \left|\mathcal{M}_{q\bar{q}+1}\right|^2 \Pi(s, t_1, \{p\}_{q\bar{q}}) \\
&= \frac{1}{2s}\int d\Phi_{q\bar{q}} \bar{\sum_\lambda} \left|\mathcal{M}_{q\bar{q}}\right|^2 \Pi(s, Q^2_{\rm cut}, \{p\}_{q\bar{q}}) \\
&\quad + \frac{1}{2s}\int_{\{p\}_{q\bar{q}+1} > Q^2_{\rm cut}} d\Phi_{q\bar{q}+1} \bar{\sum_\lambda} \left|\mathcal{M}_{q\bar{q}+1}\right|^2 \Pi(s, t_1, \{p\}_{q\bar{q}}) \Pi(t_1, Q^2_{\rm cut}, \{p\}_{q\bar{q}+1}) \\
&\quad + \frac{1}{2s}\int_{\{p\}_{q\bar{q}+2} > Q^2_{\rm cut}} d\Phi_{q\bar{q}+2} \bar{\sum_\lambda} \left|\mathcal{M}_{q\bar{q}+2}\right|^2 \Pi(s, t_1, \{p\}_{q\bar{q}}) \Pi(t_1, t_2, \{p\}_{q\bar{q}+1}) \Pi(t_2, Q^2_{\rm cut}, \{p\}_{q\bar{q}+2}) \\
&\quad + \cdots .
\end{aligned}
\tag{4.12}
$$

In order to calculate the Sudakov form factor $\Pi(s, Q^2_{\rm cut}, \{p\}_{q\bar{q}})$ without double counting or missed phase spaces, the following strategy is used. We execute the shower program on the $q\bar{q}$ event, starting from the scale s, as before. After the first evolution produces a $q\bar{q}+1$ event, we look at the kinematics of the $q\bar{q}+1$ event. If the $q\bar{q}+1$ event passes the merging scale $Q^2_{\rm cut}$ i.e. $\{p\}_{q\bar{q}+1} > Q^2_{\rm cut}$, we throw away this event and go to the next event sample. If it does not, this evolution is continued until the cut off scale $t_{\rm had}$ and this event sample contributes to the inclusive event samples. It might be imagined that, even though $\{p\}_{q\bar{q}+1} < Q^2_{\rm cut}$ after the first evolution, the second evolution can produce a $q\bar{q}+2$ event which fills $\{p\}_{q\bar{q}+2} > Q^2_{\rm cut}$ and this event can cause a double counting with an event coming from the third term in eq. (4.12). Let us look at Figure 12. The vertical axis represents the evolution variable t, the transverse axis represents some variables which determine kinematics such as the energy fraction variable z. The diagonal line indicates the merging scale cut $Q^2_{\rm cut}$. The left panel

shows a situation after two evolutions from a $q\bar{q}$ event. This event satisfies $\{p\}_{q\bar{q}+1} < Q^2_{\rm cut}$ after the first evolution, thus it is already accepted as a contribution to the inclusive event samples. However, after the second evolution, it goes to $\{p\}_{q\bar{q}+2} > Q^2_{\rm cut}$. Let us consider a $q\bar{q}+2$ event generated according to the matrix elements i.e. the third term in eq. (4.12). A $q\bar{q}+1$ event together with a scale t_2 and a $q\bar{q}$ event together with a scale t_1 will be constructed as a parton shower history. In the CKKW-L algorithm, the double counting issue is avoided by requiring the merging scale cut on constructed events too, namely $\{p\}_{q\bar{q}+1} > Q^2_{\rm cut}$ which is the case shown in the right panel in Figure 12. Thus, eq. (4.12) should be rewritten in the following form,

$$
\begin{aligned}
&\sigma(q\bar{q}, s) \\
&= \frac{1}{2s}\int d\Phi_{q\bar{q}} \bar{\sum_\lambda} \left|\mathcal{M}_{q\bar{q}}\right|^2 \Pi(s, Q^2_{\rm cut}, \{p\}_{q\bar{q}}) \Big|_{\{p\}_{q\bar{q}+1}<Q^2_{\rm cut}} + \frac{1}{2s}\int_{\{p\}_{q\bar{q}+1}>Q^2_{\rm cut}} d\Phi_{q\bar{q}+1} \bar{\sum_\lambda} \left|\mathcal{M}_{q\bar{q}+1}\right|^2 \Pi(s, t_1, \{p\}_{q\bar{q}}) \\
&= \frac{1}{2s}\int d\Phi_{q\bar{q}} \bar{\sum_\lambda} \left|\mathcal{M}_{q\bar{q}}\right|^2 \Pi(s, Q^2_{\rm cut}, \{p\}_{q\bar{q}}) \Big|_{\{p\}_{q\bar{q}+1}<Q^2_{\rm cut}} \\
&\quad + \frac{1}{2s}\int_{\{p\}_{q\bar{q}+1}>Q^2_{\rm cut}} d\Phi_{q\bar{q}+1} \bar{\sum_\lambda} \left|\mathcal{M}_{q\bar{q}+1}\right|^2 \Pi(s, t_1, \{p\}_{q\bar{q}}) \Pi(t_1, Q^2_{\rm cut}, \{p\}_{q\bar{q}+1}) \Big|_{\{p\}_{q\bar{q}+2}<Q^2_{\rm cut}} \\
&\quad + \frac{1}{2s}\int_{\{p\}_{q\bar{q}+2}>Q^2_{\rm cut}} d\Phi_{q\bar{q}+2} \bar{\sum_\lambda} \left|\mathcal{M}_{q\bar{q}+2}\right|^2 \Pi(s, t_1, \{p\}_{q\bar{q}}) \Pi(t_1, t_2, \{p\}_{q\bar{q}+1}) \Pi(t_2, Q^2_{\rm cut}, \{p\}_{q\bar{q}+2}) \Big|^{\{p\}_{q\bar{q}+1}>Q^2_{\rm cut}}_{\{p\}_{q\bar{q}+3}<Q^2_{\rm cut}} \\
&\quad + \cdots .
\end{aligned}
\tag{4.13}
$$

The merging strategy discussed so far can be applied to the improved DGLAP equation for hadronic collisions given in eq. (4.8). Thus we do not repeat it here and emphasize only the differences from the e^+e^- case. An apparent difference is that we need to calculate PDF weight factors, which can be easily calculated once a parton shower history is constructed. A more technical difference is the central scale. In order to discuss this issue, let us write the generalized and simplified version of the improved DGLAP equation below,

$$
\begin{aligned}
&\sigma(X) \\
&= \sigma(X)\Pi(t_X, Q^2_{\rm cut}, \{p\}_X) \Big|_{\{p\}_{X+1}<Q^2_{\rm cut}} \\
&\quad + \sigma\big(X+1, \{p\}_{X+1} > Q^2_{\rm cut}\big)\Pi(t_X, t_1, \{p\}_X)\Pi(t_1, Q^2_{\rm cut}, \{p\}_{X+1}) \Big|_{\{p\}_{X+2}<Q^2_{\rm cut}} \\
&\quad + \sigma\big(X+2, \{p\}_{X+2} > Q^2_{\rm cut}\big)\Pi(t_X, t_1, \{p\}_X)\Pi(t_1, t_2, \{p\}_{X+1})\Pi(t_2, Q^2_{\rm cut}, \{p\}_{X+2}) \Big|^{\{p\}_{X+1}>Q^2_{\rm cut}}_{\{p\}_{X+3}<Q^2_{\rm cut}} \\
&\quad + \cdots ,
\end{aligned}
\tag{4.14}
$$

where the PDFs and the PDF weight factors are implicit. Event configurations denoted by $\{p\}_{X+n}$ include the two incoming partons. First of all, the scale t_X must be determined

from the events $\{p\}_X$. This scale is uniquely set to the total energy s for the e^+e^- case, however which is not the case for hadronic collisions. Second, since we construct scales from matrix element events, it happens that $t_X < t_1$. This should be considered as an important prediction from the matrix elements, since this will never happen in the shower program. In such a case, the first Sudakov form factor $\Pi(t_X, t_1, \{p\}_X)$ is set to unity. Note that the parton shower starting scale for calculating the next Sudakov form factor $\Pi(t_1, Q^2_{\rm cut}, \{p\}_{X+1})$ must be set to t_X, not t_1.

The scale t_X is often called the parton shower starting scale. Since it determines hardness of radiation, it can be easily imagined that predictions can depend significantly on this parameter when we rely only on a shower program for generating QCD radiation. It has been confirmed that this dependence is reduced once we use the merging algorithm [32]. We can read this reason from eq. (4.14). The hardness of radiation parametrized by the evolution scales such as t_1 and t_2 is determined from matrix elements, thus is nothing to do with t_X. The starting scale t_X affects the first Sudakov factor $\Pi(t_X, Q^2_{\rm cut}, \{p\}_X)$ or $\Pi(t_X, t_1, \{p\}_X)$. However, since this is considered as an overall factor, the rates of the exclusive contributions from each term will not be affected. This fact leads to a stable distribution such as jet p_T distributions. The only quantity affected by t_X is the inclusive cross section which is obtained by summing the exclusive contributions.

4.3 Construction of the PYTHIA8 parton shower history

In Section 4.2 we have learned that we need to know a parton shower history which consists of a set of the sequential intermediate processes, together with the corresponding clustering scales which are ordered. In this section, we discuss how to construct the PYTHIA8 parton shower history. Because the detailed definition of the evolution variable and the kinematics construction are different for the initial state radiation and the final state radiation in PYTHIA8, the clustering procedure is also different for the clustering of incoming and outgoing partons and that of two outgoing partons. The former procedure is described in Section 4.3.1 and the latter in Section 4.3.2. The full understanding of the kinematics construction of the parton shower program [42, 45, 46] in PYTHIA8 is necessary. We use the knowledge and notation in the original publications [42, 45, 46].

4.3.1 Reconstruction of initial state radiation

Suppose that an incoming parton a and an outgoing parton c in a process $ar \to Xc$ are clustered into a parton b and hence an intermediate process $br \to X$ together with a clustering scale $p_{\perp\rm clus}$ is produced as illustrated in Figure 13 (from left to right). The clustering has to proceed as if the process $ar \to Xc$ had been induced by the initial state radiation (ISR) $a \to bc$ from the hard process $br \to X$ in the backwards evolution [44] with the evolution scale $p_{\perp\rm evol} = p_{\perp\rm clus}$. Once a pair of the incoming parton a and the outgoing parton c is determined, the incoming parton from another side is uniquely selected as a recoiling parton

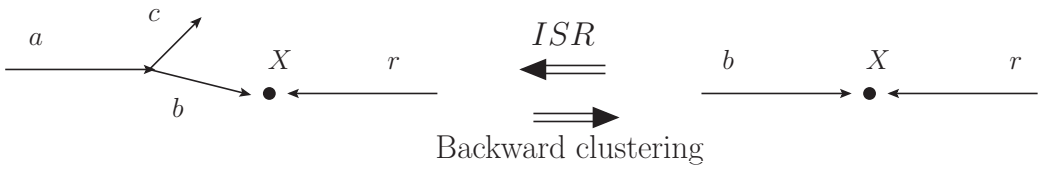

Figure 13: Illustrating that an incoming parton a and an outgoing parton c in a process $ar \to Xc$ are clustered into an incoming parton b and hence a new process $br \to X$ is produced (from left to right), and that a process $ar \to Xc$ is induced by ISR $a \to bc$ from a process $br \to X$ in the backwards evolution (from right to left).

r. The clustering scale $p_{\perp\text{clus}}$ is derived from

$$p_b = p_a - p_c, \tag{4.15a}$$

$$z = \frac{m_{br}^2}{m_{ar}^2} = \frac{(p_b + p_r)^2}{(p_a + p_r)^2}, \tag{4.15b}$$

$$p_{\perp\text{clus}}^2 = -(1-z)(p_b)^2. \tag{4.15c}$$

Here z can be interpreted as the energy fraction E_b/E_a in the pp frame. The new incoming parton b after the clustering is not moving along the z-axis and it is a spacelike particle. We need to make the b on-shell (massless) and moving along the z-axis. The algorithm is as follows. Note that X expresses all the other particles in the final state, hence $X = t\bar{t} + g$ for instance.

1. Read the azimuthal angle ϕ_c of c.
2. Rotate c and X in azimuth by $-\phi_c$.
3. Calculate the 4-momentum of b from $p_b = p_a - p_c$.
4. Boost b, r and X to the $b + r$ rest frame, and then rotate them in polar angle to have b and r moving along the z-axis.
5. Rotate X in azimuth by $+\phi_c$.
6. Construct the 4-momenta of the massless incoming partons b and r in the $b + r$ rest frame, $p_b = (m_{br}/2, 0, 0, m_{br}/2)$ and $p_r = (m_{br}/2, 0, 0, -m_{br}/2)$.
7. Boost b, r and X along the z-axis to have r having its original momentum.

With the algorithm, the transverse momentum of the clustered parton b is translated into the kinematics of X. As required, b is put on mass shell (massless) and it moves along the z-axis. The kinematics of r does not change. The algorithm is tested as follows. We apply the algorithm to a process $ar \to Xc$ which has been induced by ISR $a \to bc$ of PYTHIA8 from a hard process $br \to X$ and then we confirm that the algorithm correctly reproduces the process $br \to X$.

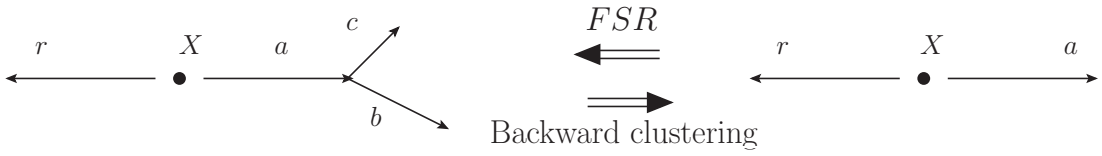

Figure 14: Illustrating that two outgoing partons b and c are clustered into an outgoing parton a (from left to right), and that a set of partons b, c and r is induced by FSR $a \to bc$ from a set of partons a and r (from right to left).

4.3.2 Reconstruction of final state radiation

Suppose that two outgoing partons b and c are clustered into an outgoing parton a and hence a set of partons a and r together with a clustering scale $p_{\perp\text{clus}}$ is produced as illustrated in Figure 14 (from left to right). The recoiling parton r is either incoming or outgoing. The clustering has to proceed as if the set of the partons b, c and r had been induced by the final state radiation (FSR) $a \to bc$ from the set of the partons a and r with the evolution scale $p_{\perp\text{evol}} = p_{\perp\text{clus}}$. Unlike the reconstruction of ISR, the recoiling parton r will not be uniquely determined. In our analysis, the recoiler is randomly chosen. The clustering scale $p_{\perp\text{clus}}$ for a given set of the partons is derived from,

$$p_a = p_b + p_c, \tag{4.16a}$$
$$p_0 = p_a + p_r, \tag{4.16b}$$
$$z = \frac{p_0 \cdot p_b}{p_0 \cdot p_a}\left(1 - \frac{p_0 \cdot p_c}{p_0 \cdot p_b}\frac{m_a^2}{2p_0 \cdot p_a + m_r^2 - m_a^2 - p_0^2}\right), \tag{4.16c}$$
$$p_{\perp\text{clus}}^2 = z(1-z)\big((p_a)^2 - m_a^2\big), \tag{4.16d}$$

where m_a and m_r are on-shell masses of the parton a and r, respectively. The mass effect is taken into account. This is relevant particularly in the clustering $\text{top}(p_b) + \text{gluon}(p_c) \to \text{top}(p_a)$ or $\text{antitop}(p_b) + \text{gluon}(p_c) \to \text{antitop}(p_a)$. When r is an incoming parton, the 4-momentum $p_0 = p_a + p_r$ is not conserved during the FSR. Therefore, p_0 must be calculated by using p_a and p_r which are obtained after the parton a made on mass shell with the algorithm given below. The new outgoing parton a after the clustering is off mass shell. We need to make a on mass shell. There are the two approaches depending on whether the recoiling parton r is outgoing or incoming.

When r is an outgoing parton, the parton a is put on mass shell by giving energy and momentum of the parton a to the parton r, while the 4-momentum $p_0 = p_a + p_r$ is kept unchanged. The kinematics of all the other partons indicated by X in Figure 14 will not be affected. The algorithm is as follows.

1. Boost a and r to the $a + r$ rest frame, $p_{a,0}$ and $p_{r,0}$.

2. Construct the energy and absolute value of momentum of the partons a and r which

are put on mass shell with the on-shell mass m_a and m_r in the $a+r$ rest frame,

$$m_{ar}^2 = (p_{a,0} + p_{r,0})^2, \tag{4.17a}$$

$$E_{a,\mathrm{new}} = \frac{m_{ar}^2 + m_a^2 - m_r^2}{2m_{ar}}, \tag{4.17b}$$

$$E_{r,\mathrm{new}} = \frac{m_{ar}^2 - m_a^2 + m_r^2}{2m_{ar}}, \tag{4.17c}$$

$$|\vec{p}_{a,\mathrm{new}}| = |\vec{p}_{r,\mathrm{new}}| = \sqrt{E_{a,\mathrm{new}}^2 - m_a^2}. \tag{4.17d}$$

3. Modify the magnitude of the momentum of a and r to $|\vec{p}_{a,\mathrm{new}}|$ and $|\vec{p}_{r,\mathrm{new}}|$ respectively, while the direction of the momentum is kept unchanged,

$$p_a^i = \frac{p_{a,0}^i}{|\vec{p}_{a,0}|}|\vec{p}_{a,\mathrm{new}}|, \qquad p_r^i = \frac{p_{r,0}^i}{|\vec{p}_{r,0}|}|\vec{p}_{r,\mathrm{new}}|. \qquad (i = 1,2,3) \tag{4.18}$$

4. Boost these back to the original $a+r$ frame.

When r is an incoming parton, the parton a is put on mass shell by reducing the 4-momentum of both a and r, while the 4-momentum $p_r - p_a$ is kept unchanged. The 4-momentum of the partons a and r is derived from,

$$\alpha = \frac{p_r^3}{E_r} = 1 \text{ or } -1, \tag{4.19a}$$

$$p_{r,\mathrm{after}}^\mu = \left(E_r - \frac{(p_a)^2 - m_a^2}{2(E_a - \alpha p_a^3)},\ 0,\ 0,\ \alpha\left(E_r - \frac{(p_a)^2 - m_a^2}{2(E_a - \alpha p_a^3)} \right) \right), \tag{4.19b}$$

$$p_{a,\mathrm{after}}^\mu = \Big(E_a + E_{r,\mathrm{after}} - E_r,\ p_a^1,\ p_a^2,\ p_a^3 + p_{r,\mathrm{after}}^3 - p_r^3 \Big). \tag{4.19c}$$

Our algorithm is tested as follows. We apply the algorithm to a process which was induced by FSR of PYTHIA8 from a hard process and then we confirm that the algorithm correctly reproduces the hard process before the FSR occurs.

4.4 Merging procedure

In this section, we describe the procedure of event generation based on the CKKW-L merging algorithm which we have discussed so far. The event generation for the process $pp \to X$+anything proceeds as follows [11].

[11] The event generation procedure for the process e^+e^- →jets should be guessed easily.

1. Generate the unweighted event samples the $pp \to X + 0, 1, 2 \ldots, N$-parton processes according to the tree level matrix elements. N is the maximal number of QCD partons provided by the matrix elements. We use MadGraph5_aMC@NLO[38] version 5.2.2.1 for this purpose. The soft and collinear singularities are regularized by a cutoff on the longitudinal-boost invariant $k_\perp$ variable [47]

$$\begin{aligned} k_{\perp iB} &= p_{Ti}, \\ k_{\perp ij} &= \min(p_{Ti}, p_{Tj}) \sqrt{(y_i - y_j)^2 + (\phi_i - \phi_j)^2}/R, \end{aligned} \tag{4.20}$$

where p_{Ti}, y_i and ϕ_i are the transverse momentum with respect to the beam, rapidity and azimuthal angle of particle i. R is the radius parameter and $R = 1$ is used if not otherwise specified. This variable is also used as the merging scale definition. A fixed value is used for the scales in α_s and in parton distribution functions (PDFs) at this step. For e^+e^- annihilation, the Durham $k_\perp$ variable [48] is used,

$$\begin{aligned} k^2_{\perp ij} &= 2\min(E_i^2, E_j^2)(1 - \cos\theta_{ij}), \\ y_{ij} &= k^2_{\perp ij}/s, \end{aligned} \tag{4.21}$$

where E_i is the energy of particle i, θ_{ij} is the angle between particle s i and j and s is the center-of-mass energy squared.

2. Select an event sample for the $pp \to X + n$-parton process with a probability proportional to its integrated cross section obtained in step 1,

$$P_n = \frac{\sigma(pp \to X + n)}{\sum_{i=0}^{N} \sigma(pp \to X + i)}. \tag{4.22}$$

3. A parton shower history of the event sample is constructed by successively clustering two partons into one parton, as explained in Section 4.3. This procedure yields a set of the sequential intermediate processes $pp \to X$, $pp \to X + 1$-parton, $\ldots$, $pp \to X + (n-1)$-parton together with the corresponding clustering scales $p_{\perp 1} > p_{\perp 2} > \cdots > p_{\perp n}$ which are ordered.

4. Weight the event sample by α_s and PDF factors which are calculated based on the shower history obtained in step 3. The α_s factor is determined from the clustering scales $p_{\perp 1} > p_{\perp 2} > \cdots > p_{\perp n}$,

$$\frac{\alpha_s(p_{\perp 1})\alpha_s(p_{\perp 2}) \ldots \alpha_s(p_{\perp n})}{\alpha^n_{s,\text{fixed}}}, \tag{4.23}$$

where $\alpha_{s,\text{fixed}}$ is the one used in step 1. If the event sample is rejected, select a new event sample according to step 2.

5. Calculate the Sudakov form factors by making trial emission with PYTHIA8 on the set of the sequential intermediate processes $pp \to X$, $pp \to X + 1$-parton, $\ldots$, $pp \to X + (n-1)$-parton and on the generated process $pp \to X + n$-parton. The parton shower starting scale is determined from the core process $pp \to X$, and the same value is also used in the PDFs. If the event sample is rejected, select a new event sample according to step 2.

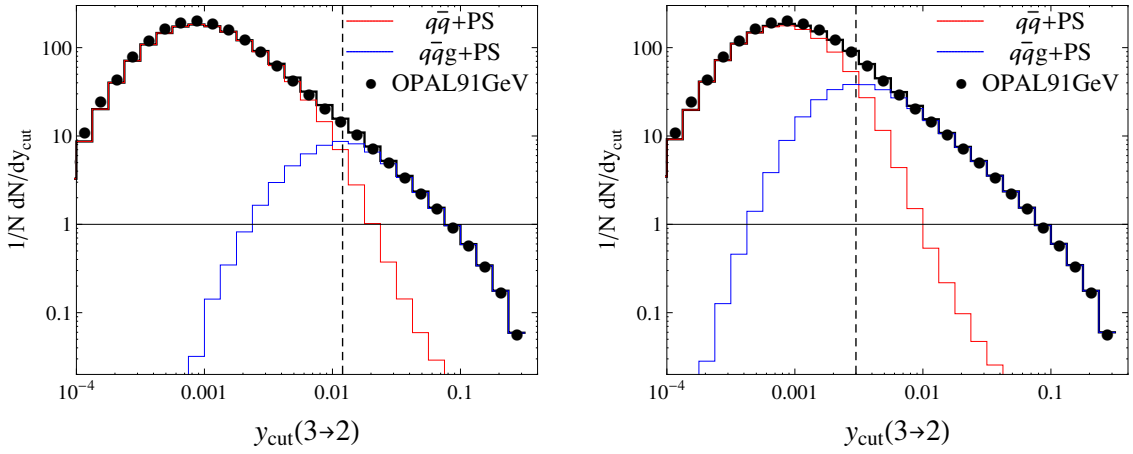

Figure 15: The distributions of $y_{\rm cut}(3 \to 2)$ in the Durham algorithm. The black solid curve represents the result, while the red solid curve represents the contributions of the $q\bar{q}$ matrix elements and the blue solid curve represents the contributions of the $q\bar{q}g$ matrix elements. A vertical dashed line indicates the merging scale $y_{\rm MS}$, $y_{\rm MS} = 0.012$ for the left graph and $y_{\rm MS} = 0.003$ for the right graph. The result is compared to the OPAL data (points) [49].

6. Repeat the algorithm from step 2 until a large number of the accepted event samples is accumulated.

4.5 Test of the algorithm

In this section, the implementation of the merging algorithm is tested. The jet production in e^+e^- annihilation (Section 4.5.1) and the Drell-Yan lepton pair production in pp collisions (Section 4.5.2) are chosen. Smoothness of the merging at the merging scale and dependence on the merging scale are carefully studied. The comparison of the predictions with experimental data is also presented.

4.5.1 Jet production in e^+e^- annihilation

The distributions of differential jet rate $y_{\rm cut}(3 \to 2)$ in the Durham algorithm are plotted in Figure 15. The black solid curve represents the result, while the red solid curve represents the contributions of the $q\bar{q}$ matrix elements and the blue solid curve represents the contributions of the $q\bar{q}g$ matrix elements A vertical dashed line indicates the merging scale $y_{\rm MS}$, $y_{\rm MS} = 0.012$ for the left graph and $y_{\rm MS} = 0.003$ for the right graph. The result is compared to the OPAL data (points) [49]. The results are stable under varying the merging scale $y_{\rm MS}$ between 0.003 (right) and 0.012 (left), which indicates that the cancellation of the merging scale dependence is satisfactory. The merging is smooth around the merging scale, thus it

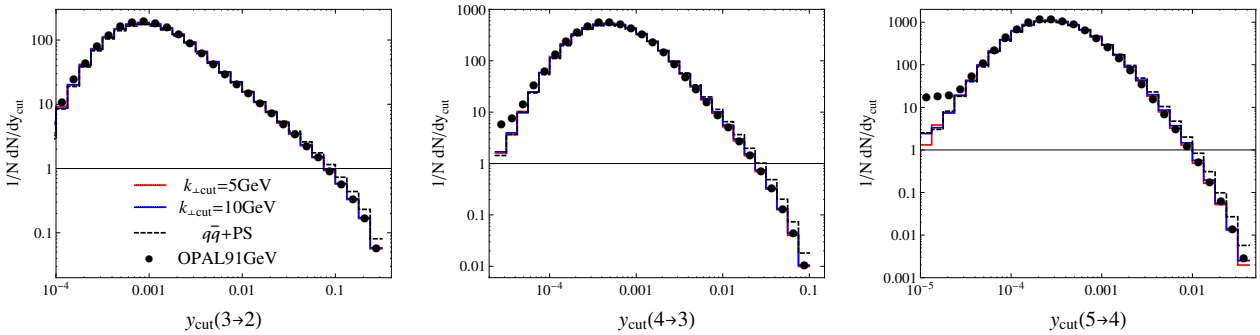

Figure 16: The distributions of $y_{\rm cut}(n \to n-1)$ for $n = 3$ (left), $n = 4$ (middle) and $n = 5$ (right) in the Durham algorithm. The red solid curve represents the result of $y_{\rm MS} = 0.003$ and the blue solid curve $y_{\rm MS} = 0.012$. The matrix elements for up to 5 partons are included in the merging. The black dashed curve represents the pure shower prediction. The results are compared to the OPAL data (points) [49].

can be concluded that the problem of double counting and missed phase space is avoided.

In Figure 16 the distributions of $y_{\rm cut}(n \to n-1)$ for $n = 3$ (left), $n = 4$ (middle) and $n = 5$ (left) in the Durham algorithm are plotted. The red solid curve represents the result of the merging with $y_{\rm MS} = 0.003$ and the blue solid curve $y_{\rm MS} = 0.012$. The matrix elements for up to 5 partons (3 partons additionally) are included in the merging. The black dashed curve represents the result of only the parton shower program [12]. It is found that the merging algorithm improves the predictions at higher energy scales.

4.5.2 $Z/\gamma \to l\bar{l}$ plus jets production in pp collisions

The Drell-Yan lepton pair production in pp collisions at 7 TeV is studied in this section. The differential jet rates are calculated by using the longitudinal-boost invariant $k_\perp$ definition in eq. (4.20) with a radius parameter $R = 1$. In Figure 17, the differential jet rates for $1 \to 0$ and $2 \to 1$ jets (left to right) are plotted. The maximal number N of partons provided by the matrix elements is set to two. A vertical dashed line indicates the merging scale.In the top graphs of Figure 17, we can observe a smooth merging of the matrix elements contributions with the parton shower around the merging scale, $k_{\perp\rm cut} = 10$ GeV. In the bottom graphs of Figure 17 the differential jet rates with the different values of the merging scale are plotted. The red solid curve represents the result with $k_{\perp\rm cut} = 10$ GeV, the blue solid curve represents the result with $k_{\perp\rm cut} = 40$ GeV. The black dashed curve represents the result without the merging i.e. jet production relies only on the shower program. It is found that the results are stable under varying the merging scale from 10 GeV to 40 GeV. A slight difference is observed around $k_\perp = 30$ GeV, which implies that 40 GeV as the merging scale is a little

[12] The matrix element correction implemented in PYTHIA8 is turned off.

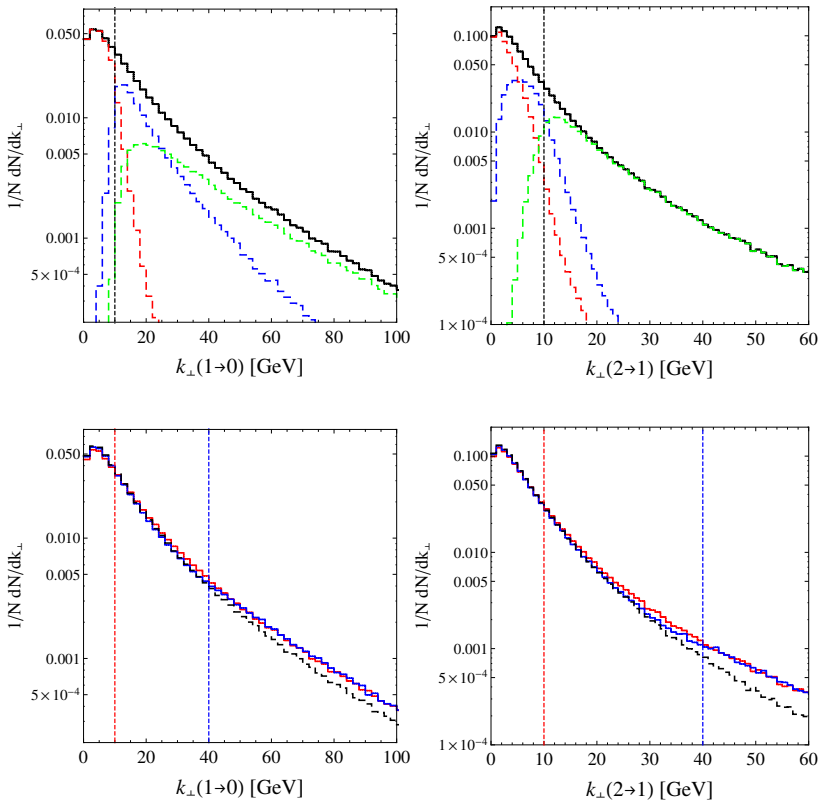

Figure 17: Differential jet rates for $1 \to 0$ and $2 \to 1$ jets. A vertical dashed line indicates the merging scale $k_{\perp\text{cut}}$. *top*: The black solid curve represents the combined result, while the other colored dashed curves the matrix element contributions for different parton multiplicity, $n = 0$ (red), $n = 1$ (blue) and $n = 2$ (green). *bottom*: The red solid curve represent the result with $k_{\perp\text{cut}} = 10$ GeV, the blue solid curve $k_{\perp\text{cut}} = 40$ GeV. The black dashed curve represents the pure shower result.

too high.

In Figure 18, the dependence of the exclusive jet multiplicity and the Z boson p_T on the maximal number N of partons provided by the matrix elements is studied. The merging scale is set to $k_{\perp\text{cut}} = 10$ GeV. The ATLAS 7 TeV data (points) [50, 51] are compared to the results. It is found that the results are improved for a higher values of N.

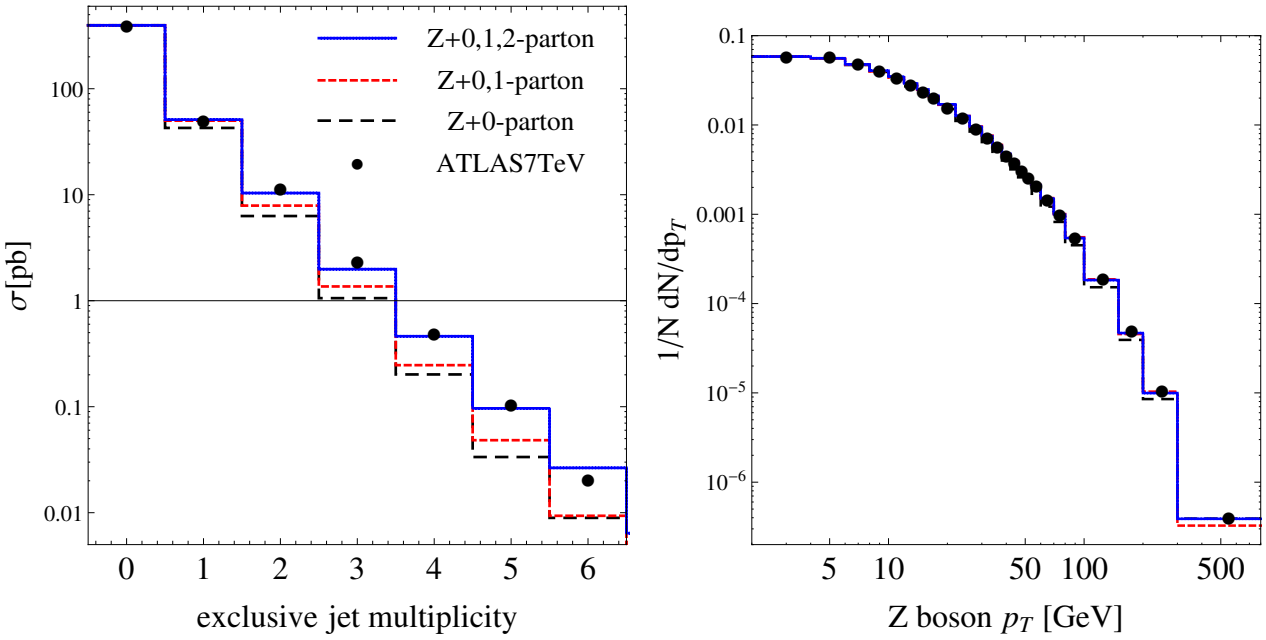

Figure 18: The exclusive jet multiplicity (left) and the Z boson p_T (right). The merging scale is $k_{\perp\text{cut}} = 10$ GeV. The ATLAS 7 TeV data (points) [50, 51] are compared to the results.

5 The azimuthal angle correlation between two jets in the top quark pair production

The merging algorithm is applied to the event generation of the top quark pair production at the 14 TeV LHC, and the azimuthal angle correlation between the two jets is studied in this section. Section 5.1 provides setups for the simulation and for analyzing the azimuthal angle correlation. In Section 5.2, we study the dependence of the simulation result on the parameter which exist in the merging algorithm, namely the merging scale and the parton shower starting scale. A discussion on the merging scale and the jet definition is presented in Section 5.3. In Section 5.4 we study the impacts of including the $t\bar{t}$ + 3-parton matrix elements in the merging algorithm. The comparison with the naive approach is performed in Section 5.5. Section 5.6 gives the conclusion of this section.

5.1 Event generation

To start with, a setup for our event generation and analyses is introduced. The unweighted event samples of the top quark pair plus multi-jet process at the 14 TeV LHC are generated with the merging algorithm described in Section 4. The scale t_X in eq. (4.14) is calculated from the core process $pp \to t\bar{t}$ as

$$t_X = E_T^2(t) = E_T^2(\bar{t}), \tag{5.1}$$

and this is used for the scale μ_F in the PDFs and for the scale μ_R in α_s^2 of the core process. The merging scale $k_{\perp\text{cut}}$ and the maximal number of partons N obtained by the leading order matrix elements (MEs) are important parameters in the merging algorithm and they are subject to study in the following sections.

The physical observable which we are interested in is the azimuthal angle difference between the two hardest jets, $\Delta\phi = \phi_1 - \phi_2$. An event sample with two or more jets is picked up and the following requirement which is often called vector boson fusion (VBF) cut is applied to the two hardest jets,

$$y_1 \times y_2 < 0, \quad |y_1 - y_2| > 4. \tag{5.2}$$

The transverse momentum p_T with respect to the beam of an object describes the hardness of the object. Therefore a jet which has the highest p_T is called the hardest jet and another jet which has the second highest p_T is called the second hardest jet, and these jets are assigned to the two hardest jets. To enhance the azimuthal angle correlation, an additional cut is applied [14],

$$m_{t\bar{t}} < 500 \text{ GeV}. \tag{5.3}$$

No other cuts are applied to the top and anti-top quarks and they are left undecayed. All particles satisfying a rapidity cut $|y| < 4.9$ except the top and anti-top quarks are clustered

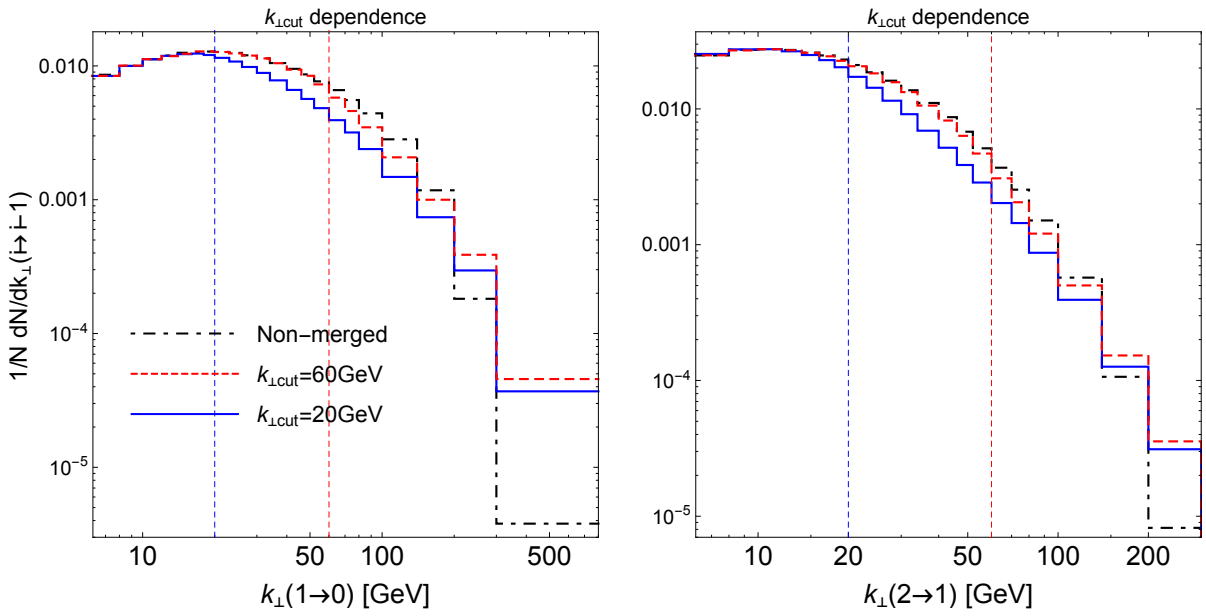

Figure 19: The differential jet rates for $1 \to 0$ (left) and $2 \to 1$ (right) jets. The blue solid curve represents the result of the merging with the merging scale $k_{\perp\mathrm{cut}} = 20$ GeV, the red dashed curve represents that with $k_{\perp\mathrm{cut}} = 60$ GeV and the black broken curve represents the pure shower prediction.

to construct inclusive jets according to the anti-k_T algorithm [52]. The radius parameter is $R = 0.4$ if not otherwise specified. Fastjet [53] version 3.1.0 is used for this purpose. All the unweighted event samples according to the leading order MEs are generated by MadGraph5_aMC@NLO [38] version 5.2.2.1 and the parton shower (PS) is performed by PYTHIA8 [36, 37] version 8186. The parton distribution function (PDF) set CTEQ6L1 [54] is used for all needs including the PDF factors for the initial state radiation in PYTHIA8. The default tune of the version 8186 is basically used in PYTHIA8 while some functions are turned off. The hadronization after the PS is turned off because it is not intended to study detector effect. To simplify the analysis, the multiple interaction is turned off. The rapidity ordering in the ISR is turned off as suggested in ref. [35]. All functions inducing azimuthal asymmetry in the PS are turned off, since azimuthal angle information of hard partons is provided by exact MEs in our study.

5.2 Parameter dependence in the merging algorithm

The dependence of the differential jet rates on the merging scale $k_{\perp\mathrm{cut}}$ is analyzed in this Section. The dependence of the differential jet rates on the merging scale $k_{\perp\mathrm{cut}}$ has been studied already for the jet production at e^+e^- annihilation and for the Drell-Yan lepton pair production at pp collisions in Section 4.5, and the smallness of the merging scale dependence has been confirmed. We repeat the same analysis for the $t\bar{t}$ production and find a clear

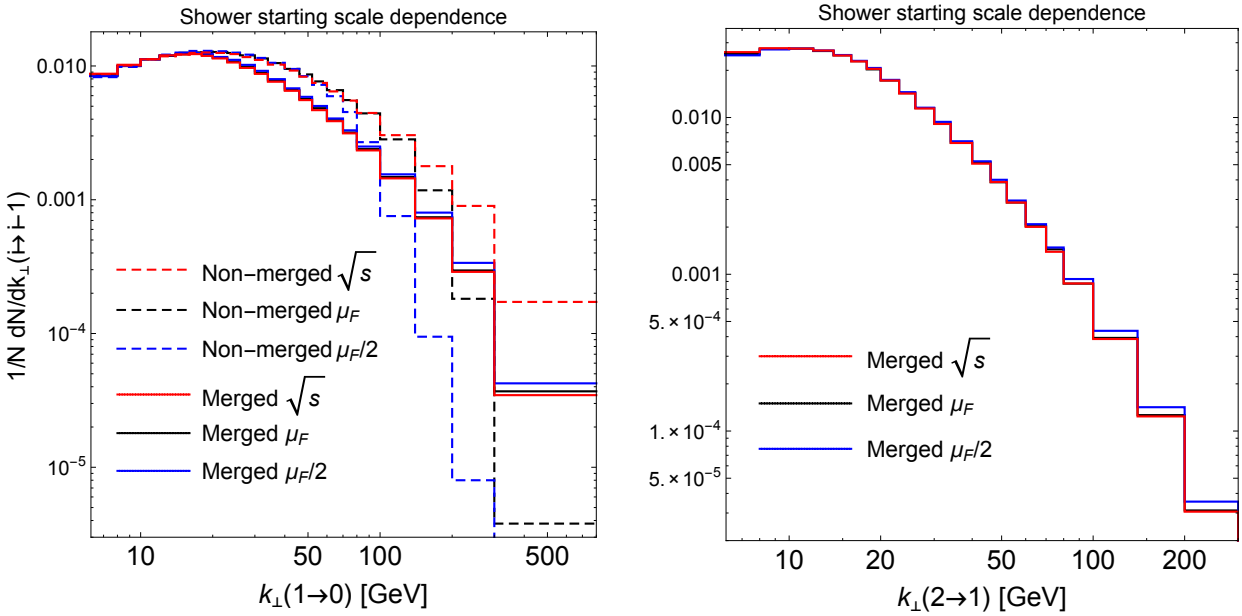

Figure 20: The differential jet rates for $1 \to 0$ (left) and $2 \to 1$ (right) jets. The dependence on the parton shower starting scale with and without the merging algorithm is studied.

dependence on the merging scale. The origin is investigated. The parton shower starting scale dependence is also studied. All the merged predictions use up to the 3-parton matrix elements.

The differential jet rates are calculated by using the longitudinal-boost invariant $k_\perp$ definition in eq. (4.20) with a radius parameter $R = 1$. In Figure 19 the differential jet rates for $1 \to 0$ (left) and $2 \to 1$ (right) jets are plotted. A vertical dashed line indicates the merging scale $k_{\perp\text{cut}}$. The blue solid curve represents the result of $k_{\perp\text{cut}} = 20$ GeV, the red dashed curve represents that of $k_{\perp\text{cut}} = 60$ GeV and the black broken curve represents the result of non-merging i.e. only the shower prediction. These three results are set equal at the bin between 10 and 12 GeV.

First of all, it should be emphasized that the merged predictions are smooth around their merging scale. This tells that the problem of double counting and missed phase space is avoided. A clear difference is, however, observed by varying the merging scale from 20 to 60 GeV. The reason for this is that the merged results already deviate from the parton shower prediction in the soft and/or collinear region. By comparing the merged prediction with $k_{\perp\text{cut}} = 20$ GeV and the shower prediction, it is clear that the merged prediction starts to deviate from the shower prediction at around its merging scale 20 GeV. It is also the case for the merged prediction with $k_{\perp\text{cut}} = 60$ GeV. This behavior of the merged predictions is quite natural, considering the idea of the merging algorithm, namely parton showering populate below a merging scale and matrix elements above the merging scale. This observation does not simply imply a potential instability of our algorithm but leads to a suggestion that

$p_{\perp \text{ start}}$	σ_{inc} (pb)	$\sigma_{\text{exc}}(0)/\sigma_{\text{inc}}$	$\sigma_{\text{exc}}(1)/\sigma_{\text{inc}}$	$\sigma_{\text{exc}}(2)/\sigma_{\text{inc}}$	$\sigma_{\text{exc}}(3)/\sigma_{\text{inc}}$
$\sqrt{s}$ (hard)	347	0.29	0.33	0.22	0.17
μ_F (normal)	424	0.28	0.33	0.22	0.17
$\mu_F/2$ (soft)	559	0.27	0.33	0.22	0.18

Table 1: Inclusive cross section and rates of each exclusive cross section, with different parton shower starting scales. The inclusive cross section without the merging is 562 pb.

we should choose a smaller merging scale for the $t\bar{t}$ pair production when the current shower model is used.

As the second check of the algorithm, we study the parton shower starting scale dependence. This parameter, which we define $p_{\perp \text{ start}}$, corresponds to the scale t_X in the improved DGLAP equation in eq. (4.14). At the end of Section 4.2, we have already discussed that distributions such as the differential jet rates will not depend largely on $p_{\perp \text{ start}}$ when the merging algorithm is correctly performed, as long as the scale choice is reasonable. We confirm this below. In Figure 20 the $p_{\perp \text{ start}}$ dependence of the differential jet rates for $1 \to 0$ (left) and $2 \to 1$ (right) with and without the merging algorithm is studied. The merging scale is set to $k_{\perp\text{cut}} = 20$ GeV. The Figure clearly shows that the $p_{\perp \text{ start}}$ dependence significantly reduces in the merged predictions.

As we have also discussed at the end of Section 4.2, it is expected that inclusive cross sections are not insensitive to $p_{\perp \text{ start}}$. The inclusive cross section is obtained by summing the exclusive contributions,

$$\sigma_{\text{inc}} = \sigma_{\text{exc}}(0) + \sigma_{\text{exc}}(1) + \sigma_{\text{exc}}(2) + \sigma_{\text{exc}}(3) \tag{5.4}$$

where $\sigma_{\text{exc}}(n)$ is the cross section from the n-parton matrix elements. In Table 1, the inclusive cross section and the rates of each exclusive cross section which are obtained with different $p_{\perp \text{ start}}$ scales are shown. The inclusive cross section without the merging is 562 pb. While the inclusive cross section is reduced as $p_{\perp \text{ start}}$ is increased, the rates of the exclusive cross sections are little affected. From this observation, the stable distribution in Figure 20 can be explained. A small increase of $\sigma_{\text{exc}}(3)$ at $p_{\perp \text{ start}} = \mu_F/2$ explains the small enhance at high $k_\perp$ regions found in Figure 20. Smaller inclusive cross sections imply less efficient event generation. We therefore choose $p_{\perp \text{ start}} = \mu_F/2$ for generating the event samples which will be analyzed in the following sections.

5.3 Merging scale and jet definition

In order for each of the two hardest jets to have the correct azimuthal angle information, each of them must have its origin in a parton obtained by the matrix elements (MEs). If one or both of them originate from a parton generated by the parton shower (PS), angular

Jet p_T cut (GeV)	20	30	40
Jet radius $R = 0.4$	11.0	4.0	2.2
Jet radius $R = 0.7$	16.4	5.3	2.7

Table 2: Contamination rate (%) with different jet definitions. The event samples are generated with the merging parameters $N = 3$ and $k_{\perp\text{cut}} = 20$ GeV. Only those which pass the cuts in eqs. (5.2) (5.3) are analyzed.

correlations between them disappear. We have observed this in Section 3.4. The minimum requirement on the merging parameters is therefore

1. $N \geq 2$.
2. $k_{\perp\text{cut}} < p_{T\text{cut}}^{\text{jet}}$.

The requirement on the maximal number of partons N provided by the MEs is obvious, since the leading order prediction of $\Delta\phi$ is obtained from the MEs for the $pp \to t\bar{t}+2$-parton process [14]. It is discussed how much the $\Delta\phi$ prediction can be improved for $N = 3$ in Section 5.4. The requirement on the merging scale $k_{\perp\text{cut}}$ is introduced to avoid that the two hardest jets have their origin in a parton generated by the PS. The $\Delta\phi$ distribution will not be stable if $k_{\perp\text{cut}} > p_{T\text{cut}}^{\text{jet}}$. However it is not obvious how smaller $k_{\perp\text{cut}}$ should be than $p_{T\text{cut}}^{\text{jet}}$ for a stable result. A too small $k_{\perp\text{cut}}$ is undesirable at all, since it can significantly reduce the efficiency of event generation. We, therefore, at first explore a relationship between $k_{\perp\text{cut}}$ and $p_{T\text{cut}}^{\text{jet}}$ from which $\Delta\phi$ is expected to be stable.

The contamination rate, which is defined as a rate of the contributions of the MEs event samples for the $pp \to t\bar{t}+0, 1$-parton processes, is calculated with different jet definitions and summarized in Table 2 in units of percentage. The merging parameters are set to $N = 3$ and $k_{\perp\text{cut}} = 20$ GeV. Note that the almost identical result is obtained when $N = 2$ and $k_{\perp\text{cut}} = 20$ GeV, as expected. Only those which pass the cuts in eqs. (5.2) (5.3) are considered. It is shown that more than 10% of the azimuthal angle correlation $\Delta\phi$ will be contaminated i.e. lost when $k_{\perp\text{cut}}$ is set equal to the jet p_T cut (= 20 GeV). The rate decreases with a rise in the jet p_T cut as expected. In order to suppress the contamination rate while avoiding too inefficient event generation, $k_{\perp\text{cut}} = 20$ GeV is chosen for the merging scale and a radius parameter $R = 0.4$ with $p_{T\text{cut}}^{\text{jet}} = 30$ GeV is used for the jet definition hereafter.

5.4 Result of the merging and impacts of the 3-parton MEs

The requirement on the maximal number of partons N provided by the matrix elements (MEs), $N \geq 2$ is briefly discussed in Section 5.3. In general a more precise description of multi-jet processes is expected for larger values of N. Thus $\Delta\phi$ is also expected to be more precise for $N = 3$ than for $N = 2$. However it is not obvious how and how much the $\Delta\phi$ prediction can be improved. In the present section this issue is clarified from a detailed study

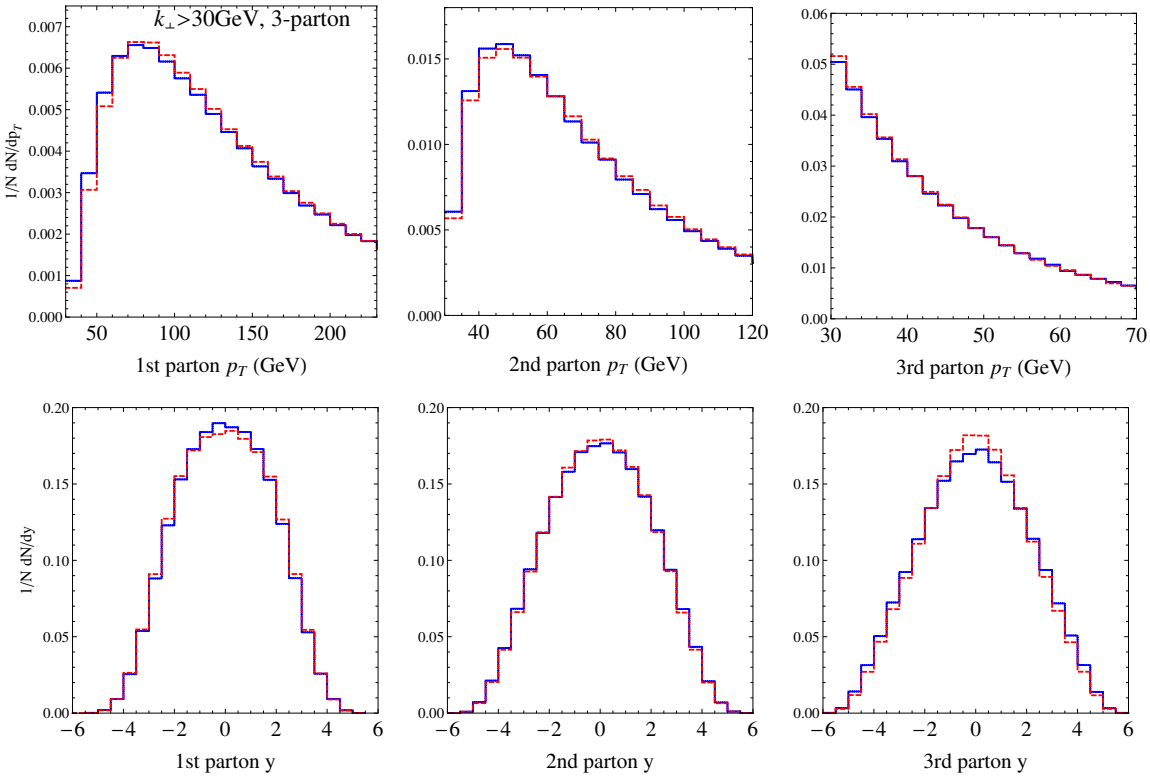

Figure 21: p_T and rapidity of the three partons in the event samples of the $pp \to t\bar{t} + 3$-parton process generated in the two different approaches (5.5) (5.6). The blue solid curves represent the approach (5.5) and the red dotted curves represent the approach (5.6).

on the impacts of including the $t\bar{t} + 3$-parton MEs.

When the parton shower (PS) generates additional partons from the MEs event samples for the highest parton multiplicity N in the merging algorithm, these additional partons are constrained to be softer than the N partons provided by the MEs in terms of the PS evolution variable. More precisely, by using the words in the merging algorithm in Section 4.4, the starting scale of the PS evolution variable from the $pp \to t\bar{t} + N$-parton process is set to the smallest clustering scale, $p_{\perp N}$. In order to explicitly confirm that the PS is well controlled, the event samples of the $pp \to t\bar{t}+3$-parton process are exclusively generated in the following two different approaches (5.5) (5.6) and p_T and rapidity of the generated three partons are compared in Figure 21. The three partons satisfy $k_\perp > 30$ GeV defined in eq. (4.20).

- An event sample of the $pp \to t\bar{t} + 3$-parton process is generated by the MEs and weighted by the Sudakov factors. (blue solid) . (5.5)
- An event sample of the $pp \to t\bar{t}+2$-parton process is generated by the MEs and weighted by the Sudakov factors. Then 1 parton is added by the PS. (red dotted) (5.6)

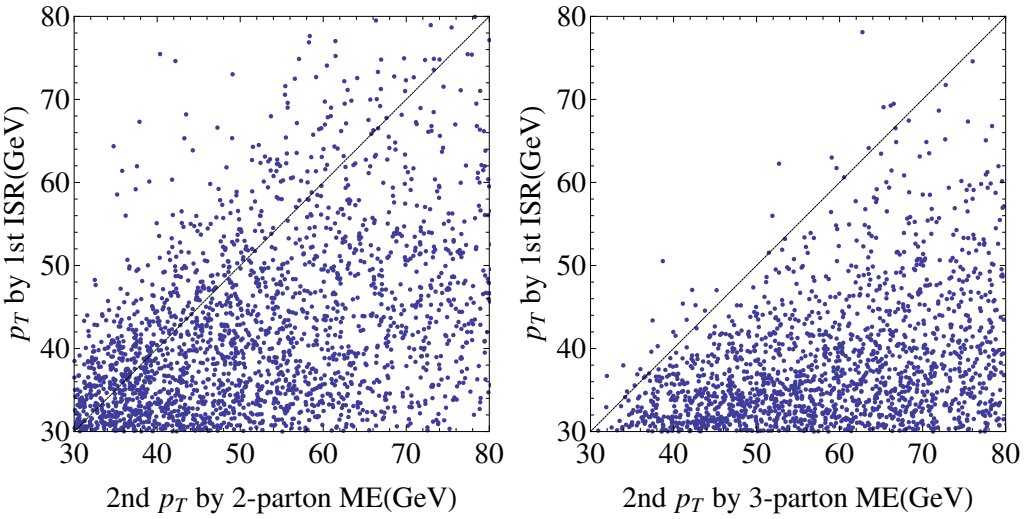

Figure 22: *Left*: The horizontal axis represents p_T of the second hardest parton generated by the MEs, the vertical axis represents p_T of the parton added by the ISR, in the event samples of the $pp \to t\bar{t} + 3$-parton process generated in the approach (5.6). *Right*: The horizontal axis represents p_T of the second hardest parton generated by the MEs, the vertical axis represents p_T of the parton added by the ISR, in the event samples of the $pp \to t\bar{t} + 4$-parton process generated in the approach (5.7).

A good agreement between the two approaches is found. Note that when we mention that an event sample is weighted by the Sudakov factors, not only the Sudakov factors but also the α_s and PDF factors are included in the weight factor. The latter procedure (5.6) is actually performed in the merging algorithm with $N = 2$ (of course not only the 1 parton but more partons are generated by the PS until the evolution variable reaches a cutoff scale). An important finding in the latter approach (5.6) is that the 1 parton added by the PS does not necessarily have a lower p_T than the 2 partons obtained by the MEs. In order to make it clearer, in the left graph of Figure 22 the horizontal axis represents p_T of the second hardest parton generated by the MEs and the vertical axis represents p_T of the parton added by the PS in the event samples of the $pp \to t\bar{t} + 3$-parton process generated in the approach (5.6). Only the samples which pass the cuts in eqs. (5.2) (5.3) and in which the additional parton is generated by the initial state radiation (ISR) are plotted. The graph shows that in the considerable fraction $\sim 21\%$ of the event samples indicated by the dots in the upper left of the graph, the parton added by the ISR has a higher p_T than either or both of the 2 partons generated by the MEs. Note that about 82% of the first PS from the $pp \to t\bar{t} + 2$-parton process is ISR. This fact can cause a non-negligible loss of the correlation $\Delta\phi$ in the following way. A parton with the highest or second highest p_T generated by the PS gives rise to the hardest or second hardest jet, which is thus selected for constructing $\Delta\phi$. We note that this problem exists, even though the merging scale is properly chosen.

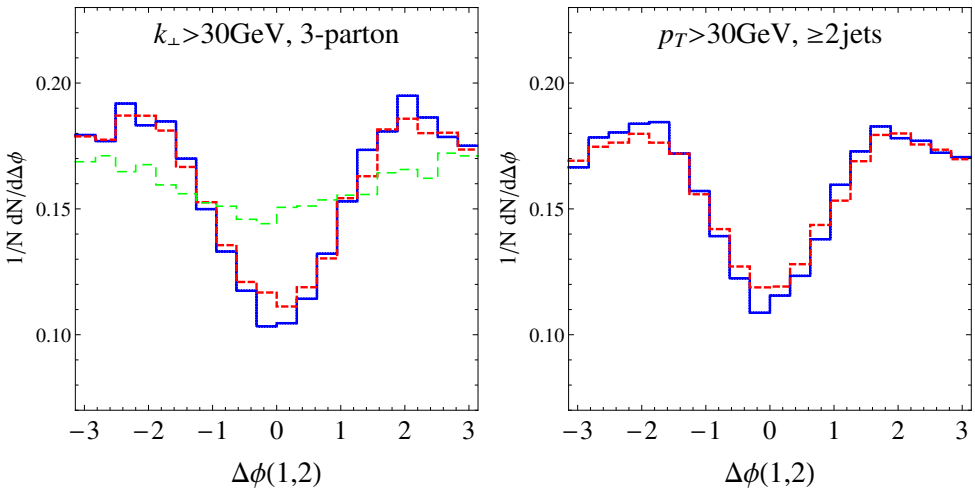

Figure 23: *Left*: $\Delta\phi$ distribution between the two hardest *partons* in the $pp \to t\bar{t}$+3-parton process generated in the three different approaches (5.5) (5.6) (5.8). *Right*: $\Delta\phi$ distribution. The blue solid curve represents the merging with $N = 3$, and the red dotted curve represents the merging with $N = 2$.

The problem of generating the hardest or second hardest parton with the PS can be solved by including the $t\bar{t}$ + 3-parton MEs. The event samples of the $pp \to t\bar{t}$ + 4-parton process are exclusively generated in the following approach (5.7), which is actually performed in the merging algorithm with $N = 3$,

- An event sample of the $pp \to t\bar{t}$+3-parton process is generated by the MEs and weighted by the Sudakov factors. Then 1 parton is added by the PS. (5.7)

The 1 parton added by the PS does not necessarily have a lower p_T than the 3 partons generated by the MEs, which is the same as the procedure (5.6). An important difference from the procedure (5.6) is that the parton added by the PS seldom has a higher p_T than the second hardest parton generated by the MEs. This fact is clearly shown in the right graph of Figure 22, where the horizontal axis represents p_T of the second hardest parton generated by the MEs and the vertical axis represents p_T of the parton added by the ISR, in the event samples of the $pp \to t\bar{t}$+4-parton process generated in the approach (5.7). Only the samples which pass the cuts in eqs. (5.2) (5.3) are plotted. This can effectively avoid that a jet which has its origin in a parton generated by the PS has the highest or second highest p_T, thus this jet is selected for a construction of $\Delta\phi$. Consequently, a loss of the correlation $\Delta\phi$ is reduced significantly in the merging with $N = 3$.

A loss of the correlation should be apparent when $\Delta\phi$ distributions are compared. At first, $\Delta\phi$ between the two hardest *partons* in the event samples of the $pp \to t\bar{t}$ + 3-parton process exclusively generated in the above two approaches (5.5) (5.6) is plotted in the left

graph of Figure 23, where the blue solid curve represents the approach (5.5) and the red dotted curve the approach (5.6). The green dashed curve represents the following approach,

- An event sample of the $pp \to t\bar{t} + 1$-parton process is generated by the MEs and weighted by the Sudakov factor. Then 2 partons are added by the PS. (green dashed) (5.8)

In this approach (5.8) the correlation $\Delta\phi$ should be absent and only an enhancement at $|\Delta\phi| \sim \pi$ from kinematic reasons is shown in the graph. Note that, as is clear from the blue solid curve, the $t\bar{t} + 3$-parton MEs do exhibit the strong correlation $\Delta\phi$ between the two hardest *partons* with large rapidity separation, just like in the $t\bar{t} + 2$-parton MEs. When the blue solid curve and the red dotted curve are compared, a clear difference is found. The loss of about 20% of the correlation between the two hardest *partons* in the approach (5.6) can explain the difference. Note that it is clear from Figure 21 that the difference cannot be explained from the kinematic differences of the three partons.

Finally the $\Delta\phi$ distribution in the merging with $N = 3$ (blue solid curve) and that in the merging with $N = 2$ (red dotted curve) are shown in the right graph of Figure 23. A difference is clearly seen. This observation confirms the non-negligible loss of the correlation in the merging with $N = 2$ and the avoidance of a loss of the correlation in the merging with $N = 3$ which are expected from the above parton level analyses. Therefore it can be concluded that the prediction of $\Delta\phi$ can be improved significantly by extending the merging algorithm from $N = 2$ to $N = 3$, namely by including the $t\bar{t} + 3$-parton MEs in the merging.

5.5 Comparison with the non-merging

In this section a naive approach, which we call the non-merging approach, is introduced. In the non-merging approach, only the $t\bar{t} + 2$-parton matrix elements (MEs) are used, and the parton shower (PS) evolution is applied to the MEs event samples of the $pp \to t\bar{t} + 2$-parton process. The two hardest jets can have their origin in a parton provided by the MEs and have a realistic representation of the internal jet structure generated by the PS, therefore the event samples should exhibit the correlation $\Delta\phi$. The Sudakov weight is absent, thus the $\Delta\phi$ prediction should be closer to the prediction of the leading order MEs. The result is compared to our best result obtained by the merging algorithm. A clear difference in the $\Delta\phi$ distribution is found, which is induced by the large Sudakov suppression.

The setup for generating the event samples in the non-merging approach is summarized at first. When generating the MEs event samples of the $pp \to t\bar{t} + 2$-parton process, α_s values are determined from

$$\alpha_s^2(\mu_R)\alpha_s(p_{T1})\alpha_s(p_{T2}), \tag{5.9a}$$

$$\mu_R^2 = E_T^2(t) + E_T^2(\bar{t}) + p_{T1}^2 + p_{T2}^2, \tag{5.9b}$$

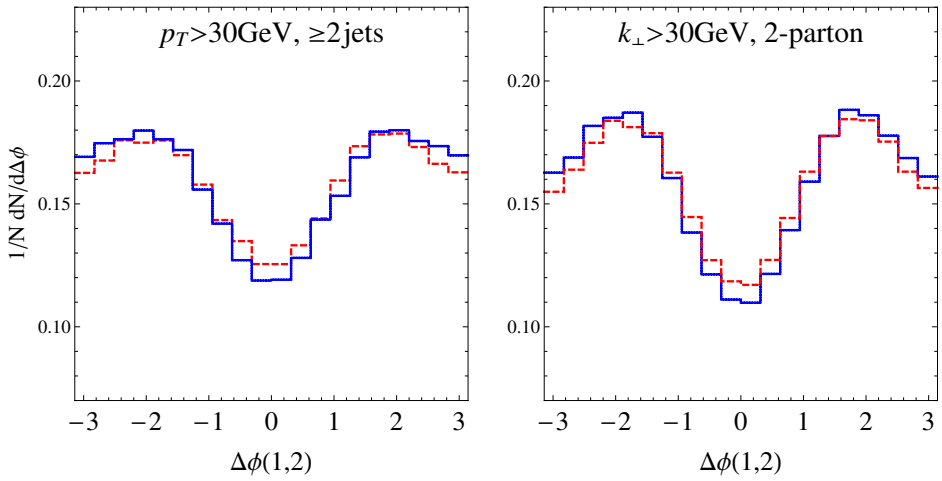

Figure 24: *Left*: $\Delta\phi$ distribution. The blue solid curve represents the merging with $N = 2$, and the red dotted curve represents the non-merging. *Right*: $\Delta\phi$ distribution between the two *partons* in the $pp \to t\bar{t} + 2$-parton process obtained by the MEs including the Sudakov weight (blue solid curve) and by the MEs (red dotted curve).

and the scale in the PDFs is set to

$$\mu^2_{\rm PDF} = p^2_{T1} + p^2_{T2}, \tag{5.10}$$

where p_{T1} and p_{T2} represent p_T of the two partons. The starting scale of the PS evolution variable is set to the lowest p_T of the two partons obtained by the MEs on event by event basis.

In the left graph of Figure 24 the $\Delta\phi$ distribution in the merging (blue solid curve) and that in the non-merging (red dotted curve) are compared. For a fair comparison, the result of the merging with $N = 2$ is plotted. A clear difference is found. There are more events at $\Delta\phi \sim 0$ and less events at $|\Delta\phi| \sim \pi$ in the non-merged result. The origin of the difference can be apparent through a parton level analysis. In the right graph of Figure 24, $\Delta\phi$ between the two *partons* in the event samples of the $pp \to t\bar{t} + 2$-parton process exclusively generated by the MEs (red dotted curve) and by the MEs including the Sudakov weight (blue solid curve) are plotted, where the same difference is found. This tells that the difference is induced by Sudakov effects.

Sudakov effects should be more apparent in p_T distributions of jets or partons. The p_T distributions of the two jets used in the left graph of Figure 24 are shown in the left two graphs of Figure 25, likewise the p_T distributions of the two *partons* used in the right graph of Figure 24 are shown in the right two graphs of Figure 25. Clearly there is strong Sudakov suppression of events with relatively low p_T jets and partons. The kinematic differences of the jets induced by the Sudakov suppression can explain the difference between the merged and non-merged results in the left graph of Figure 24. The two jets in the non-merged result

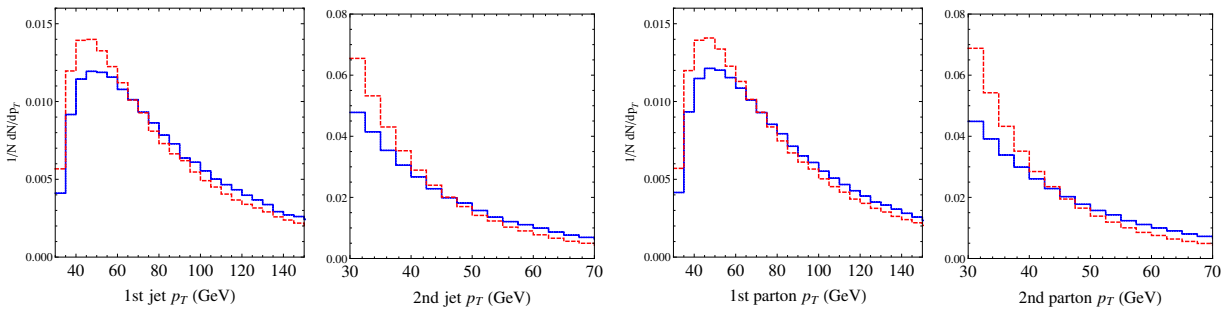

Figure 25: p_T of the two jets used in the left graph of Figure 24 is plotted in the left two graphs. p_T of the two *partons* used in the right graph of Figure 24 is plotted in the right two graphs.

are less energetic, as a result there are less events with back to back jets in azimuth, $|\Delta\phi| \sim \pi$.

In addition to the clear difference in the $\Delta\phi$ distribution, the strong Sudakov suppression indicates that the non-merged result is not reliable. Therefore it can be concluded that the non-merging approach does not accommodate the correct prediction of $\Delta\phi$.

5.6 Conclusion

The azimuthal angle correlation between the two highest p_T jets, $\Delta\phi = \phi_1 - \phi_2$ in the top quark pair plus multi-jet process at the 14 TeV LHC has been studied. Our objective is to clarify theoretical issues which are important when producing a reliable simulation of the process which accommodates the correct $\Delta\phi$ distributions. The event samples are generated by a merging algorithm of the leading order matrix elements (MEs) with parton shower (PS) evolution. The merging algorithm has been validated by confirming the smooth merging around the merging scale and the small dependence on the parton shower starting scale in the distributions of differential jet rates.

The generated event samples exhibit the strong correlation in $\Delta\phi$, when the maximal number of partons N provided by the MEs in the merging is set to 2 or 3 and when the merging scale is properly chosen. The difference between the merging with $N = 3$ and that with $N = 2$, namely the impacts of including the $t\bar{t}$ + 3-parton MEs in the merging, has been studied carefully. From a parton level analysis using the exclusive $pp \to t\bar{t}$ + 3-parton event samples, it is found that a parton generated by the PS has the second highest p_T in a considerable fraction $\sim 20\%$ of the event samples of the merging with $N = 2$, even though the merging scale is properly chosen. This can cause a non-negligible loss of the correlation $\Delta\phi$ in the merging with $N = 2$, because a parton with the highest p_T generated by the PS gives rise to the hardest or second hardest jet, which is thus selected for a construction of $\Delta\phi$. We have explicitly shown that a parton generated by the PS seldom has the largest or second highest p_T if the $t\bar{t}$ + 3-parton MEs are included in the merging, thus the loss of the correlation is significantly reduced in the merging with $N = 3$. It is worth noting here that the $t\bar{t}$ + 3-parton MEs do exhibit the strong $\Delta\phi$ correlation between the two highest p_T

partons with large rapidity separation, just like in the $t\bar{t}+2$-parton MEs. The non-negligible loss of the correlation in $N = 2$ and its avoidance in $N = 3$ which are estimated from the parton level analyses are observed as a clear difference in the $\Delta\phi$ distribution. We therefore conclude that the impact of including the $t\bar{t} + 3$-parton MEs is not negligible and the prediction of $\Delta\phi$ can be improved significantly by extending the merging algorithm from $N = 2$ to $N = 3$.

Our result has also been compared to the result of a naive approach in which PS evolution is applied to the MEs event samples of only the $pp \to t\bar{t} + 2$-parton process. The strong Sudakov suppression of events with low p_T jets has been observed, which indicates that the naive approach is not reliable. Moreover, a clear difference in the $\Delta\phi$ distribution is found and this can be explained from the kinematic differences of the jets induced by the Sudakov suppression. Therefore, we conclude that the naive approach does not accommodate the correct prediction of the correlation $\Delta\phi$.

We note that our findings from the study on the top quark pair production should be applicable equally to other heavy particle production by gluon fusion.

6 Conclusions and Outlook

In this thesis, the azimuthal angle correlation between the two jets in the top quark pair production at the LHC is studied. The azimuthal angle correlation is interesting not only in its own light, but also it is similar to the azimuthal angle correlation between the two jets produced in association with the parity odd Higgs boson via gluon fusion. What I expect is that the experimental technique to measure such an angular correlation between jets can be established first by using the top quark pair production which has a larger cross section.

My research presented in this thesis is divided into three main parts. In the first part, the azimuthal angle correlations between the 2 partons produced in association with the Higgs boson and with the heavy quark pair are studied both analytically and numerically. The second part is concerned with the jet simulation based on the DGLAP equation and the merging algorithm combining this approach with the matrix element approach. In the third part, the merging algorithm is applied to the event generation of the top quark pair production at the 14 TeV LHC, and the azimuthal angle correlation between the two jets is studied.

One of technical challenges in the merging algorithm for angular correlation studies is inefficient event generation due to a strong Sudakov suppression which arises because the merging scale must be chosen smaller than a jet scale. This is a common issue in the CKKW type merging algorithm. It can be an important research topic to explore merging strategies which can avoid this issue.

7 Acknowledgments

Many people have supported me during my Ph.D. studies at SOKENDAI and deserve gratitude. Some of them are particularly prominent:

First and foremost, my adviser Kaoru Hagiwara for making it possible to do excellent research in particle physics and have such a great experience. I am grateful to him for teaching me over the four years and for the patience he has shown during it. He has given me the several opportunities to do collaboration with the other physicists, which were invaluable for me. Most notably he did not abandon me, when I was thinking about quiting physics, and he has encouraged me to go to CERN to learn QCD, which I am now really enjoying;

The staff members of the KEK theory center for making the institute such a great place to study for students. In particular: Yutaka Sakamura and Takashi Kaneko for supervising the group discussion on the quantum field theory, twice a week and more than four hours on each day sometimes! They taught me physics very kindly with great patience, despite I asked too many stupid questions and I was a bit too rude. Mihoko Nojiri for supervising the group discussion on Collider physics, from which I have learned a lot;

My collaborators and colleagues for their help and inspirations. In particular: Jae Sik Lee for collaborating with me for the Higgs paper. Kentarou Mawatari for the collaboration and for letting me stay in Brussels twice. Satya Mukhopadhyay for the collaboration and for writing a great paper about the $Q\bar{Q}jj$. Without this, my thesis subject would have been absolutely different. Rikkert Frederix for giving a couple of impressive lectures about QCD in Tohoku University, since then I have been attracted by QCD, and for supervising me when I came to CERN after that. Yukinari Sumino for inviting Rikkert as a lecturer and for inviting me too, despite that we had met only once before! Yoshitaro Takaesu for helping me with calculations and with many programming problems. Junichi Kanzaki for giving me several advices for the paper;

My colleagues in the KEK theory center for making my life at KEK so enjoyable. In particular: Yohei Kikuta for being such a good friend. It was a great moment for me to look at the four hits by Ichiro Suzuki together. It is a quite shame, however, that we could not do collaboration. Yasuhito Sakaki for many enjoyable discussions on QCD. He has been the only researcher in KEK who has the same physical interest with me. Goto Hajime and Masaya Yata for discussions on non-physics topics. Masashi Fujitsuka, Hirohisa Kubota, Yoshihiko Oyama and Kengo Shimada for being a great colleague, who I wish the best of luck in their future work whatever they are;

JSPS, SOKENDAI and KEK for funding my studies.

Finally I would like to thank those closest to me: my brother, my sister and my grandparents for their love, support and encouragement, and most importantly my parents for everything. Thank you!

References

[1] T. Plehn, D. L. Rainwater and D. Zeppenfeld, "Determining the structure of Higgs couplings at the LHC," Phys. Rev. Lett. **88** (2002) 051801 [hep-ph/0105325].

[2] V. Del Duca, W. Kilgore, C. Oleari, C. Schmidt and D. Zeppenfeld, "Gluon fusion contributions to H + 2 jet production," Nucl. Phys. B **616** (2001) 367 [hep-ph/0108030].

[3] G. Klamke and D. Zeppenfeld, "Higgs plus two jet production via gluon fusion as a signal at the CERN LHC," JHEP **0704** (2007) 052 [hep-ph/0703202 [HEP-PH]].

[4] K. Hagiwara, Q. Li and K. Mawatari, "Jet angular correlation in vector-boson fusion processes at hadron colliders," JHEP **0907** (2009) 101 [arXiv:0905.4314 [hep-ph]].

[5] K. Odagiri, "On azimuthal spin correlations in Higgs plus jet events at LHC," JHEP **0303** (2003) 009 [hep-ph/0212215].

[6] V. Del Duca, G. Klamke, D. Zeppenfeld, M. L. Mangano, M. Moretti, F. Piccinini, R. Pittau and A. D. Polosa, "Monte Carlo studies of the jet activity in Higgs + 2 jet events," JHEP **0610** (2006) 016 [hep-ph/0608158].

[7] C. Ruwiedel, N. Wermes and M. Schumacher, "Prospects for the measurement of the structure of the coupling of a Higgs boson to weak gauge bosons in weak boson fusion with the ATLAS detector," Eur. Phys. J. C **51** (2007) 385.

[8] J. R. Andersen, V. Del Duca and C. D. White, "Higgs Boson Production in Association with Multiple Hard Jets," JHEP **0902** (2009) 015 [arXiv:0808.3696 [hep-ph]].

[9] J. R. Andersen, K. Arnold and D. Zeppenfeld, "Azimuthal Angle Correlations for Higgs Boson plus Multi-Jet Events," JHEP **1006** (2010) 091 [arXiv:1001.3822 [hep-ph]].

[10] G. Aad *et al.* [ATLAS Collaboration], "Measurements of Higgs boson production and couplings in diboson final states with the ATLAS detector at the LHC," Phys. Lett. B **726** (2013) 88 [Erratum-ibid. B **734** (2014) 406] [arXiv:1307.1427 [hep-ex]].

[11] G. Aad *et al.* [ATLAS Collaboration], "Measurements of fiducial and differential cross sections for Higgs boson production in the diphoton decay channel at $\sqrt{s} = 8$ TeV with ATLAS," JHEP **1409** (2014) 112 [arXiv:1407.4222 [hep-ex]].

[12] S. Chatrchyan *et al.* [CMS Collaboration], "Measurement of the properties of a Higgs boson in the four-lepton final state," Phys. Rev. D **89** (2014) 092007 [arXiv:1312.5353 [hep-ex]].

[13] V. Khachatryan *et al.* [CMS Collaboration], "Observation of the diphoton decay of the Higgs boson and measurement of its properties," Eur. Phys. J. C **74** (2014) 10, 3076 [arXiv:1407.0558 [hep-ex]].

[14] K. Hagiwara and S. Mukhopadhyay, "Azimuthal correlation among jets produced in association with a bottom or top quark pair at the LHC," JHEP **1305**, 019 (2013) [arXiv:1302.0960 [hep-ph]].

[15] K. Hagiwara and D. Zeppenfeld, "Helicity Amplitudes for Heavy Lepton Production in e+ e- Annihilation," Nucl. Phys. B **274** (1986) 1.

[16] K. Hagiwara and D. Zeppenfeld, "Amplitudes for Multiparton Processes Involving a Current at e+ e-, e+- p, and Hadron Colliders," Nucl. Phys. B **313** (1989) 560.

[17] K. Hagiwara, H. Murayama and I. Watanabe, "Search for the Yukawa interaction in the process e+ e- —¿ t anti-t Z at TeV linear colliders," Nucl. Phys. B **367**, 257 (1991).

[18] H. Murayama, I. Watanabe and K. Hagiwara, "HELAS: HELicity amplitude subroutines for Feynman diagram evaluations," KEK-91-11.

[19] V. N. Gribov and L. N. Lipatov, "Deep inelastic e-p scattering in perturbation theory, Sov. J. Nucl. Phys. 15 (1972) 438.

[20] G. Altarelli and G. Parisi, "Asymptotic freedom in parton language, Nucl. Phys. B126 (1977) 298318.

[21] Y. L. Dokshitzer, "Calculation of the structure functions for deep inelastic scattering and e+ e annihilation by perturbation theory in quantum chromodynamics, Sov. Phys. JETP 46 (1977) 641653.

[22] M. L. Mangano, M. Moretti and R. Pittau, "Multijet matrix elements and shower evolution in hadronic collisions: $Wb\bar{b}$ + n jets as a case study," Nucl. Phys. B **632** (2002) 343 [hep-ph/0108069].

[23] S. Catani, F. Krauss, R. Kuhn and B. R. Webber, "QCD matrix elements + parton showers," JHEP **0111**, 063 (2001) [hep-ph/0109231].

[24] L. Lonnblad, "Correcting the color dipole cascade model with fixed order matrix elements," JHEP **0205** (2002) 046 [hep-ph/0112284].

[25] F. Krauss, "Matrix elements and parton showers in hadronic interactions," JHEP **0208**, 015 (2002) [hep-ph/0205283].

[26] S. Mrenna and P. Richardson, "Matching matrix elements and parton showers with HERWIG and PYTHIA," JHEP **0405** (2004) 040 [hep-ph/0312274].

[27] N. Lavesson and L. Lonnblad, "W+jets matrix elements and the dipole cascade," JHEP **0507** (2005) 054 [hep-ph/0503293].

[28] M. L. Mangano, M. Moretti, F. Piccinini and M. Treccani, "Matching matrix elements and shower evolution for top-quark production in hadronic collisions," JHEP **0701** (2007) 013 [hep-ph/0611129].

[29] J. Alwall, S. Hoche, F. Krauss, N. Lavesson, L. Lonnblad, F. Maltoni, M. L. Mangano and M. Moretti *et al.*, "Comparative study of various algorithms for the merging of parton showers and matrix elements in hadronic collisions," Eur. Phys. J. C **53** (2008) 473 [arXiv:0706.2569 [hep-ph]].

[30] W. T. Giele, D. A. Kosower and P. Z. Skands, "A simple shower and matching algorithm," Phys. Rev. D **78**, 014026 (2008) [arXiv:0707.3652 [hep-ph]].

[31] N. Lavesson and L. Lonnblad, "Merging parton showers and matrix elements: Back to basics," JHEP **0804** (2008) 085 [arXiv:0712.2966 [hep-ph]].

[32] J. Alwall, S. de Visscher and F. Maltoni, "QCD radiation in the production of heavy colored particles at the LHC," JHEP **0902** (2009) 017 [arXiv:0810.5350 [hep-ph]].

[33] S. Hoeche, F. Krauss, S. Schumann and F. Siegert, "QCD matrix elements and truncated showers," JHEP **0905** (2009) 053 [arXiv:0903.1219 [hep-ph]].

[34] K. Hamilton, P. Richardson and J. Tully, "A Modified CKKW matrix element merging approach to angular-ordered parton showers," JHEP **0911** (2009) 038 [arXiv:0905.3072 [hep-ph]].

[35] L. Lonnblad and S. Prestel, "Matching Tree-Level Matrix Elements with Interleaved Showers," JHEP **1203** (2012) 019 [arXiv:1109.4829 [hep-ph]].

[36] T. Sjostrand, S. Mrenna and P. Z. Skands, "A Brief Introduction to PYTHIA 8.1," Comput. Phys. Commun. **178** (2008) 852 [arXiv:0710.3820 [hep-ph]].

[37] T. Sjostrand, S. Mrenna and P. Z. Skands, "PYTHIA 6.4 Physics and Manual," JHEP **0605** (2006) 026 [hep-ph/0603175].

[38] J. Alwall, R. Frederix, S. Frixione, V. Hirschi, F. Maltoni, O. Mattelaer, H.-S. Shao and T. Stelzer *et al.*, "The automated computation of tree-level and next-to-leading order differential cross sections, and their matching to parton shower simulations," JHEP **1407**, 079 (2014) [arXiv:1405.0301 [hep-ph]].

[39] R. K. Ellis, W. J. Stirling and B. R. Webber, "QCD and collider physics," ed. 1, vol. 8, Cambridge Monogr. Part. Phys. Nucl. Phys. Cosmol., 1996.

[40] T. Sjostrand, "Monte Carlo Generators," hep-ph/0611247.

[41] P. Skands, "Introduction to QCD," arXiv:1207.2389 [hep-ph].

[42] T. Sjostrand and P. Z. Skands, "Transverse-momentum-ordered showers and interleaved multiple interactions," Eur. Phys. J. C **39** (2005) 129 [hep-ph/0408302].

[43] G. P. Salam, "Elements of QCD for hadron colliders," CERN Yellow Report CERN-2010-002, 45-100 [arXiv:1011.5131 [hep-ph]].

[44] T. Sjostrand, "A Model for Initial State Parton Showers," Phys. Lett. B **157** (1985) 321.

[45] R. Corke and T. Sjostrand, "Interleaved Parton Showers and Tuning Prospects," JHEP **1103** (2011) 032 [arXiv:1011.1759 [hep-ph]].

[46] E. Norrbin and T. Sjostrand, "QCD radiation off heavy particles," Nucl. Phys. B **603**, 297 (2001) [hep-ph/0010012].

[47] S. Catani, Y. L. Dokshitzer, M. H. Seymour and B. R. Webber, "Longitudinally invariant K_t clustering algorithms for hadron hadron collisions," Nucl. Phys. B **406** (1993) 187.

[48] S. Catani, Y. L. Dokshitzer, M. Olsson, G. Turnock and B. R. Webber, "New clustering algorithm for multi - jet cross-sections in e+ e- annihilation," Phys. Lett. B **269** (1991) 432.

[49] P. Pfeifenschneider *et al.* [JADE and OPAL Collaborations], "QCD analyses and determinations of alpha(s) in e+ e- annihilation at energies between 35-GeV and 189-GeV," Eur. Phys. J. C **17** (2000) 19 [hep-ex/0001055].

[50] G. Aad *et al.* [ATLAS Collaboration], "Measurement of the production cross section of jets in association with a Z boson in pp collisions at $\sqrt{s} = 7$ TeV with the ATLAS detector," JHEP **1307** (2013) 032 [arXiv:1304.7098 [hep-ex]].

[51] G. Aad *et al.* [ATLAS Collaboration], "Measurement of the Z/γ^* boson transverse momentum distribution in *pp* collisions at $\sqrt{s} = 7$ TeV with the ATLAS detector," JHEP **1409** (2014) 145 [arXiv:1406.3660 [hep-ex]].

[52] M. Cacciari, G. P. Salam and G. Soyez, "The Anti-k(t) jet clustering algorithm," JHEP **0804** (2008) 063 [arXiv:0802.1189 [hep-ph]].

[53] M. Cacciari, G. P. Salam and G. Soyez, "FastJet User Manual," Eur. Phys. J. C **72** (2012) 1896 [arXiv:1111.6097 [hep-ph]].

[54] J. Pumplin, D. R. Stump, J. Huston, H. L. Lai, P. M. Nadolsky and W. K. Tung, "New generation of parton distributions with uncertainties from global QCD analysis," JHEP **0207** (2002) 012 [hep-ph/0201195].